Heriot Watt University

Institute of GeoEnergy Engineering

Mechanistic Study of Immiscible and Near-miscible CO_2 Water-Alternating-Gas Process

Gang Wang

A dissertation submitted for the degree of Doctor of Philosophy

July 2020

Abstract

CO_2 Water-Alternating-Gas injection (CO_2-WAG) under near-miscible conditions is a multifaceted process due to the complex interaction of thermodynamic phase behaviour, multiphase flow behaviour and the heterogeneity of the porous medium. The central objective of this study is to improve the fundamental understanding of fluid behaviour during the injection process of CO_2-WAG, with an emphasis on the transition from immiscible to miscible conditions. This work presents a detailed simulation study of both continuous and WAG displacements with unfavourable mobility ratios for 1D and 2D areal systems. Various flow regimes were investigated, including viscous fingering and channelling displacements within heterogeneous random correlated fields.

The key novelty/contribution of this thesis is to bring a new synthesis, which incorporates both compositional effects (M_{CE}) and interfacial effects (M_{IFT}), to improve the numerical simulation of near-miscible processes. Based on this newly developed synthesis, this study was then further extended to investigate a range of key physics, including gas trapping, water hysteresis and capillarity, all of which may occur in 3-phase systems. For the first time, the significance of these mechanisms has been clearly identified with the use of very-fine scale compositional simulations (Δx=0.05m), where all the physics of interest can be fully represented. The efforts of studying the key processes separately leads to a greater insight into how these physical processes positively or negatively affect the sweep and local displacement efficiency. Issues such as front stability, local displacement efficiency, formation of fingering/channelling and viscous crossflow during CO_2 near-miscible displacement can lead to behaviour that is significantly different from immiscible flooding in these systems. From the modelling perspective, it demonstrates convincingly that field-scale reservoir models should properly address these small-scale effects to lay claim to reasonable accuracy in forecasts of flow/reservoir behaviour. The complete dataset and results of this study are available online as a model case example for compositional flows in heterogeneous systems. DOI is 10.17861/fc1c90bb-9d3f-4a6c-9170-7b7fe10ec7b9.

Acknowledgements

Undertaking this PhD has been a truly life-changing experience for me, and it would not have been possible to do without the help and support that I received from many people, particularly my supervisors Dr Gillian Pickup, Prof. Ken Sorbie and Prof. Eric Mackay. As my first supervisor, Gillian has been extremely supportive through each stage of my PhD and drove my project to progress smoothly. As the "legend" of Institute of GeoEnergy Engineering (IGE), Ken's enormous expertise in the field surrounding my research was invaluable and the key to formulating the research topic and methodology. Eric has taught me a lot on how to build the mind-set to be a better researcher and will be the mentor of my fellowship awarded by Leverhulme Trust. Their immense patience, considerate encouragement, great sense of humour and positive attitude have always kept me motivated throughout the course of the study as well as life. Many thanks also go to Prof. Arne Skauge at Bergen University for his valuable input and inspiring discussions on my work. I am amazed that the chemistry worked perfectly well between my supervisory team and myself throughout my PhD journey.

I also wish to thank Prof. Erling Stenby from Technical University of Denmark and Dr. Rink van Dijke at IGE for examining this thesis and their very useful feedback. I am greatly appreciative for the funding by Energi Simulation, Petronas, Uzma Engineering Sdn. Bhd., which allowed me to concentrate on my research without having any financial concerns. Dr. Vijay Shrivastava, Mr. Marco Misenta, Dr. Faraj Zarei and Ms. Susan Fellows at Computer Modelling Group are thanked for their great support for the use of reservoir simulator, i.e. CMG/GEM. I also appreciate the insightful discussions with Dr. Quan Chen, who has assured me to pursue a higher degree at Heriot-Watt University.

My thanks also go out to the support I received from my colleagues of IGE, Dr. Saeed Ghanbari, Dr. Eltazy Khalid, Dr. Akindolu Dada and Dr. Ehsan Nikjoo. I am especially grateful to Mr. Victor Gutierrez for making my learning process of MATLAB highly efficient and joyful. Special thanks to Ms. Heather O'Hara and Mr. Alan Brown, for their excellent admin and computer support, respectively.

Finally, my deep and sincere gratitude to my family for their unconditional love. I am forever indebted to my parents, my wife and my wife's parents for their tremendous support.

Declaration Statement

I hereby declare that this work is original research undertaken by me and that no part of this thesis has been submitted for consideration towards another degree at this or any other institution. In this thesis, any work that is not my own work has been properly referenced.

Gang Wang
July 2020

List of Publications

Peer-reviewed papers:

- **Wang, G.**, Pickup, G., Sorbie, K., Mackay, E. and Skauge, A. (2020) 'Numerical Study of CO_2 Injection and the Role of Viscous Crossflow in Near-miscible CO_2-WAG', *Journal of Natural Gas Science and Engineering*, 74, p. 103112.
- **Wang, G.**, Pickup, G. E., Sorbie, K. S. and Mackay, E. J. (2019b) 'Detailed Assessment of Compositional and Interfacial Tension Effects on the Fluid Behaviour During Immiscible and Near-Miscible CO_2 Continuous and WAG Displacements', *Transport in Porous Media*, 131(3), pp. 805-830.
- **Wang, G.**, Pickup, G. E., Sorbie, K. S. and Mackay, E. J. (2019a) 'Analysis of Compositional Effects on Global Flow Regimes in CO_2 Near-Miscible Displacements in Heterogeneous Systems', *Transport in Porous Media*, 129(3), pp. 743-759.

Conference papers:

- **Wang, G.**, Pickup, G. E., Sorbie, K. S., Mackay, E. J. and Skauge, A. (2019c) 'Analysis of Near-Miscible CO_2-WAG Displacements: the Distinction between Compositional and Interfacial Tension Effects', SPE-193907-MS, *Proceedings of the SPE Reservoir Simulation Conference.* Society of Petroleum Engineers, 10-11 April, Galveston, Texas. doi: 10.2118/193907-MS.
- **Wang, G.**, Pickup, G., Sorbie, K. and Mackay, E. (2018a) 'Numerical Analysis Of Immiscible/Near-Miscible CO_2-WAG Displacement, Incorporating Compositional And Interfacial Tension Effects', *Proceedings of the Fifth CO_2 Geological Storage Workshop*. EAGE, 21 - 23 November Utrecht, Netherlands. doi: 10.3997/2214-4609.201802985
- **Wang, G.**, Pickup, G. E., Sorbie, K. S. and Mackay, E. J. (2018b) 'The Analysis of Compositional Effects on Global Flow Regimes in CO_2 Near-Miscible Displacements in Heterogeneous Systems ', SPE-190273-MS, *Proceedings of the SPE Improved Oil Recovery Conference*. Society of Petroleum Engineers, 14-18 April, Tulsa, Oklahoma. doi: 10.2118/190273-MS.
- **Wang, G.**, Pickup, G. and Mackay, E. (2016) 'Synergy between Carbon Dioxide Storage and Incremental Oil Recovery', *Proceedings of the 78th EAGE Conference and Exhibition 2016*. EAGE, 30 May-2 June, Vienna, Austria. doi: 10.3997/2214-4609.201601073

Research Thesis Submission

Name*:*	Gang Wang		
School:	Energy Geoscience Infrastructure and Society		
Version: *(i.e. First, Resubmission, Final)*	Final	Degree Sought:	PhD in Petroleum Engineering

Declaration

In accordance with the appropriate regulations I hereby submit my thesis and I declare that:

1. The thesis embodies the results of my own work and has been composed by myself
2. Where appropriate, I have made acknowledgement of the work of others
3. The thesis is the correct version for submission and is the same version as any electronic versions submitted*.
4. My thesis for the award referred to, deposited in the Heriot-Watt University Library, should be made available for loan or photocopying and be available via the Institutional Repository, subject to such conditions as the Librarian may require
5. I understand that as a student of the University I am required to abide by the Regulations of the University and to conform to its discipline.
6. I confirm that the thesis has been verified against plagiarism via an approved plagiarism detection application e.g. Turnitin.

Signature of Candidate*:*		Date:	29/07/2020

Submission

Submitted By *(name in capitals):*	GANG WANG
Signature of Individual Submitting:	
Date Submitted:	29/07/2020

For Completion in the Student Service Centre (SSC)

Limited Access	Requested	Yes		No		Approved	Yes		No	
E-thesis Submitted (mandatory for final theses)										
Received in the SSC by *(name in capitals):*						Date:				

Inclusion of Published Works

Declaration

This thesis contains one or more multi-author published works. In accordance with Regulation 6 (9.1.2) I hereby declare that the contributions of each author to these publications is as follows:

Citation details	**Wang, G.**, Pickup, G., Sorbie, K., Mackay, E. and Skauge, A. (2020) 'Numerical Study of CO_2 Injection and the Role of Viscous Crossflow in Near-miscible CO_2-WAG', *Journal of Natural Gas Science and Engineering*, 74, p. 103112.
Author 1	Conceptualization, Methodology, Software, Visualization, Investigation, Writing- Original draft preparation
Author 2	Data curation, Visualization, Supervision, Writing- Reviewing and Editing, Funding acquisition;
Author 3	Conceptualization, Methodology, Investigation; Writing- Reviewing and Editing
Author 4	Methodology, Data curation, Supervision, Resources, Funding acquisition**;** Reviewing and Editing
Author 5	Conceptualization, Methodology.
Signature:	
Date:	

Citation details	**Wang, G.**, Pickup, G. E., Sorbie, K. S. and Mackay, E. J. (2019b) 'Detailed Assessment of Compositional and Interfacial Tension Effects on the Fluid Behaviour During Immiscible and Near-Miscible CO_2 Continuous and WAG Displacements', *Transport in Porous Media*, 131(3), pp. 805-830.
Author 1	Conceptualization, Methodology, Software, Visualization, Investigation, Writing- Original draft preparation
Author 2	Data curation, Visualization, Supervision, Writing- Reviewing and Editing, Funding acquisition;
Author 3	Conceptualization, Methodology, Investigation; Writing- Reviewing and Editing
Author 4	Methodology, Data curation, Supervision, Resources, Funding acquisition**;** Reviewing and Editing
Signature:	
Date:	

Citation details	**Wang, G.**, Pickup, G. E., Sorbie, K. S. and Mackay, E. J. (2019a) 'Analysis of Compositional Effects on Global Flow Regimes in CO_2 Near-Miscible Displacements in Heterogeneous Systems', *Transport in Porous Media*, 129(3), pp. 743-759.
Author 1	Conceptualization, Methodology, Software, Visualization, Investigation, Writing- Original draft preparation
Author 2	Data curation, Visualization, Supervision, Writing- Reviewing and Editing, Funding acquisition;
Author 3	Conceptualization, Methodology, Investigation; Writing- Reviewing and Editing
Author 4	Methodology, Data curation, Supervision, Resources, Funding acquisition**;** Writing- Reviewing and Editing
Signature:	
Date:	

Table of Contents

List of Figures

List of Tables

List of Abbreviations

α_{lk}- Longitudinal dispersivity

α_{tk}- Transverse dispersivity

D_{ik}^{*}- Molecular diffusion coefficient of component i in phase k

f- Weighting factor for IFT effects

F_k- Formation resistivity factor for phase k

J_i- Total mass flux (rate of mass flow per unit area) of component i

K_{rg}- Gas relative permeability

K_{rgt}- Total gas relative permeability (under IFT effects)

K_{rg}^{dr} - Gas relative permeability during drainage process

K_{rg}^{im}- Gas relative permeability during imbibition process

K_{rw}^{imb}- Imbibition relative permeability

K_{rw}^{2phase}- Relative permeability of water in two-phase system (equal to K_{rw}^{imb})

K_{rw}^{3phase}- Relative permeability of water in three-phase system (under the effect of water hysteresis)

K_{ro}- Oil relative permeability

K_{rocw}- Oil relative permeability at connate water saturation

K_{rot}- Total oil relative permeability (under IFT effects)

K_{rw}-Water relative permeability

M_{CE}- Compositional effects

MCM- Multiple-Contact Miscibility

M_{IFT}- Interfacial tension effects

n- Exponent of the equation for weighting factor

P_c- Capillary pressure,

S_g- Gas saturation

S_g^{*}- Normalised gas saturation

S_{gc}- Critical gas saturation

S_{gf}- Free gas saturation (under the effect of gas trapping)

S_g^{I}- Gas saturation from the former process (under the effect of water hysteresis)

S_{gr}- Trapped gas saturation (under the effect of gas trapping)

S_{gi}- Gas saturation at the start of the decreasing gas saturation process (under the effect of gas trapping)

S_{gmax}- Maximum attainable gas saturation

S_o- Oil saturation

S_o^*- Normalised oil saturation

S_{org}- Residual oil saturation to gas

S_{orw}- Residual oil saturation to water

S_w- Water saturation

S_w^*- Normalised water saturation

S_{wc}- Connate water saturation

PVI- Pore volume injection

$\overrightarrow{u_k}$- Flow velocity of phase k

y_{ik}- Mass fraction of component i in phase k (oil, water and gas)

σ_{go}^0- Threshold value when IFT effects are triggered

σ_{go}- Interfacial tension between oil and gas

3PRP- three-phase relative permeability

Chapter 1 Introduction and Research Objectives

1.1 Introduction

Global demand for liquid fuels is expected to increase from 98 to 108 million barrels per day in the next decade as a result of economic development and population growth (BP, 2019). Since much of the easy-to-produce oil has been recovered, Enhanced Oil Recovery (EOR) is becoming an essential technique in global oil production to guarantee the energy security. EOR, by definition, is a stage of hydrocarbon production that involves an injection of materials not normally present in petroleum reservoirs to recover incremental oil (Lake *et al.*, 2014). There are three main types of EOR, including thermal -injection (steam), chemical injection (such as polymer), and gas injection (such as CO_2). The main goal of any EOR project is to achieve the best performance in terms of economic and recovery prospects. For more than 40 years of field practice, CO_2 injection has been widely applied to extend the field life following the primary production and water flood, especially in the North America (Christensen *et al.*, 1998; Alvarado and Manrique, 2010). Taking the year of 2008 as an example, there were more than 100 CO_2-EOR projects implemented globally and collectively led to an incremental oil recovery of 250,000 barrels per day (Perera *et al.*, 2016). According to the outlook report by BP (2019), the global production from CO_2-EOR will experience further increase given the additional policy support for efforts to advance carbon capture utilisation and storage (CCUS).

There are a number of advantages of applying CO_2 injection to improve the displacement performance, such as oil swelling and lowered oil viscosity, which are a result of CO_2 dissolution in oil. Most importantly, CO_2 flooding is able to unlock the trapped oil and significantly improve the displacement efficiency through developing miscibility with oil. Miscibility is a physical state when multiple substances mix without forming any interface. Minimum miscibility pressure (MMP) is defined as the minimum pressure that is required for the miscibility to occur between fluids. If the reservoir pressure is sustained above MMP, miscibility can be either achieved directly at the first contact or after multiple contacts through mass transfer between the oil and gas (Stalkup, 1983).

CO_2 flooding is therefore commonly grouped into the immiscible and the miscible displacement. Although both types of CO_2 displacement have been applied successfully (Christensen *et al.*, 1998), it is preferably to implement miscible CO_2 flooding in practice,

so that local displacement efficiency can be greatly improved. Strictly speaking, it is difficult to distinguish between the two situations in terms of compositional effects. This is because mass transfer will occur as long as CO_2 starts to contact oil, even at the condition that is typically defined as immiscible conditions. Therefore, in this study, the ***immiscible*** displacement here refers to a condition with an operation pressure well below MMP, whereas ***miscible*** displacement with an operation pressure well above MMP. As for the concept of ***near-miscible***, the displacement is operated slightly below MMP. The development of miscibility and the process of mass transfer will be demonstrated in detail in the following chapters.

CO_2 can be injected either continuously or alternately with water under both immiscible and miscible conditions. In general, CO_2 injection has an issue of unstable displacing front due to the adverse mobility ratio. This may lead to early gas breakthrough and therefore bypassing of a great amount of oil. For this reason, CO_2 is often injected alternately with water to improve the mobility control, namely Water-Alternating-Gas injection (WAG). Typically, water and gas slugs are pumped into the oil reservoir with a certain WAG ratio. WAG ratio is defined as the volume of injected water to the volume of injected gas at reservoir conditions. Note that too much water may lead to poor microscopic efficiency whereas too much gas may have a very poor sweep due to the rapid gas breakthrough. For this reason, various injection schemes and well control techniques have been developed in practice to optimise the displacement performance of WAG, such as Simultaneous Water and Gas injection (SWAG) and Foam Assisted Water and Gas injection (FAWAG). The selection of an appropriate WAG scheme is dependent on a range of factors, such as the reservoir fluids, rock properties, CO_2 source and economic status. In particular, this mechanistic study is focused on the fluid behaviour with a fixed WAG injection ratio (1:1), which has been frequently tested/applied in the oil industry (Alvarado and Manrique, 2010).

Compared with water injection, it is more problematic to simulate WAG injection due to the complexity of multi-phase flow behaviour. First, there is an additional requirement of a 3-phase relative permeability (3PRP) model for the reservoir simulations. Since reliable and complete experimental data of 3PRP is seldom available, it is a common practice to evaluate 3PRP through interpolating from two-phase data using an empirical model, such as Stone 1, Stone 2 and Baker (Ranaee *et al.*, 2016). Secondly, the fluid saturations (water and gas) experience strong cyclic changes and present a hysteresis flow

feature during the WAG injection. Permeability hysteresis refers to the relative permeability dependent on the history of saturation path. The relative permeability of the non-wetting phase during the imbibition cycle is generally lower than that during the drainage cycle at the same saturation. Finally yet importantly, the analysis of multi-phase flow will be even more complex when the flow functions are also affected by the mass transfer process. According to Asar and Handy (1988), one important issue is that the relative permeabilities of gas and oil should increase with decreasing gas/oil interfacial tension (IFT), which can be changed dramatically by mass transfer when moving towards miscibility.

1.2 Research motivations and objectives

In fact, both immiscible and miscible CO_2-WAG have been actively analysed since the 1970s. However, the understanding of the CO_2-WAG process is still incomplete. One of the major concerns is the flow behaviour in the transition from immiscible to miscible conditions, i.e. near-miscible conditions. Near-miscible displacement refers to a process in which the injected CO_2 does not quite develop complete miscibility with the oil, but comes close (Sohrabi *et al.*, 2008a). Strictly speaking, near-miscible displacement should be classified as a special type of immiscible displacement, which involves strong compositional effects (and therefore is close to miscibility) but still has multi-phase behaviour. It has been reported that many miscible projects encountered loss of pressure during operations and therefore becoming more of a near-miscible displacement. Surprisingly, these near-miscible displacements still achieve a very good incremental recovery (Christensen *et al.*, 1998). For this reason, it is highly necessary to analyse the key physics occurring in near-miscible CO_2-WAG injection in terms of the improved oil recovery.

With the use of commercial simulator (CMG/GEM) and Matlab, the central objective of this numerical study is to provide a fundamental knowledge of the multi-phase flow behaviour in the process of near-miscible CO_2-WAG displacement. In particular, we managed to identify the impacts of fine-scale heterogeneity, which are usually ignored in large-scale simulations, on actions of multi-physics involved. We identified how four key influencing mechanisms drive the sweep efficiency, local displacement performance and the distribution of the remaining oil. These physical processes include compositional effects, interfacial tension effects, gas trapping and capillary forces (wettability). With a striking development of computational power, it is now feasible to conduct a simulation-

based mechanistic study using very fine-scale models, which are required to simulate a range of key physics that are sensitive to numerical dispersion.

The main objectives of the research presented in this thesis are:

1) To capture/recognise the key physics and the corresponding modelling methods through a comprehensive literature review.
2) To assess the contribution of the mass transfer process to the improved oil recovery and how it interacts with the typical flow regimes i.e. fingering and channelling.
3) To properly reflect the interfacial-tension effect in flow simulations and investigate how it influences the microscopic and macroscopic displacement efficiency.
4) To explicitly evaluate the contribution of viscous crossflow to the oil recovery.
5) To investigate the impacts of other key multiphase physics, such as the impacts of gas trapping, water hysteresis effects and capillary pressure on the displacement performance.

The fine-scale simulations presented here resolves details of flow behaviour driven by the major mechanisms occurring in near-miscible CO_2 WAG displacements. This detailed analysis based on fine-scale models unavoidably entails a high computational cost. The average CPU time for a 2D WAG case is up to two weeks. In fact, some methods have been developed for upscaling compositional simulations such as Li and Durlofsky (2016), who managed to produce reasonable agreement between small-scale example simulations (Δx=20 feet) and their upscaled work. However, no one has yet developed a procedure for satisfactorily upscaling from the very fine scales (Δx=0.05m) studied in this thesis to reservoir scale. The impacts of the fine-scale effects can be significant and should be properly addressed when moving up to larger scales, such as simulating field-scale CO_2-EOR processes. Therefore, we would like to kindly invite and encourage other researchers to test various upscaling methods for simulations presented in this work. The complete dataset and results of this study are available online as a model case example for compositional multi-phase flows in heterogeneous systems. DOI is 10.17861/fc1c90bb-9d3f-4a6c-9170-7b7fe10ec7b9.

1.3 Synthesis and Novel Achievements

The analysis of ***immiscible*** WAG displacement was usually focused on multi-phase flow functions, such as the 3PRP model, IFT effects and hysteresis effects, but rarely incorporated a dynamic mass transfer process. On the other hand, the analysis of ***miscible***

gas displacement was mostly based on the assumption of first-contact miscibility, with neither account of the mass transfer process nor 3PRP flow functions. As aforementioned, near-miscible CO_2-WAG involves both strong mass transfer and complex multi-phase behaviour, and this requires a more rigorous synthesis.

In a near-miscible CO_2-WAG displacement, there are two factors that improve displacement efficiency significantly, i.e. compositional effects (denoted as M_{CE} here) and interfacial tension effects (denoted as M_{IFT} here). As seen in Figure 1-1, a new synthesis incorporating both compositional effects (thermodynamic phase behaviour) and IFT effects (3PRP flow functions) is formed to improve the numerical simulations of near-miscible CO_2-WAG displacements. With this new synthesis, a range of key physics was investigated to fill in the gap of fundamental knowledge in the transition from immiscible to miscible displacement. Here are the main novelties and contributions of this thesis.

1) For the first time, a fully converged fine-scale model based on the new synthesis was developed to provide a reliable and consistent test bed for a range of key physics considered here. The fine-scale simulation results presented here, which resolve the full details of multi-phase flow behaviour, can be used as *input* for any potential upscaling methods for large-scale simulations of near-miscible process.
2) This thesis clearly demonstrates that fine-scale effects are important, and therefore should not be ignored in full-filed simulations. Ideally, these small-scale effects should be upscaled in stages for full-field simulations. However, no one has yet upscaled from the scale studied in this thesis to full field simulation (Pickup *et al.*, 2005). We argued that a few small-scale simulations might be better than one, probably inaccurate, large-scale one. Therefore, the results achieved from these small-scale simulations provide useful insights and estimations on the reservoir behaviour, which are typically dismissed in industry.
3) A pseudo-tracer analysis was successfully designed and conducted in a full-compositional model. I managed to correlate the tracer distribution and the extent of viscous crossflow on the oil recovery explicitly. Very importantly, it can now be ascertained that the contributions and the obstacles of multiple mechanisms involved in near-miscible CO_2 WAG process to the bypassed oil recovery.
4) The modelling of IFT effects in CMG/GEM was originally based on the work of Betté *et al.* (1991). It is identified that the current model does not have a proper

treatment on the residual oil saturation. Therefore, my supervisors and I have made formal recommendations to CMG to adapt the model of Coats (1980), which has been coded and will be presented in a future version of CMG/GEM.

5) A detailed and thorough analysis was conducted to assess and evaluate how different mechanisms (compositional effects, IFT effects, gas trapping and capillarity) work in different parts of a reservoir model (preferential and non-preferential routes), and for different processes (continuous CO_2 injection and WAG) at different conditions (immiscible and near miscible).

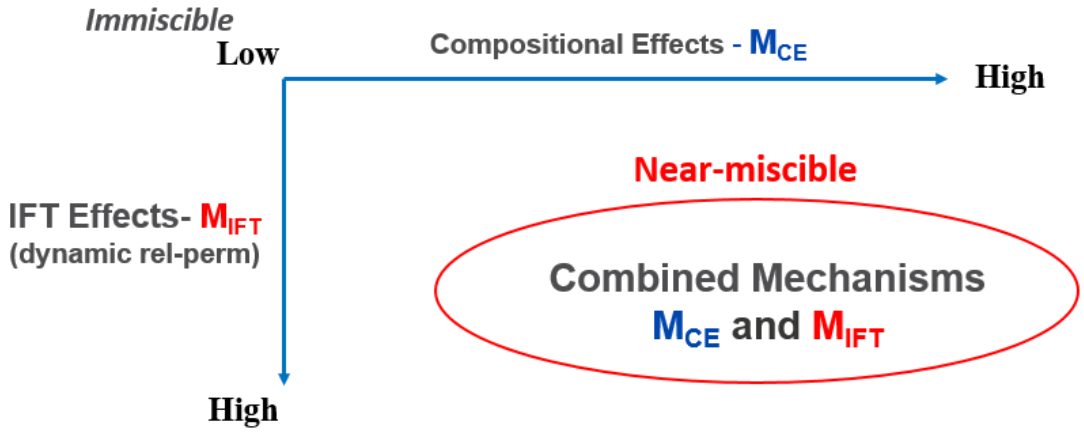

Figure 1-1 Schematic of a new synthesis incorporating with two key mechanistic processes.

1.4 Thesis outline

The theme of this thesis essentially reflects a development of an effective methodology to analyse the flow behaviour involving multi-phase (from 2-phase to 3-phase) and multi-physics (from single to multiple) in multi-dimensional systems (from 1D to 2D). With a building-up strategy, this thesis is organised as follows:

In **Chapter 2**, a comprehensive literature review is presented to demonstrate the key physics occurring during CO_2-WAG, such as compositional effects, IFT effects and hysteresis effects.

In **Chapter 3,** the mass transfer process was investigated during near miscible and immiscible CO_2-oil displacements. Because of mass transfer, the changed saturations and properties of the flowing phases can have a great impact on the issues of front stability, local displacement efficiency, and formation of fingering/channelling in specific

heterogeneous systems. The results of this chapter provided a baseline for other physics to build on in the following chapters.

In **Chapter 4,** the new synthesis as aforementioned was developed. Various combinations between oil-stripping effects and IFT effects were tested to evaluate the impacts of each mechanism (M_{CE} and M_{IFT}) on the flow behaviour, i.e. their separate and joint effects on quantities such as the local displacement efficiency, phase flow vectors and the ultimate oil recovery. ***Viscous crossflow,*** which is well recognised during polymer flooding (Sorbie, 2013), was explicitly evaluated here and found to be also a major recovery mechanism in near-miscible WAG displacement. Very importantly, such mechanism, which is the key to recovering the bypassed oil, can be only captured based on the new synthesis developed here.

In **Chapter 5**, a range of other important physics including gas trapping, water hysteresis and capillary pressure were analysed based on the new synthesis. The positive or negative effects on the oil recovery in near-miscible WAG process have been ascertained following a systematic sensitivity analysis.

In **Chapter 6,** main conclusions of this study are presented. In addition, this chapter provides suggestions for future work, such as using 3D models to include gravity effect or incorporating geological structures of interest (e.g. fault and fractures).

Chapter 2 Theoretical Background

2.1 Introduction

Although CO_2-WAG has been successfully applied in the oil industry over the last few decades, it is still a challenging task to properly simulate and investigate such a process. One of the main reasons is the complexity induced by the interactions of multiple physical processes, particularly at near-miscible conditions. Therefore, a full understanding of the physical processes during CO_2-WAG injection is the first step to make reliable predictions on the flow behaviour and the oil recovery.

In this chapter, a comprehensive review of the literature was conducted to capture the major flow physics/mechanisms occurring in a CO_2 displacement, with a particular interest in the transition from immiscible to miscible conditions. A range of key papers on CO_2 displacements is presented here with an aim to provide the theoretical background and define the scope of this research. The modelling methods of multi-phase flow, particularly those that have been incorporated in CMG/GEM (CMG, 2019), are demonstrated in detail to explain the underlying theory of the tool for this study. Starting with an introduction of CO_2 characteristics (Section 2.2), this chapter includes a detailed demonstration of compositional effects (Section 2.3), methods of fluid modelling (Section 2.4), multi-phase flow functions (Section 2.5), and typical flow regimes such as fingering and channelling (Section 2.6).

2.2 CO_2 characteristics

There are several characteristics, which make CO_2 an effective displacing solvent, superior to others. Since reservoir conditions are often above the critical conditions of CO_2 (73.9 KPa and 31.1 °C), the injected supercritical CO_2 is of a liquid-like density, which is much greater than other typical solvents such as methane and nitrogen (Holstein *et al.*, 2007). Therefore, the displacement performance is possibly less affected by the issue of gravity segregation using CO_2 injection than other gases. Secondly, the great solubility of CO_2 in oil is another favourable feature to recover oil. This is because the oil viscosity can be reduced by the dissolved CO_2 (Barclay and Mishra, 2016). In fact, this is one of the key reasons that even immiscible CO_2 flood can still improve the oil recovery and be applied in heavy oil reservoirs (Chung *et al.*, 1988). At the same time, the dissolution of CO_2 in crude oil could also possibly lead to oil swelling, which can

push oil out of dead end pores and helps oil production (Whitson and Brulé, 2000). In addition, the residual oil situation to gas is generally lower than the residual oil saturation to water (Lake *et al.*, 2014). For this reason, the displacement efficiency in the zone swept by gas will be greater than in a water-swept area.

2.3 Miscible displacement

2.3.1 Multiple-contact miscibility

Besides the mechanisms of pressure support, lowering oil viscosity and swelling the oil as mentioned above, the main objective of injecting CO_2 is to develop the miscibility between CO_2 and crude oil. Ideally, the displacement efficiency in a miscible displacement can be 100% in the swept zone. As mentioned in Chapter 1, there are two types of miscibility between oil and the injected solvent, i.e. first contact or multiple contacts. First-contact miscibility (FCM) suggests that the injected solvent can mix with reservoir oil instantly at the first contact in all proportions without forming any interface (Stalkup, 1983). Theoretically, first-contact miscibility may be achieved in a highly rich gas flood or in a CO_2-oil system at very high pressure. However, it is barely economical, and sometimes not technically feasible, to achieve FCM with the oil (Al-Wahaibi, 2010).

On the other hand, the in-situ oil and the injected CO_2 can also develop a dynamic miscibility through multiple stages of component transfer, namely multiple-contact miscibility (MCM). Many laboratory experiments investigating MCM displacement have been carried out since the 1970s. Rathmell *et al.* (1971) presented the development process of the multiple-contact miscibility in CO_2-oil systems with ternary phase diagrams. They found that CO_2 is progressively enriched with oil components to achieve miscibility with the in-situ oil. Their results showed that the local displacement efficiency of a CO_2 flood is highly dependent on the mass transfer process, which can be reflected by the composition path.

Holm and Josendal (1974) discussed and summarized the various mechanisms occurring in CO_2-oil systems. They claimed that CO_2 enhances the oil recovery most efficiently by stripping of hydrocarbons. In other words, the oil components are recovered in the vapour phase due to the strong stripping effects. At the same time, the procedures of slim-tube tests applied in their study became established. Therefore, their methods have been generally used to measure the minimum miscible pressure (MMP) since then. They also investigated the effect of oil constituents on achieving miscibility between CO_2 and oil

(Holm and Josendal, 1982). They found that gasoline-range hydrocarbons in the oil are particularly efficient in achieving miscibility.

Orr *et al.* (1983) designed continuous multiple-contact (CMC) tests (essentially a multiple mixing vessel) to measure the details of phase compositions and phase properties. They showed that most of the oil components were stripped from the liquid phase if the pressure is sufficiently high. Based on the comparisons between CMC tests and slim-tube tests, they highlighted the roles of phase behaviour and volume change on mixing in the slim-tube tests.

Yang and Gu (2004) visualized the interaction between CO_2 and oil by using axisymmetric drop shape analysis and reported the phenomena such as the gradually disappearing phase interface with contact time and the presence of asphaltene precipitations during the later stage of mass transfer, due to the fact that light components have been preferentially stripped out. In a most recent study, Rezk and Foroozesh (2019) investigated the time taken for a certain CO_2-oil system to be equilibrated and the impact of such mass-transfer process on the oil properties (such as viscosity).

To summarise, MCM in a CO_2-oil system can be achieved through a set of component exchanges between the oil phase and the vapour phase. The improved displacement performance is a combined outcome of both condensing and vaporising (stripping effects) mechanisms. Note the focus of this thesis is the near-miscible displacement, where a true miscibility is not achieved. However, it is highly necessary to fully understand and capture the process of mass transfer. This is because the mass transfer process can possibly lead to dramatic changes of saturations and properties of flowing phases, which may have a great impact on the flow behaviour. Very importantly, according to Danesh (1998), such thermodynamic phase behaviour occurs most significantly under a pressure near MMP, i.e. at near-miscible conditions (my simulations also reproduced/confirmed this issue). Therefore, a detailed demonstration of MCM development led by mass transfer is presented as below.

2.3.2 Mass transfer with forward contacts- miscibility development

According to Stalkup (1983), hundreds of oil components can be found in an in-situ oil. However, to describe a MCM development, it is a common practice to classify fluid components into three simplified groups, i.e. CO_2, extractable hydrocarbons (light-

medium components) and heavy hydrocarbons, and to use a ternary diagram to demonstrate the mass transfer process (Figure 2-1). Therefore, the reservoir fluid can be treated as a three-component mixture, whose compositions can be reflected by the position in this ternary diagram. Each corner of a ternary diagram represents a 100% mole fraction of the aforementioned simplified component. The closer to one corner, the greater fraction of this component in the fluid. For instance, the point of an example oil M represents a mixture consisting of 55% heavy hydrocarbons, 45% light hydrocarbons and 0% CO_2.

The envelope, denoted by ABC, represents a two-phase region (pre-defined by experiments in practice) whereas outside this envelop is a single-phase region. Any mixture within the two phase region will form a vapour and a liquid phase eventually in equilibrium (Danesh, 1998). The resulting gas and oil composition will fall on the envelope boundary.

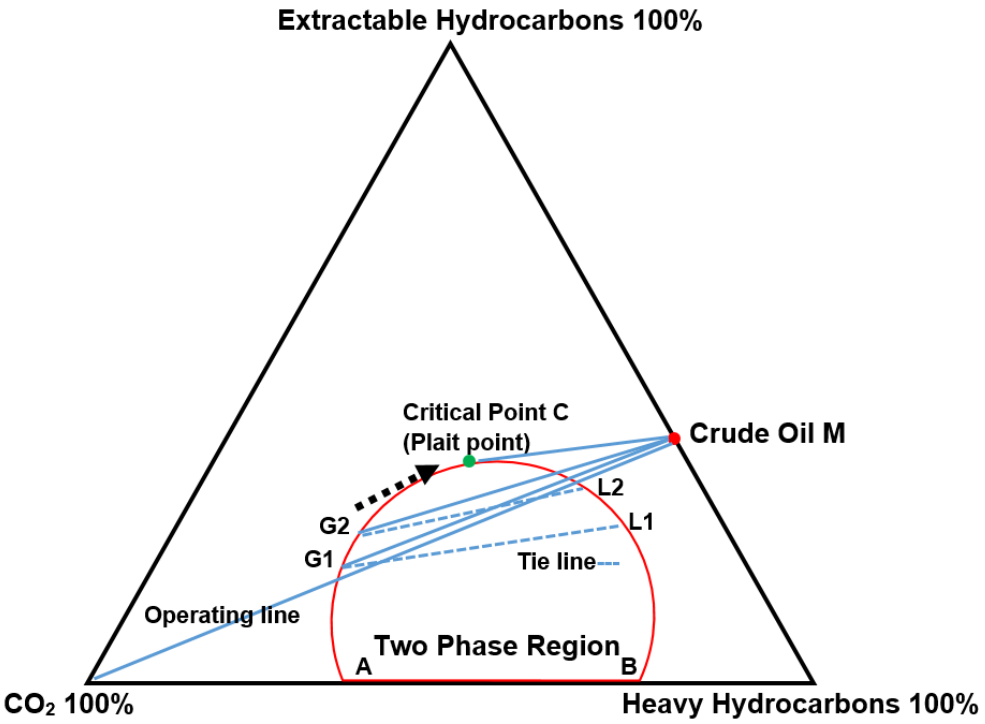

Figure 2-1 Conceptual phase behaviour of simple hydrocarbons in forward-contact process (Danesh, 1998).

Figure 2-1 shows an example assuming that pure CO_2 is injected to develop MCM with an example oil M. Since the connecting line of oil and CO_2 intersects the two-phase region, they are not miscible initially but will be later through mass transfer. At the first

contact, light oil components are extracted whereas CO_2 is dissolved into oil, forming the new gas (G1) and the new liquid (L1). The consequent compositions of G1 and L1 are dependent on the tie line, which the connecting line of oil and CO_2 intercepts. A tie-line (pre-defined in practice) is a straight line in the two-phase region joining an equilibrium-vapour composition with its equilibrium-liquid composition (Whitson and Brulé, 2000). Any system with an overall composition lying on this tie line will split into the same pair of equilibrated liquid and vapour compositions. Therefore, in this particular case, G1 and L1 are formed because of the first contact of CO_2 and oil. Then, this new vapour phase (G1) keeps flowing forward and contact with the fresh oil. At the second contact, gas G2 and liquid L2 are formed respectively, and their compositions are getting closer to the critical point. The critical point is the position where the connecting line with the fresh oil is tangent to the two-phase region (i.e. starting to form single phase). With continuous contacts afterwards, the composition of the resulting gas will eventually reach the critical point and become miscible with fresh oil at the displacing front.

In this ternary diagram, miscibility is achieved when the line joining the initial oil composition and the injected gas lies above the critical point. Therefore, the success of the miscibility depends on the fact that size of the two-phase region is sufficiently small. According to Danesh (1998), the area of two-phase region shrinks with increasing pressure. As another way of seeing this concept, MMP is the condition where the tangent line of the two-phase envelop at the critical point just goes through the initial oil composition.

The key influencing factors of MMP are reservoir temperature, purity of solvent (CO_2 fraction) and crude oil composition (Stalkup, 1983). MMP increases with temperature due to the fact that two-phase region expands with temperature. Compared with other gases, CO_2 has the lowest MMP. In other words, impurities (such as N_2 and CH_4) will increase the MMP of the system. As for the oil composition, the more light-to-intermediate components (C5 to C12) contained in the oil, the lower the MMP will be (Yellig and Metcalfe, 1980).

Note such classification of immiscible and miscible displacement is simply to distinguish if true miscibility is achieved or not. However, one should not confuse with the fact that the compositional effects, occur at almost all conditions in a CO_2-oil system. This is because, whether miscibility is achieved or not, the process of mass transfer (vaporization

and condensation) between vapour and liquid phase still happens in a CO_2-oil system, as long as it is not under thermodynamic equilibrium. The closer to MMP in a CO_2-oil system, the greater mass transfer should occur (Danesh, 1998). Therefore, it is more of a matter how significant the compositional effects are in terms of classification between the immiscible (well below MMP with minor/negligible compositional effects) and near-miscible displacement (close to MMP with strong compositional effects).

2.3.3 Mass transfer with backward contacts- oil stripping effects

It has been demonstrated how MCM in a CO_2-oil system is achieved at the displacing front through forward contacts occurring along the direction of flow. At the same time, there is also a significant mass transfer process due to the backward contacts occurring at the displacing trail (Whitson and Brulé, 2000). Interestingly, the remaining oil compositions will become increasingly heavier at the displacing trail. This is because the light-to-medium components have been mostly vaporised, namely stripping effects. Here a theoretical demonstration of the process is presented.

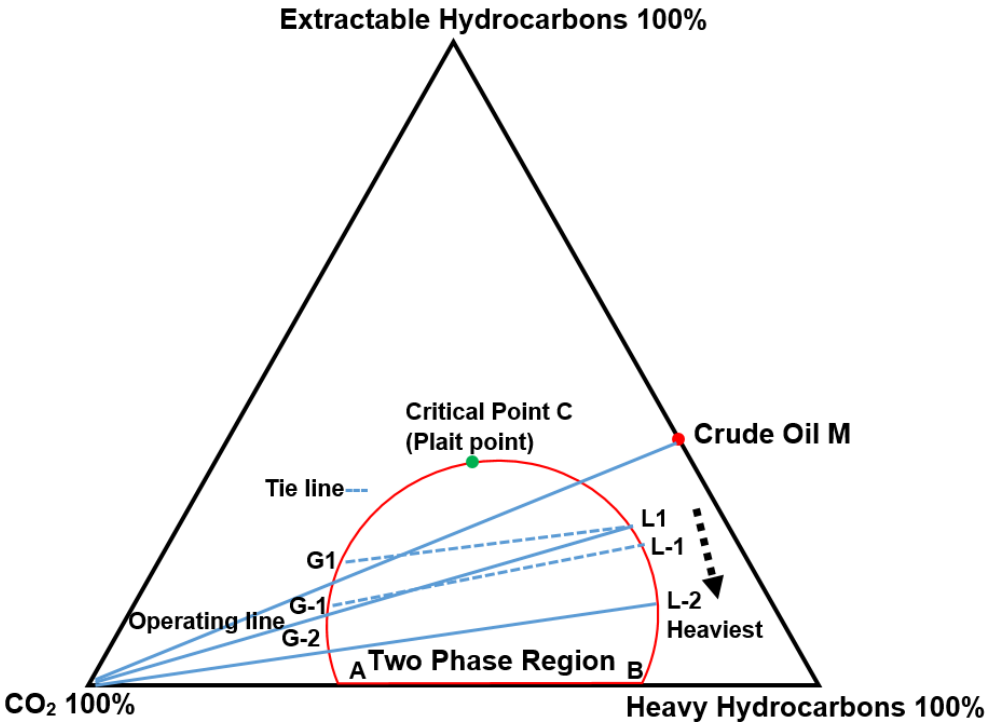

Figure 2-2 Conceptual phase behaviour of simple hydrocarbons in backward-contact process (Danesh, 1998).

As seen in Figure 2-2, which is modified from the work by Danesh (1998), the ternary diagram is used to demonstrate the stripping effects. After the first contact between oil and CO_2, the consequent gas (G1) will move forward to contact fresh oil (demonstrated

in Section 2.3.3) whereas the resulting liquid (L1) will further contact newly arrived CO_2. The light-medium components in L1 will be stripped into the vapour phase. As a result, L-1 and G-1 are formed respectively at equilibrium. The outcome of next round of contact between L-1 and CO_2 will then be L-2 and G-2. With a continuous process of stripping out, only heavy components left behind in the liquid phase. Note that although miscibility inevitably disappears due to the increasingly heavier liquid phase, the overall displacement performance can still be improved by stripping effects. This is because the oil components are now recovered in the vapour phase, which generally has a greater mobility than the liquid. In fact, this is one of two major mechanisms (together with IFT effects) that even near-miscible displacement can recover the oil efficiently. Here such stripping/compositional effects, which can be significant at near-miscible conditions, are denoted as M_{CE} (the Mechanism of Compositional Effects).

Although ternary diagram is very useful to demonstrate the process of component transfer, one of the important thermodynamic phase behaviour i.e. heavy components are left behind, will be missed in a 3-component system. Figure 2-1 and Figure 2-2 are depicted here to qualitatively describe the process of mass transfer, i.e. CO_2 condensation (dissolution) and oil stripping (vaporization). In fact, a seven-component system is used in this research to capture such complex thermodynamic phase behaviour involved in the oil displacement by CO_2. A further discussion on the process of component can be found in Chapter 3.

2.4 Fluid modelling

2.4.1 Black-oil model

Now the question is how to reflect such phase behaviour in a reservoir simulation. There are currently two main methods of fluid modelling, i.e. the black-oil model and compositional models. The key difference between these two models is the way of determining the fluid state/properties of each grid cell in a simulation. A black oil model entails simple interpolation of PVT properties, such as oil formation volume factor (B_o) and the gas solution ratio (R_s), to represent the phase behaviour as a function of pressure (Lake *et al.*, 2014). B_o is the ratio of the volume of oil at reservoir conditions to that at stock tank conditions. R_s is defined as the amount of gas dissolved in the oil (or water) at any pressure. Typically, if an oil has a R_s less than 750scf/stb and a B_o less than 1.4bbl/stb, this system can be simulated using black-oil model (Cao, 2002).

2.4.2 Compositional model

On the other hand, a compositional model entails using a range of thermodynamic functions, namely an equation of state (EOS), to describe complex phase behaviour. In a compositional simulator, the overall fluid compositions in each grid cell are used to calculate the equilibrated fluid state, i.e. flash calculations. At each time step, a set of flash calculations using an EOS is performed to determine the equilibrated fluid state. According to Orr (2007), the equilibrated fluid state suggests a minimum Gibbs free energy, which leads to the fact that the partial fugacity of any component (i) in the vapour phase (f_{iV}) should be equal to its partial fugacity in the liquid phase (f_{iL}). The component fugacity in a mixture is defined as the products of its partial pressure and the fugacity coefficient (Equation 2-2).

$$f_{iL} = f_{iV} \qquad \text{Equation 2-1}$$

$$f_i = P_i \times \varphi_i \qquad \text{Equation 2-2}$$

$$\ln \varphi_i = \int_0^P (\overline{Z}_\iota - 1) \frac{dP}{P} \qquad \text{Equation 2-3}$$

where f_i is the fugacity of a component in a mixture; φ_i is the fugacity coefficient and $\overline{Z}_\iota$ is the partial molar compressibility factor which can be calculated using an EOS. The acquired fluid state such as the number of phases (water, oil and gas), phase saturations, component constitutions, phase properties (such as density), and the interfacial tension (IFT) between phases will then be used to calculate the flow behaviour (Cao, 2002).

Compared with the black-oil model, a compositional simulator is more capable of modelling realistic phase behaviour accurately, especially in a CO_2-oil system that involves complex component partitioning. However, the improved accuracy of the fluid modelling is at a price of very high computational cost induced by the flash calculations. In addition, the mass transfer process in a CO_2-oil system can be very sensitive to numerical dispersion (Jessen *et al.*, 2004). In other words, any numerical analysis (based on finite-difference simulators) with the focus on the compositional effects may have to address the concerns on the size of the grid cell in the simulation. In fact, Leach and Yellig (1981) have pointed out the great necessity of using compositional simulation for CO_2 studies to properly reflect the strong phase behaviour (i.e. vaporization and

condensation). However, modelling of mass transfer was historically over-simplified, which was simply because of the limited computational power at that time (Young and Stephenson, 1983).

Here, a full-compositional simulator (CMG/GEM) based on EOS, which can consistently reflect hydrocarbon phase behaviour, was used in this study. In addition, a particular need of using compositional simulations is the appropriate IFT calculation as a function of the compositions of oil and gas. This is because the IFT could change dramatically in a near-miscible displacement and may have a huge impact on the residual oil saturation. A more extensive literature review of the IFT effects can be found in section 2.5.3.

Note that even with the striking development of computational power of today, some assumptions (such as using numerical dispersion to mimic physical dispersions) are still necessary to reduce the computational cost but do not compromise the main focus/scope of this thesis. A detailed demonstration of the set-up of numerical simulations and assumptions of this study can be seen in Section 3.3.

2.4.3 Equation of state

The earliest equation of state for Vapour-Liquid Equilibrium (VLE) calculations were found in the work of Van der Waals (1873). This method is based on a two-term semi-empirical relationship, i.e. the pressure of an equilibrated system is equal to the sum of a repulsion pressure P_R and an attraction pressure P_A between molecules. Since then, many authors have proposed various modifications to his equations to improve the prediction accuracy. In terms of the oil industry, the first application of an equation of state was developed by Soave (1972), namely the Soave-Redlich-Kwong (SRK) equation. Generally, SRK can be used to produce acceptable predictions of the vapour properties. However, one of the major shortcoming of this method is the failure to produce satisfactory density values for the liquid. Therefore, Peng and Robinson (1976) modified the SRK equations to improve the prediction of liquid phase densities, namely the PR-EOS (Equation 2-4 to Equation 2-9).

$$P = \frac{RT}{V_m - b} - \frac{a\alpha}{V_m^2 + 2bV_m - b^2} \qquad \text{Equation 2-4}$$

$$a \approx 0.45724 \frac{R^2 T_c^2}{P_c} \qquad \text{Equation 2-5}$$

$$b \approx 0.07780 \frac{R^2 T_c^2}{P_c} \quad \text{Equation 2-6}$$

$$\alpha = (1 + \kappa(1 - T_r^{0.5}))^2 \quad \text{Equation 2-7}$$

$$\kappa \approx 0.37464 + 1.54226\omega - 0.26992\omega^2 \quad \text{Equation 2-8}$$

$$T_r = \frac{T}{T_c} \quad \text{Equation 2-9}$$

where M_w is molar weight; T_c is critical temperature; P_c is critical pressure; R is the universal gas constant; V_m is the molar volume; ω is acentric factor.

Due to its relative simplicity and improved accuracy, the PR-EOS has achieved a wide acceptance of the industry and has been coded in the simulators of CMG/GEM (CMG, 2017) and E300 (Schlumberger, 2015). In fact, numerous EOS have been developed today, such as the correlations proposed by Elliott *et al.* (1990), to further improve the prediction accuracy. However, there is no single EOS universally applicable to predict the fluid properties of all substances under all conditions. Since PR-EOS has a relatively good track-record of providing reliable predictions of phase behaviour in a CO_2-oil system (Jhaveri and Youngren, 1988; Orr, 2007), the PR-EOS is therefore selected here.

2.5 Fundamentals of multiphase flow functions

2.5.1 Concept of relative permeability

Reservoir simulations, which are based on the fundamental principles of mass conservation and Darcy's law, are a useful a tool to describe the flow process in porous media. Mass conservation reflects the fact that the net accumulation of mass of the unit volume must equal the net flux over the boundaries, as specified by Equation 2-10. Since mass transfer occurs in compositional flow, the total mass of each component must be also conserved.

$$\frac{\partial(\rho\emptyset)}{\partial t} + \nabla \cdot (\rho\vec{v}) = \rho q, \quad \text{Equation 2-10}$$

$$\partial_t[\emptyset(x_i\xi_o S_o + y_i\xi_g S_g)] + \partial_t[\emptyset(x_i\xi_g S_g + y_i\xi_o S_o)] = x_i q_o + y_i q_g \quad \text{Equation 2-11}$$

where ρ is the density of the fluid; $\emptyset$ is the rock porosity; $\vec{v}$ is the flow velocity; ∂_t denotes times differentiation; g, o and w refer to gas, oil, and water phases; x_i and y_i denote the mole fractions of the component "i" in the gas and oil phases; ξ_g and ξ_o are

the molar densities of gas and oil; S_g and S_o are saturations of gas and oil; q denotes the outflow and inflow of fluids.

With the fluid state and properties calculated based on an EOS (PR-EOS here), the phase fluxes within the reservoir are then determined by Darcy's law. The theory of flow in the porous media is derived from the work of Darcy, who proposed an equation to describe the water flow through a vertical sand pack, i.e. Darcy's Law. Muskat (1949) developed an extensional form of Darcy's Law to fit the needs of petroleum industry. With the account of all three driving forces (viscous, capillary and gravity), a dimensionless parameter, relative permeability ($k_{r\alpha}$), is introduced to reflect the fact that the flow of each phase, α, is inhibited by the other phase(s) in a multiphase system (Equation 2-12). Relative permeability is defined as ratio of the effective permeability to a given fluid to the absolute permeability. This concept measures impediment to phase flow because of the co-existence of other phases.

$$q_\alpha = -\frac{k_{abs}k_{r\alpha}}{\mu_\alpha}(\nabla P_\alpha - \rho_\alpha g),\ \alpha = water, oil\ and\ gas \qquad \text{Equation 2-12}$$

where q is the volumetric fluid flux; k_{abs} is the absolute permeability; $k_{r\alpha}$is the relative permeability of each phase; μ is the dynamic viscosity of the fluid; P_α is the each phase pressure; ρ is the fluid density; g is the gravitational acceleration.

Many researchers attempted to investigate the key influencing factors of the relative permeability and to develop a sound correlation functions of relative permeabilities for the use in reservoir simulations. Rose and Bruce (1949) found that tortuosity (the ratio of the length of effective flow path to the length of core sample) has a great impact on the relative permeability. Later, Burdine (1953) derived the formula for the relationship between the tortuosity and phase saturations. Based on those works, Corey (1954) and Brooks and Corey (1964) developed a 2-phase relative permeability function which depended on saturation only. The underlying theory (channel flow theory) is that each pore is occupied by a single mobile fluid and the relative permeabilities are therefore only dependent on the mobile amount of that flowing phase. Because of its simplicity, Corey's model (Equation 2-13 to Equation 2-16) has been widely used since then.

Water-oil system

$$S_{wn} = \frac{S_w - S_{wc}}{1 - S_{wc} - S_{orw}} \quad \text{Equation 2-13}$$

$$S_{own} = \frac{S_o - S_{orw}}{1 - S_{wc} - S_{orw}} \quad \text{Equation 2-14}$$

$$K_{rw}(S_w) = K_{rwiro} S_{wn}^{N_w} \quad \text{Equation 2-15}$$

$$K_{row}(S_o) = K_{rocw} S_{own}^{N_{ow}} \quad \text{Equation 2-16}$$

where S_{wn} and S_{on} are normalised water and oil saturations to represent the fraction of mobile phase; N_w and N_{ow} are curve shape factors which are dependent on the distribution of pore sizes; K_{rwiro} and K_{rocw} are water and oil relative permeability at end-points respectively (i.e. maximum values of relative permeabilities respectively); S_{wc} is connate water saturation; S_{orw} is the residual oil saturation to water.

Similarly, such correlations shown above can be used for an immiscible gas-oil system (Equation 2-17 to Equation 2-20). Note that the gas-oil system may involve low-interfacial tension effects at near-miscible conditions, which can change both the shape and end-points (residual oil saturation) of the curves of relative permeabilities. A detailed demonstration on IFT effects is presented in Section 2.5.3.

Gas-oil system (immiscible)

$$S_{gn} = \frac{S_g - S_{gc}}{1 - S_{wc} - S_{org} - S_{gc}} \quad \text{Equation 2-17}$$

$$S_{ogn} = \frac{S_o - S_{org}}{1 - S_{wc} - S_{org}} \quad \text{Equation 2-18}$$

$$K_{rg}(S_g) = K_{rgcl} S_{wn}^{N_g} \quad \text{Equation 2-19}$$

$$K_{rog}(S_o) = K_{rogcg} S_{ogn}^{N_{og}} \quad \text{Equation 2-20}$$

where S_{gn} and S_{ogn} are normalised gas and oil saturations to represent the fraction of mobile phase; N_g and N_{og} are curve shape factors; K_{rgcl} and K_{rogcg} are gas and oil relative permeability at end-points respectively (i.e. maximum values of relative permeabilities respectively); S_{gc} is critical gas saturation; S_{org} is the residual oil saturation to gas.

Typically, all the above parameters are determined through conducting a set of core flood tests, at either steady state (uniform fluid saturations at any cross section perpendicular to the flow direction) or unsteady state (Lake *et al.*, 2014). No matter which method is used, the key concern of determining relative permeabilities is that the experiments should reproduce the initial reservoir conditions and correctly reflect the saturation change in the reservoir. For example, the test of water-oil imbibition (increasing wetting-phase saturation, water) should be used to describe the oil displacement by water (water flooding). On the other hand, the test of gas-oil drainage (decreasing wetting phase saturation, oil) should be used to describe the oil displacement by gas.

In this study, I assumed a water-wet system with water-oil (imbibition) and gas-oil (drainage) relative permeabilities, which were provided by one of our sponsors.

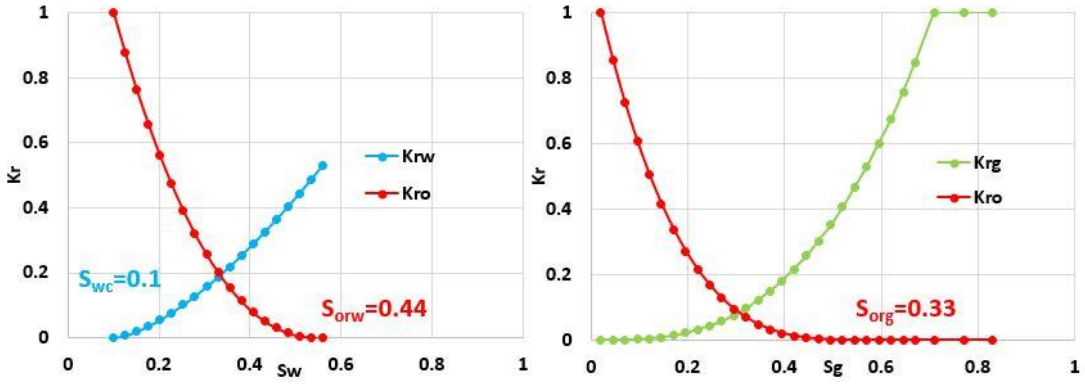

Figure 2-3 Oil-water and gas-oil relative permeability curves.

2.5.2 3-phase relative permeability

The simultaneous flow of three phases may occur in various circumstances in hydrocarbon reservoirs, such as the WAG injection, which is often applied for the oil displacement by CO_2. For this reason, an estimate or measurement of 3-phase relative permeabilities (3PRP) is mandatory for the numerical simulations. Ideally, such 3PRP data should be determined through conducting laboratory experiments, i.e. core flood displacements. However, the laboratory measurement of 3PRP is prohibitively difficult, expensive and impractical (Blunt, 2000). Unlike the phase saturations changing in a simple path (one phase saturation increases and the other phase must decrease) during a two-phase displacement test, any three-phase displacement test involves two independent phase saturations, which leads to an infinite number of different displacement paths. For instance, the increase of gas does not necessarily lead to a simultaneous decrease of both

oil and water in a fixed manner. Therefore, it is a common practice to estimate three-phase relative permeabilities from two-phase data using an empirical correlation method. Currently, there are three main methods of empirical 3PRP models i.e. Stone 1 (Stone, 1970) and Stone 2 (Stone, 1973) and saturation-weighted model (Baker, 1988), which have been widely coded in commercial software packages, such as CMG (CMG, 2017) and Eclipse (Schlumberger, 2015).

Stone (1970) proposed his first empirical model to predict oil relative permeability, i.e. Stone 1. This method entails an extrapolation of two-phase relative permeability data for K_{ro} in three-phase applications. This is based on an underlying assumption that the water is the most wetting phase whereas gas is the least wetting phase, i.e. a strongly water-wetting condition. In other words, water and gas will always seek to occupy the smallest and largest pores respectively. For this reason, both K_{rg} and K_{rw} are the same between 2-phase and 3-phase system and are only dependent on their own saturation respectively. On the other hand, the oil occupies the rest of pores (i.e. intermediate-size) and is dependent on both water and gas saturation.

One of the potential advantages of this model is that the 3-phase residual oil saturation (S_{om}) is a function of gas saturation rather than a constant value. Fayers and Matthews (1984) claimed that a linear function should be sufficient to reflect the fact that the 3-phase residual oil in most immiscible systems is between S_{orw} and S_{org}. The normalized version of Stone 1 proposed by Aziz and Settari (1979), which has been generally used in commercial simulators, is presented below (Equation 2-21 to Equation 2-28). In addition, the oil isoperm in a ternary diagram based on the two-phase data of Figure 2-3, is plotted in Figure 2-4 using Matlab codes (Theune, 2018).

$$S_{om} = \alpha S_{orw} + (1-\alpha) S_{org} \qquad \text{Equation 2-21}$$

$$\alpha = 1 - \frac{S_g}{1 - S_{wc} - S_{org}} \qquad \text{Equation 2-22}$$

$$S_w^* = \frac{S_w - S_{wc}}{1 - S_{wc} - S_{om}} \qquad \text{Equation 2-23}$$

$$S_g^* = \frac{S_g - S_{gc}}{1 - S_{wc} - S_{om}} \qquad \text{Equation 2-24}$$

$$S_o^* = \frac{S_o - S_{om}}{1 - S_{wc} - S_{om}} \quad \text{Equation 2-25}$$

$$\beta_w = \frac{K_{row}(S_w)/K_{rocw}}{1 - S_w^*} \quad \text{Equation 2-26}$$

$$\beta_g = \frac{K_{rog}(S_g)/K_{rocw}}{1 - S_g^*} \quad \text{Equation 2-27}$$

$$K_{ro} = K_{rocw} S_o^* \beta_w \beta_g \quad \text{Equation 2-28}$$

where S_{om} is 3-phase residual oil saturation; S_w^*, S_o^* and S_g^* are normalised water, oil and gas saturations; β_w and β_g are factors account for the decrease in K_{ro} due to the presence of water and gas respectively.

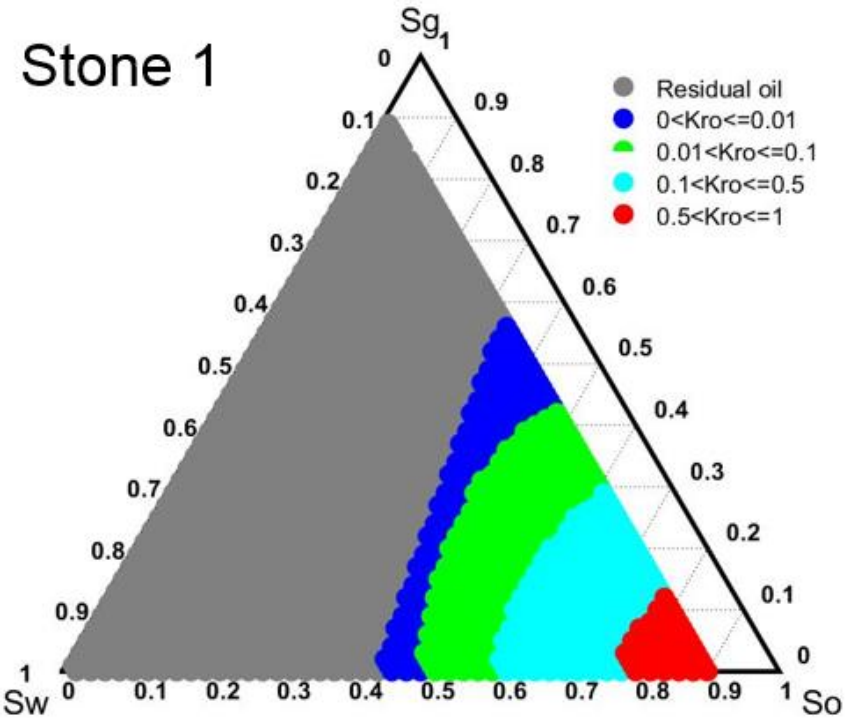

Figure 2-4 Three-phase oil isoperms predicted Stone 1 model.

Later, Stone (1973) proposed his second model, Stone 2, with the aim to improve the prediction accuracy of the 3PRP oil relative permeability. In addition to the different 3PRP function for oil relative permeability (Equation 2-29), the 3-phase residual oil saturation (S_{om}) is not required in Stone 2. Here the oil isoperm in a ternary diagram using Stone 2 is presented in Figure 2-5.

$$K_{ro} = K_{rocw}[\left(\frac{K_{row}}{K_{rocw}} + K_{rw}\right)\left(\frac{K_{rog}}{K_{rocw}} + K_{rg}\right) - (K_{rw} + K_{rg})] \qquad \text{Equation 2-29}$$

where K_{rocw} is oil relative permeability at the connate water saturation.

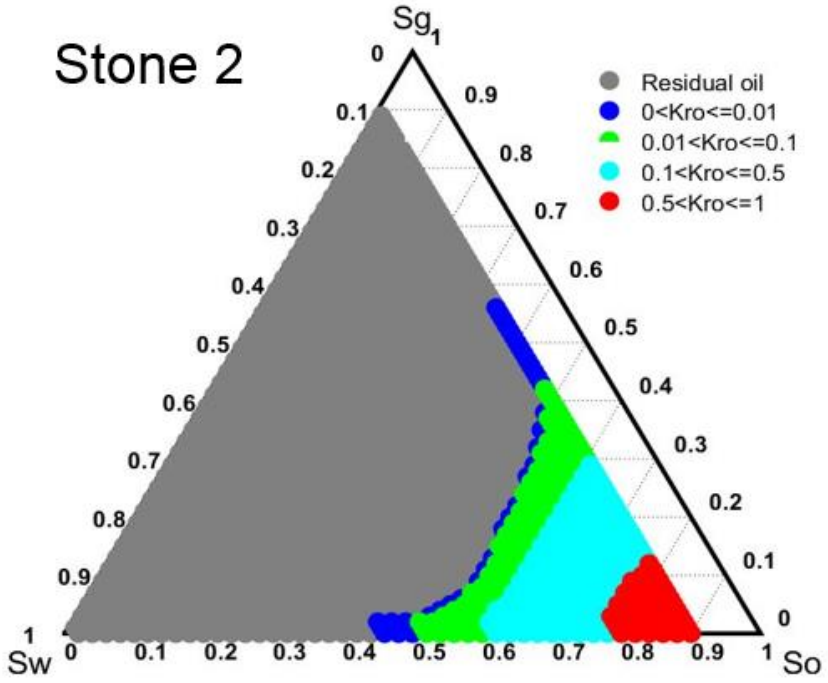

Figure 2-5 Three-phase oil isoperms predicted Stone 2 model.

Baker (1988) made a thorough review of the 3PRP model, which had been published at that time. In order to improve the fit to experimental results, he proposed the saturation–weighted method to predict 3PRP. One of the key features of this method is to release one of the important assumptions that K_{rw} is same in oil-water and gas-water systems or Krg is same in gas-oil and gas-water systems. Therefore, a separate set of gas-water relative permeability data is required for this model. The advantage of this treatment is to address the concerns over the complex wetting order in systems not being strongly water wet, i.e. water and gas not being the most wetting and non-wetting phase. This model has been implemented in Eclipse as the default method to calculate 3PRP (Schlumberger, 2015). Here the oil isoperm in a ternary diagram using the saturation-weighted model is presented in Figure 2-6.

$$K_{ro} = \frac{(S_w - S_{wc})K_{row} + (S_g - S_{gc})K_{rog}}{(S_w - S_{wc}) + (S_g - S_{gc})} \qquad \text{Equation 2-30}$$

$$K_{rw} = \frac{(S_o - S_{orw})K_{rwo} + (S_g - S_{gc})K_{rwg}}{(S_o - S_{orw}) + (S_g - S_{gc})} \quad \text{Equation 2-31}$$

$$K_{rg} = \frac{(S_o - S_{org})K_{rgo} + (S_w - S_{wc})K_{rgw}}{(S_o - S_{org}) + (S_w - S_{wc})} \quad \text{Equation 2-32}$$

where K_{rwg} and K_{rgw} are water and gas relative permeabilities in the gas-water system. Note that neither K_{rwg} nor K_{rgw} is available in this study and therefore they were assumed to be same as K_{rwo} and K_{rgo} respectively.

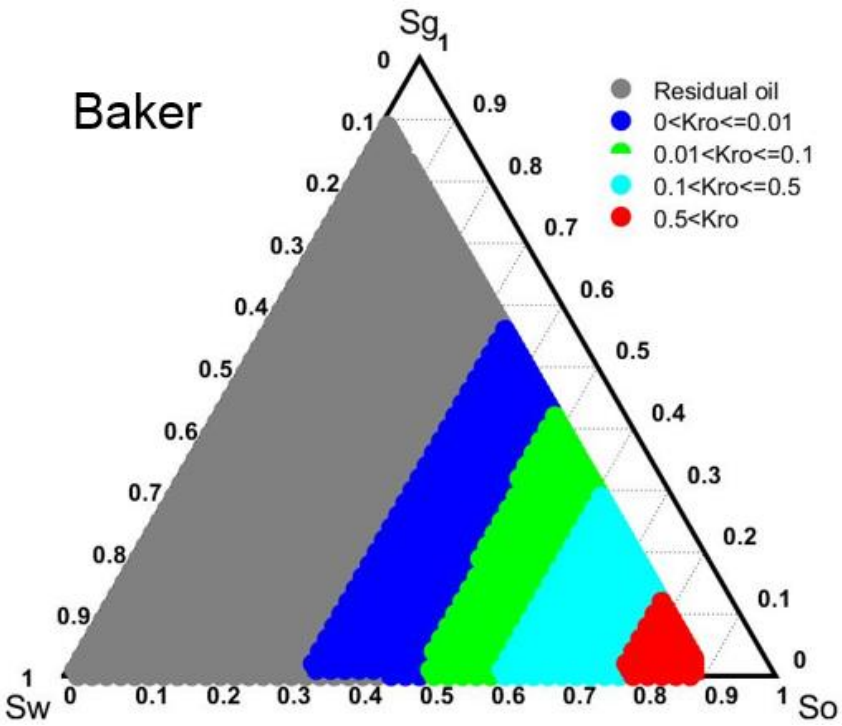

Figure 2-6 Three-phase oil isoperms predicted Baker's saturation-weighted model.

Due to the importance of 3PRP for the prediction of flow behaviour, all three models have been widely tested in literature. It has been argued that none of them is able to guarantee a consistent accuracy of 3PRP predictions. In fact, many papers have presented contradictory conclusions with each other. Delshad and Pope (1989) managed to compare the prediction accuracy of a range of 3PRP models, based on three-phase experimental data obtained in Berea sandstone core samples. They claimed that Stone's models failed to predict the experimental data whereas Baker's methods generally provided a better fit to the data available at that time.

Blunt (2000) found that Baker's saturation-weighted method produced poor predictions at low oil saturations. He claimed that this was because layer drainage (oil layers formed between water and gas) can be significant in 3-phase system, which leads to an increase in the oil relative permeability. According to Spiteri and Juanes (2006), the method of Stone 2 could severely underestimate the oil relative permeability. In a most recent study, Bourgeois *et al.* (2019) improved the prediction of 3PRP during WAG in both water-wet and oil-wet systems using the Stone 1 model. They modified the model by Larsen and Skauge (1998) through adding a separate parameter (C_w) to account for trapped water saturation.

At this stage, the only agreement achieved from all these disagreements is that none of those empirical models is able to predict the relative permeabilities with consistent accuracy all the time, not mentioning when other flow mechanics are involved, such as hysteresis, low-interfacial tension effects etc. Although the main objective of this simulation-based study is not to history-match any experimental data or develop a new empirical model, it is necessary to recognise the main features of these 3PRP models before applying them in the simulations. All three models were tested with an aim to provide a base case for the new synthesis (M_{CE} & M_{IFT}) proposed here to be built on. Very importantly, a detailed investigation will be carried out to determine the discrepancy in the flow behaviour induced by the different treatments of these models, particularly during the near-miscible WAG displacement. In fact, there are many other 3PRP models existing, such as the model developed by Blunt (2000) and the model proposed by Ranaee *et al.* (2015). Since these models are much less frequently used and not available in the commercial simulator (CMG/GEM here), they will not be discussed any further.

In fact, the pore network models (Blunt, 2001; Van Dijke *et al.*, 2001) can be alternatively used to predict the relative permeabilities based on the pore structure and the displacement physics. However, empirical models are still frequently used in the oil industry for reservoir simulations. This is simply because accurate descriptions of the pore geometry and wettability are not always fully available. In fact, another reason that the 3PRP models mentioned above (Stone 1, Stone 2 and Baker) are normally coded in the commercial simulators is their simplicity, which allows them to be incorporated with other functions to reflect additional flow mechanics, such as the IFT effects and permeability hysteresis.

2.5.3 IFT-dependent relative permeability

As demonstrated earlier in Section 2.3, a significant mass transfer can occur in a near-miscible CO_2-oil system. With the continuously changing fluid constitution, the interfacial tension between gas and oil (σ_{go}) can also change dramatically during this process, which may also have a great impact on the fluid behaviour in a multi-phase system.

Longeron (1980) and Bardon (1994) performed a series of core flooding tests to investigate the IFT effects on relative permeability using a binary fluid mixture. They concluded that the residual oil saturation is highly dependent on the value of σ_{go}, especially when it is lower than 0.1 mN/m. Very importantly, the relative permeabilities to both oil and gas became linear as IFT approached zero. This is a very important result in the literature on near miscible gas injection, but it omits the effects of the presence of much heavier hydrocarbon components in real oils. For such realistic systems, the stripping/compositional effects remove the lighter components leaving the heavier ones behind and as the displacement progresses, the gas/oil IFT will frequently increase, as shown in Chapter 4.

Betté *et al.* (1991) performed a series of numerical simulations to evaluate IFT effects on fluid behaviour. They claimed that IFT effects barely affect the ultimate recovery. In fact, the IFT effects in their study were probably masked by the more dominant compositional effects. They only simulated continuous injection of CO_2 into 1D slim-tube models and cores, and they did not simulate WAG. Although the importance of IFT effects was not well resolved, their method of simulating IFT effects has been well accepted and incorporated in commercial software, such as GEM/CMG. This present work agrees with the finding of Betté et al. for continuous gas injection, but I go on to show that IFT effects are much more important in near-miscible WAG processes.

Cinar and Orr (2005) experimentally investigated the effect of σ_{go} variation on three phase relative permeabilities. A very important conclusion from their study is that oil relative permeability can be significantly improved at a σ_{go} range of 0.03 to 2.3 mN/m. On the other hand, the relative permeability of the wetting phase (water here) is hardly affected by the IFT change.

Shyeh-Yung (1991) used core flood experiments of CO_2 injection to examine the effects of pressure, initial saturation and volume of injected CO_2. He highlighted the positive effects of both mass transfer and low interfacial tension on the ultimate recovery, particularly at near-miscible conditions. In addition, he suggested that slim-tube tests might not be able to provide results as realistic as those from reservoir-condition corefloods.

Nowadays, increasing micromodel experiments and theoretical analysis have pushed forward a better understanding of the multi-phase flow at the pore-scale, particularly under near-miscible conditions. Sohrabi *et al.* (2004; 2008a; 2008b) designed a series of WAG tests to evaluate IFT effects at the pore-scale. They used etched glass micromodels to mimic the pore structure of reservoir rocks and varied the wettability conditions by injecting either water or oil before the tests. They claimed that if the IFT between oil and gas is reduced to the level of 1 - 3 mN/m, good oil recovery can be obtained through either a thick oil film (oil wetting) or an oil layer (water wetting). In other words, the local displacement efficiency can be greatly improved by means of an "oil film/layer", even though the IFT is not an ultra-low level (i.e. σ_{go} ~ 1 - 3 mN/m and not necessarily as low as σ_{go} ~ 0.001 mN/m).

Sorbie and van Dijke (2010) proposed a consistent pore-scale theory of phase flow for the transition from immiscible to miscible conditions with respect to the impact of IFT effects on the contact angles. They modified the equations originally proposed by Al-Al-Siyabi *et al.* (1999) to account for this low IFT (but not ultra-low) transition. They concluded that the "oil film" mechanism is particularly important during near-miscible WAG, where IFT is at a level of 1 - 3 mN/m for instance. In fact, this would normally be described as "immiscible", but is better described as "near-miscible".

It can be seen that IFT variations could have a great impact on the flow behaviour at both pore and laboratory scale. Skauge and Sorbie (2014) produced a review on the flow mechanisms at different scales during the process of WAG injection. They pointed out the strong link between pore-scale physics, the core-scale and field-scale oil recovery mechanisms. As motivated by their study, it was therefore proposed here that such IFT effects, which are related to the "oil-film" (oil-layer) mechanism, should be included in the reservoir simulation. However, IFT does not explicitly appear in the flow equations in a conventional reservoir simulation. In order to capture this important mechanism

(M_{IFT}), an IFT-dependent relative permeability model is applied here. Both the shape and end-point of relative permeabilities of oil and gas change as a function of σ_{go}. In fact, this is another requirement of performing a full-compositional simulation, which provides a more accurate/consistent IFT prediction based on the Equation 2-33 (CMG, 2017), i.e. McLeod-Sugden equation.

$$\sigma_{go} = (\sum_{1}^{n_c} P_{ch\_i}\ (\rho_o y_{o_i} - \rho_g x_{g_i}))^4 \qquad \text{Equation 2-33}$$

where n_c is the number of fluid components; P_{ch_i} is the parachor of component *i*; ρ_o is molar density of oil; $y_{o_i}$is mole fraction component *i* in oil phase; ρ_g is molar density of gas; $x_{o_i}$is mole fraction component *i* in gas phase.

Unlike the 3-phase relative permeability functions, the effort spent on developing a more rigorous IFT dependent relative models are fairly limited. Coats (1980) proposed the first IFT-dependent model to simulate gas displacement to take account of IFT effects. This method entails an interpolation between immiscible relative permeability and scaled phase saturations, which reflects the feature of a fully miscible relative permeability as a straight line. The weighting function (f) with a specified critical gas/oil IFT, σ_{go}^0, is introduced to control the contribution of the IFT effects. If the actual $\sigma_{go}$is above the threshold value (σ_{go}^0), the initial immiscible permeability is used. If $\sigma_{go} < \sigma_{go}^0$, the relative permeability of oil and gas will be modified and gradually become linear functions as σ_{go} approaches zero. At the same time, the residual oil saturation and critical gas saturations should also decrease with f and approach zero. As seen in Equation 2-34 to Equation 2-36, the smaller the weighting factor (f), the greater the impact IFT effects will have on the relative permeabilities.

$$K_{rog} = f * K_{rog}^{inmiscible} + (1 - f) * \overline{S_o} \qquad \text{Equation 2-34}$$

$$K_{rg} = f * K_{rg}^{immiscible} + (1 - f) * \overline{S_g} \qquad \text{Equation 2-35}$$

$$\text{The parameter } f = 1, \text{ if } \sigma_{go} > \sigma_{go}^0$$

$$= (\sigma_{go} / \sigma_{go}^0)^n, \text{ otherwise.} \qquad \text{Equation 2-36}$$

$$\overline{S_o} = \frac{1 - S_g - S_{wc} - S_{org}^*}{1 - S_{wc} - S_{org}^*} \qquad \text{Equation 2-37}$$

$$\overline{S_g} = \frac{S_g - S_{gc}^*}{1 - S_{wc} - S_{gc}^*} \quad \text{Equation 2-38}$$

$$S_{org}^* = f * S_{org}^{immiscible} \quad \text{Equation 2-39}$$

$$S_{gc}^* = f * S_{gc}^{immiscible} \quad \text{Equation 2-40}$$

Later, Betté *et al.* (1991) modified Coats' model and introduced a separate parameter, i.e. hydrocarbon relative permeability (K_{rh}). This concept reflects the fact that gas and oil should be indistinguishable when miscibility is achieved. However, it was found that this method has a major shortcoming that the residual oil saturation jumps to zero as soon as IFT effects are activated in the simulation.

$$K_{rot} = f * K_{ro} + (1 - f) * K_{rh} * (S_o/(1 - S_w)) \quad \text{Equation 2-41}$$

$$K_{rgt} = f * K_{rg} + (1 - f) * K_{rh} * (S_g/(1 - S_w)) \quad \text{Equation 2-42}$$

$$K_{rh} = 0.5 * (K_{row} + K_{rg}) \quad \text{Equation 2-43}$$

Another model of IFT-dependent relative permeability based on Coats' model can be found in CMG/GEM (CMG, 2019). This method combines both the concept of hydrocarbon relative permeability and a consistent treatment of the residual oil saturation. A more extensive discussion of modelling IFT effects on the flow behaviour using these models can be found in Chapter 4.

$$K_{rot} = f * K_{ro} + (1 - f) * K_{rh} * \left(\frac{S_o - fS_{org}}{1 - S_w - fS_{org}}\right) \quad \text{Equation 2-44}$$

$$K_{rgt} = f * K_{rg} + (1 - f) * K_{rh} * \left(\frac{S_g - fS_{gc}}{1 - S_w - fS_{gc}}\right) \quad \text{Equation 2-45}$$

2.5.4 Permeability hysteresis

Permeability hysteresis is a well-recognised phenomenon. It means that relative permeability is dependent not only on saturation but also the saturation history/direction (Killough, 1976; Spiteri and Juanes, 2006). When strong flow reversals are involved, great errors may result in reservoir simulation if the phenomenon of permeability hysteresis is ignored. There have been numerous studies on the hysteresis effects in both

2-phase systems and 3-phase systems. Here, I focused on the commonly used models, which are also available in the simulator chosen here (CMG/GEM).

2.5.4.1 Gas trapping

In a gas-oil system, the non-wetting phase presents a lower relative permeability in the imbibition process than that in the primary drainage process at the same saturation (Naar *et al.*, 1962). This is because gas can be disconnected and trapped in the form of discontinuous ganglia (Killough, 1976; De Gennes *et al.*, 2013). The greater the amount of gas entrapment, the more reduction in the gas relative permeability. Land (1968) firstly proposed a single-parameter model (i.e. Land constant, C) to predict the trapped gas saturation Equation 2-46 and this has been the basis of most subsequent gas trapping models. Carlson (1981) developed a relative-permeability model based on a concept of free gas saturation and is defined as Equation 2-47 to Equation 2-49. He proposed that gas saturation can be divided into two parts, i.e. the trapped gas saturation (S_{gr}) and the free gas saturation (S_{gf}). The calculated free gas saturation can be used to predict the gas relative permeability using the drainage curve for the imbibition process.

$$C = \frac{1}{S_{gr}} - \frac{1}{S_{gh}} \qquad \text{Equation 2-46}$$

$$S_g = S_{gf} + S_{gr} \qquad \text{Equation 2-47}$$

$$S_{gf} = S_{gc} + \frac{1}{2}\left[\left(S_g - S_{gr}\right) + \sqrt{(S_g - S_{gr})^2 + \frac{4}{C}(S_g - S_{gr})} \right] \qquad \text{Equation 2-48}$$

$$K_{rg}^{im}\left(S_g\right) = K_{rg}^{dr}\left(S_{gf}\right) \qquad \text{Equation 2-49}$$

Where S_{gh} is the value of S_g when the shift to imbibition occurs; K_{rg}^{im} is the gas relative permeability during imbibition process; K_{rg}^{dr} is the gas relative permeability during drainage process.

CMG also developed their own gas trapping model based on the same theory, although using a different formula to determine the free gas saturation (CMG, 2019).

$$S_{gf} = S_{gc} + \frac{(S_g - S_{grh})(S_{gh} - S_{gc})}{S_{gh} - S_{grh}} \qquad \text{Equation 2-50}$$

where S_{gc} is the critical gas saturation; S_{grh} is the value of S_{gc} corresponding to S_{gh} via Land's equation (CMG, 2019).

These two models (proposed by Carlson and CMG) are both developed based on the Land's theory, although they differ in the treatment of the free gas saturation. Another well-accepted model was developed by Killough (1976), which is a parametric interpolation method. Since this method has not been coded to incorporate with the subsequent 3-phase hysteresis model in CMG/GEM, it was not tested here.

2.5.4.2 3-phase hysteresis

It has also been reported that K_{rw} was appreciably reduced in the secondary water injection compared with values during the primary water injection in a WAG process (Wang, 1988; Wegener and Harpole, 1996). Based on the trapping model developed by Carlson (1981), Larsen and Skauge (1998) proposed an immiscible 3PRP model to reflect the hysteresis effects of both gas and water relative permeabilities under immiscible conditions. They managed to achieve a better agreement between this model and the experimental data available from WAG injection experiments. There are two major features in this model. One is the reduced water permeability after the primary imbibition (Equation 2-51 to Equation 2-54). The other one is the coupling of the residual oil saturation to the trapped gas saturation. This is to reflect the fact that the recovery can be improved because of the trapped gas saturation under immiscible conditions (Negron-Perez and Ali, 1973). Note that the latter feature can be only activated under the condition that Stone 1 is used to model 3PRP hysteresis (Equation 2-55). In fact, Larsen and Skauge's model is widely used in many commercial software such as CMG/GEM (CMG, 2019).

For increasing water saturation (imbibition):

$$K_{rw}^{imb} = K_{rw}^{2phase}\left(1 - \frac{S_g^I}{S_{gmax}}\right) + K_{rw}^{3phase} * \left(\frac{S_g^I}{S_{gmax}}\right) \qquad \text{Equation 2-51}$$

For decreasing water saturation (drainage):

If $S_g > S_g^I$ (gas flood), then

$$K_{rw}^{drain} = (K_{rw}^{imb})_f \left(1 - \frac{S_g - S_g^I}{S_{gmax} - S_g^I}\right) + K_{rw}^{3phase} * \left(\frac{S_g - S_g^I}{S_{gmax} - S_g^I}\right) \qquad \text{Equation 2-52}$$

If $S_g < S_g^I$ (oil flood), then

$$S_{om(mod)} = S_{om} - a * S_{gt} \qquad \text{Equation 2-53}$$

If $S_g = S_g^I$ (constant gas saturation), then

$$K_{rw}^{drain} = (K_{rw}^{imb})_f \quad \text{Equation 2-54}$$

$$S_{om(mod)} = S_{om} - a * S_{gt} \quad \text{Equation 2-55}$$

where K_{rw}^{imb} is the calculated imbibition relative permeability; K_{rw}^{2phase} is the two-phase relative permeability; S_g^I is the gas saturation from the former process; S_{gmax} is the maximum attainable gas saturation; K_{rw}^{3phase} is the water relative permeability in a three-phase system, which is the lower boundary for the scanning curve; $(K_{rw}^{imb})_f$ is the water relative permeability from the former increasing water saturation process.

As mentioned earlier, strong multi-phase flow behaviour is expected to occur in the process of near-miscible WAG displacement. Both models (gas trapping and 3PRP hysteresis) will be tested respectively based on the new synthesis developed here. Note the work presented here is mostly confined to water-wet systems, although I do address the concerns of the wettability condition on the flow behaviour in the section of 5.3.3.

2.5.5 Capillary pressure

The simultaneous existence of multiple immiscible fluids in the reservoir pores give rise to capillary pressure, which is defined as the pressure difference between two immiscible fluids at the interface (McPhee *et al.*, 2015). As defined by Equation 2-56 (Dullien, 1992), the capillary pressure P_{cow} is a function of radii of curvature r of the shared interface, the contact angle (θ) and the interfacial tension between oil and water (σ_{ow}).

$$P_{cow} = P_o - P_w = \frac{2\sigma_{ow}\cos\theta}{r} \quad \text{Equation 2-56}$$

According to Brown (1951), the magnitude of capillary pressure is dependent on a range of factors, such as the textural properties of the medium, interfacial tension between fluids, the rock wettability etc. Leverett (1941) developed a dimensionless function, the J-function (Equation 2-57), to describe the capillary pressure, which is still widely used in the current oil industry.

$$J(S_w) = \frac{P_c(S_w)\sqrt{k/\emptyset}}{\sigma\cos\theta} \quad \text{Equation 2-57}$$

where P_c is the capillary pressure, k is the absolute permeability, $\emptyset$ is the porosity; σ is the surface tension; θ is the contact angle. Assuming an immiscible system, the value of the J-function is constant for a given saturation within a reservoir.

Many researchers have proposed various modifications for J-function to improve its applicability for different rock types. Saboorian Jooybari *et al.* (2010) and Ferreira *et al.* (2015) pointed out the importance of incorporating rock microstructure-related parameters, i.e. the shape factor and the hydraulic tortuosity. Later, a general form of the J-function, which is suitable for variety of microstructures, has been proposed by Mirzaei-Paiaman *et al.* (2018). Since the focus of this study is not to improve the formula of J-function, the traditional J-function (Equation 2-57) is used for simplicity:

Capillary pressure is usually ignored in practice for reservoir simulations (Juanes and Blunt, 2006). This is because the cell size in reservoir simulation is very large (a level of 100~1000m). At this scale, the viscous pressure difference between cells is large and dominates over the capillary pressure difference between cells (Ringrose *et al.*, 1993). However, Schembre and Kovscek (2003) claimed that capillary forces might dominate multiphase flow in low-permeability rocks, where the bypassed oil is usually located. This is because the non-wetting phase must overcome the capillary pressure to flow. This study includes an extension to the flow behaviour taking into account capillary pressure. A synthetic capillary oil-water curve based on J-function was tested with various injection rates to investigate its impacts on the distribution of remaining oil saturation. Note that the J-function is not constant in practice within the realistic reservoirs due to the large variations in rock properties (rock typing), such as lithology and depositional pattern (Abedini and Torabi, 2015). Since the total system size in this study is 50m×10m, i.e. essentially the size of one "grid block" in filed-scale simulations, the J-function is assumed constant for simplicity. In fact, capillary pressure also presents hysteresis effects (Killough, 1976). Note the focus of this study is on the two major mechanisms (M_{CE} and M_{IFT}) by which oil can be mobilised under near-miscible displacements. Hysteresis of capillary pressure, although intriguing, is outside the scope of the present work.

2.5.6 Dispersion

According to Stalkup (1983), fluid dispersion or mixing could also have an impact on the recovery performance in a CO_2-oil system, especially under miscible conditions. This is

because the fluid in the miscible zone can be dissipated and therefore leads to the loss of the miscibility (Perkins and Johnston, 1963).

According to Johns and Garmeh (2010), the source of fluid mixing includes two parts, i.e. molecular diffusion and convective dispersion (velocity variations related to heterogeneity). The modelling methods of the reservoir mixing have been studied for years. A common/simple way of modelling dispersion effects (dispersive flux) is to use the Fickian-type formula, which is defined as Equation 2-58 to Equation 2-61 (Lake, 1989). This method entails using a fixed value of dispersivity in the longitudinal (parallel to the bulk flow) and transverse (perpendicular to the bulk flow) directions respectively.

$$J_i = -\sum_k \emptyset \rho_k S_k D_{ik} \nabla y_{ik} \qquad \text{Equation 2-58}$$

$$D_{ik} = \begin{bmatrix} (D_{ik})_{11} & (D_{ik})_{12} & (D_{ik})_{13} \\ (D_{ik})_{21} & (D_{ik})_{22} & (D_{ik})_{23} \\ (D_{ik})_{31} & (D_{ik})_{32} & (D_{ik})_{33} \end{bmatrix} \qquad \text{Equation 2-59}$$

$$(D_{ik})_{xx} = \frac{D_{ik}^*}{F_k \emptyset S_k} + \frac{\alpha_{lk} u_{xk}^2 + \alpha_{tk}(u_{yk}^2 + u_{zk}^2)}{\emptyset S_k |\overrightarrow{u_k}|} \qquad \text{Equation 2-60}$$

$$(D_{ik})_{xy} = \frac{(\alpha_{lk} - \alpha_{tk}) u_{xk} u_{yk}}{\emptyset S_k |\overrightarrow{u_k}|} \qquad \text{Equation 2-61}$$

where J_i is the total mass flux (rate of mass flow per unit area) of component i; y_{ik} is mass fraction of component i in phase k (oil, water and gas); D_{ik}^* is the molecular diffusion coefficient of component i in phase k; F_k is formation resistivity factor for phase k; α_{lk} and α_{tk} refers to longitudinal and transverse dispersivity respectively; $\overrightarrow{u_k}$ is flow velocity of phase k; u_{xk}, u_{yk} and u_{zk} are the flow velocity of phase k in three directions (x, y and z) respectively. The negative sign indicates that the direction of dispersion flux is from higher mass fraction to lower mass fraction. The longitudinal dispersivity (α_{tk}) is always larger (an order of magnitude higher) than the transverse dispersivity (α_{tk}), which makes $(D_{ik})_{xy}$ is always positive (Lake, 1989).

According to Gray (1975), the order of convective dispersion can be many times larger than molecular diffusion. This is because the term of convective dispersion contains

contributions from fluctuations of the velocity, if the interstitial flow velocity (superficial velocity divided by porosity) is greater that 3cm/day (Lake, 1989). Since the present analysis is confined to the flow behaviour during a short period of injection process (2.5-20 days in a 50m-long model) with fairly high injection rate (0.1-0.4PV/day), it is assumed that the dispersion effects are mostly dominated by the convective dispersion. In other words, the term with D_{ik}^{*} is neglected here.

In fact, the outcome of such physical dispersion is remarkably similar to that of the numerical dispersions (truncation errors resulting from the approximations of the partial differential equations) in a finite-difference simulation (Abou-Kassem *et al.*, 2013). According to Sorbie and Mackay (2000), it is a reasonable practice to use numerical dispersion to mimic the physical dispersions. A major concern is that the numerical dispersion of reservoir simulations in practice is much larger than physical dispersion, due to mixing within coarse grid cells. Although the level of mixing at the field scale is still debatable, a range of tests of varying cell size was performed to match the case with an assumed physical dispersion, which was determined based on the study of Arya *et al.* (1988). It is the first step to determine an appropriate cell size (sufficiently fine) in a finite-difference simulation to conduct a reliable mechanistic study of near-miscible CO_2-WAG displacements. A detailed discussion on this issue is presented in Chapter 4.

2.6 Viscous fingering and channelling flow

A gas flood inherently has an unstable displacing front due to the unfavourable mobility ratio (Equation 2-62).

$$M = \frac{K_{r1}\mu_2}{K_{r2}\mu_1} \qquad \text{Equation 2-62}$$

where $K_{r1}\ and\ \mu_1$ are the relative permeability and viscosity of the displacing fluid (gas); $K_{r2}\ and\ \mu_2$ are the relative permeability and viscosity of the displaced fluid (oil). Typically, the end-points of the relative permeability are used to calculate the mobility ratio for immiscible displacements. The smaller the value of M, the more stable displacing front.

Gardner and Ypma (1984) performed 2D areal simulations to examine the effect of viscous instability in a miscible displacement. They found that the remaining oil

saturation was significantly higher in the presence of fingering flow than in its absence. Later, Homsy (1987) produced a thorough review on both numerical and experimental (Hele-Shaw cell) studies on the viscous fingering with an aim to provide a fundamental understanding of the fingering flow. He demonstrated how the major mechanisms, such as shielding, spreading and splitting, govern the development of the flow fingers in homogeneous systems. He claimed that such phenomena should be very important in EOR processes.

Waggoner *et al.* (1992) analysed the competition between effects of adverse mobility ratio and heterogeneous permeability during miscible displacement. A set of simulations varying mobility ratio and level of heterogeneity were performed to reveal the different sources of fingering and channelling. Fingering flow means tongues of displacing fluid forming at the interface between the displacing and displaced fluids (Kargozarfard *et al.*, 2019). Fingering flow occurs when the mobility ratio is greater than one. On the other hand, channelling flow refers to the phenomenon of dominant fluid flow through a few preferred pathways of least resistance (Tsang and Neretnieks, 1998). Channelling flow occurs when the correlation length of the permeability field is of the order of the system length, even with unit mobility ratio. Correlation length (λ_D) is a dimensionless parameter to describe the distribution of the spatial properties and is determined using the formula Equation 2-63. The degree of correlation between the permeabilities at two points decreases with the increasing distance between them. When the distance is above the correlation length scale, the permeabilities are not correlated any more.

$$\lambda_D = \frac{\lambda}{L} \qquad \text{Equation 2-63}$$

where λ is the correlation length; L is the system length.

Araktingi and Orr Jr (1993) also investigated the impacts of the heterogeneity on the fingering development. They found that if the heterogeneous permeability field is not correlated, the pattern of fingering is similar to homogeneous cases. Such behaviour has been reproduced in my simulations based on a permeability field with random noise. On the other hand, if the permeability field is highly variable and of a correlation length greater than a certain fraction of system length, the fingering pattern is mostly governed by the permeability distributions. If the permeability distribution is lognormal, the

Dykstra and Parsons cofficient (Dykstra and Parsons, 1950) can be used to describe the level of the variations (Equation 2-64).

$$V_{dp} = \frac{K_{50} - K_{84.1}}{K_{50}} = 1 - e^{-\sigma_{\ln k}} \qquad \text{Equation 2-64}$$

where K_{50} is value of median permeability; $K_{84.1}$ is the permeability value at 84.1% probability; $\sigma_{\ln k}$ is the standard deviation of $\ln k$.

As motivated by these studies, a range of permeability fields were generated varying the Dykstra and Parsons cofficient ($V_{dp} \sim 0.1 - 0.7$) and correlation length ($\lambda_D \sim 0.1 - 1$) using a commercial software—Petrel (Schlumberger, 2018). Based on these fields, I managed to trigger consistent and reproducible fingering and channelling flow regimes, with an aim to test various mechanisms of interest with a same basis.

According to Christie *et al.* (1993), there are mainly two ways of investigating such unstable flows, i.e. empirical models and high-resolution numerical simulations. One of the benchmark empirical method was proposed by Todd and Longstaff (1972). They successfully modelled viscous fingering using a mixing parameter (ω, not to be confused with the parameter used in EOS) in a miscible displacement. However, their method is based on an assumption of a single hydrocarbon phase in a black oil model without the account of the dynamic compositional effects. Alternatively, many researchers also performed high-resolution numerical simulations to capture the details of the fingering flow.

Chang et al (1994) investigated the phase-behaviour effects on finger formation. Their simulations of multiple-contact miscible CO_2 displacement showed that the component transfer between oil and CO_2 causes viscosity contrast and the capillary force to decrease simultaneously. Both effects tend to reduce the growth of fingering in their 2D results. However, due to the limitations of the computational power at that time, the grid resolution (Δx= 12.5 ft.) of their simulations was probably insufficient to fully capture the details of compositional effects and gas fingers. For this reason, I built fine-cell models (Δx=0.05m) to resolve these issues.

Jessen *et al.* (2004) ran a set of slim-tube numerical tests varying grid resolution to analyse the interplay of phase behaviour and numerical dispersion. They investigated the effect of the coarse grid on composition path along the slim-tube. However, the methodology they used in the 1D model is not fully applicable to 2D models. They did not clearly differentiate the source of discrepancies between inevitably reduced heterogeneity and numerical dispersion in their upscaled cases. Instead, they only analysed the discrepancies of the viscosity and density of phases and oil recovery compared with slim-tube tests, and they did not take details of compositional effects into account.

In a recent study, Moortgat (2016) described a series of sensitivity tests on viscous fingering accounting for mechanical dispersion, Fickian diffusion, flow rate, heterogeneity etc. His study focused on the effect of changed viscosity and density on the formation of fingering. He concluded that the fingering flow at near-miscible conditions could be profoundly different from first-contact miscible conditions and immiscible conditions presented in earlier studies. However, the details of the compositional effects such as the composition path were not included in his study. The effect of component transfer in a multidimensional system (such as a real reservoir) is still an issue.

It can be seen that two important flow regimes, i.e. fingering and channelling, have been extensively analysed but only under either immiscible or miscible conditions. On the other hand, the analysis of such flow behaviour is rarely conducted based on high-resolution simulations with detailed account of compositional effects under near-miscible conditions. For this reason, the first task of this mechanistic study is to understand how the compositional effects under near-miscible conditions interact with the aforementioned flow regimes, with an aim to provide a baseline on which to build a new synthesis.

2.7 Summary

In this chapter, a comprehensive review of the literature and the theoretical background required for this study has been conducted. An overview of the key physics occurring in multiphase systems, particularly under near-miscible conditions, has been presented here. Details of the compositional effects and interfacial tension effects, which are the binary elements of the new synthesis developed in this thesis, are stated. A review of the literature related to the multiphase flow functions, such as gas trapping, hysteresis of

water permeability and capillarity is presented. To summarise, our survey of the literature highlighted a gap in the fundamental understanding in the transition from immiscible to miscible conditions. This has motivated a mechanistic study focused on near-miscible displacement to be undertaken in this thesis.

Chapter 3 Analysis of Compositional Effects on Global Flow Regimes in Heterogeneous Systems

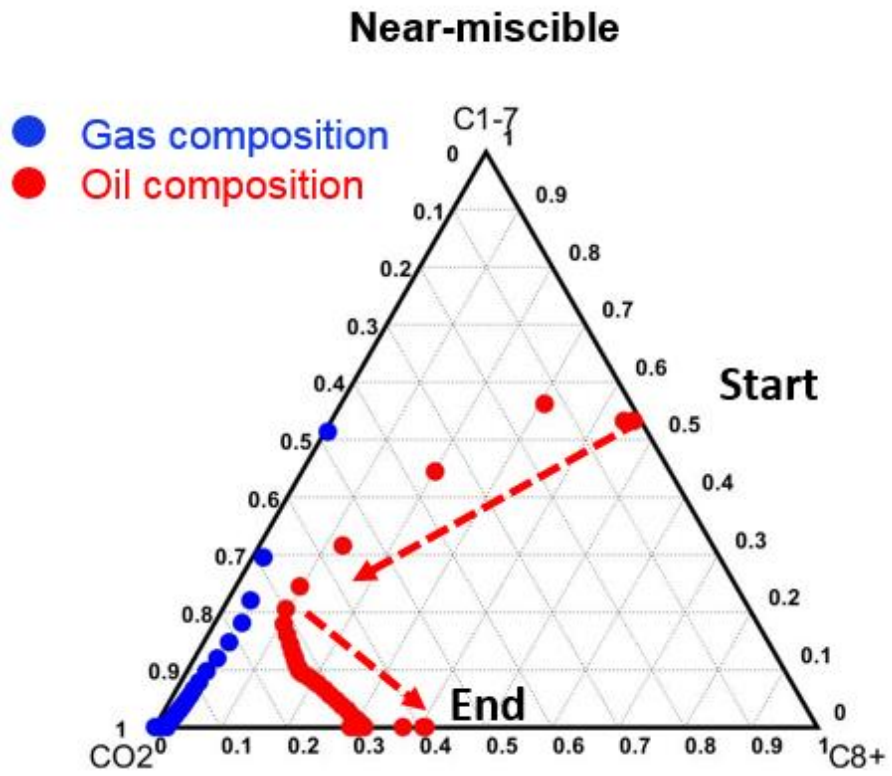

Ternary diagram: Composition path in a near-miscible CO_2 displacement

Publication:

Wang, G., Pickup, G. E., Sorbie, K. S. and Mackay, E. J. (2019a) 'Analysis of Compositional Effects on Global Flow Regimes in CO2 Near-Miscible Displacements in Heterogeneous Systems', *Transport in Porous Media*, 129(3), pp. 743-759.

3.1 Introduction

As mentioned previously, one of the challenges of properly modelling near-miscible displacement is that phase saturations and properties may experience dramatic changes due to the mass transfer between oil and CO_2. This is because the process of CO_2 dissolving into the oil phase and oil components being vaporised into the vapour phase leads to a continuous variation in composition, i.e. compositional effects. Therefore, this chapter investigates the interaction of compositional effects with the flow behaviour during near-miscible and immiscible CO_2-oil displacements in heterogeneous systems. Specifically, a series of issues have been addressed in this chapter:

- How do compositional effects interact with the underlying heterogeneity pattern of the flow field, particularly in the flow regimes of fingering and channelling?
- What are the overall influences on the local displacement efficiency and the ultimate oil/component recovery?
- How should we consistently measure and evaluate compositional effects, and thus assess the accuracy of simulations using models at different scales and dimensions?

Both 1D and 2D areal systems were simulated using a fully compositional simulator, i.e. CMG/GEM. The details of setup of the numerical models are presented below.

3.2 Model description

3.2.1 1D model

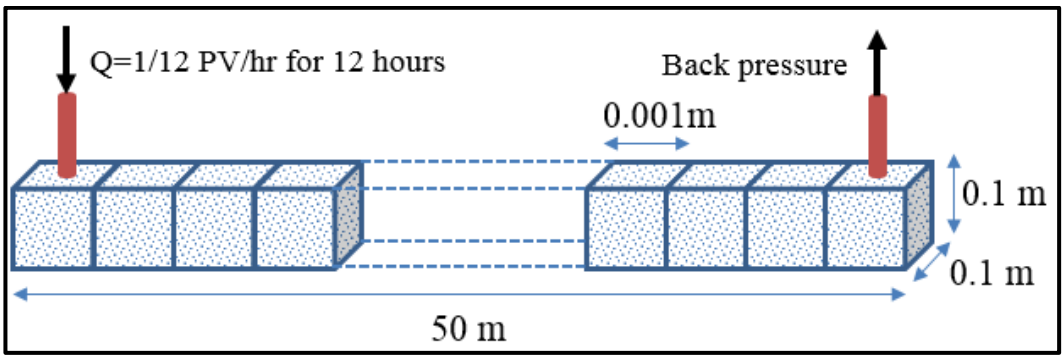

Figure 3-1 Schematic of 1D model

A very-fine-scale 1D model (i.e. Δx=0.001 m) was used as a base case to demonstrate the process of mass transfer (CO_2 displacing oil). Note that refining the cell size further has negligible influence on the results and therefore it is assumed to be a dispersion-free process. A tracer analysis (H_2O* displacing H_2O) was also performed to determine the proper cell size to introduce a certain level of numerical dispersion, which was used to

mimic the realistic physical dispersion in the subsequent 2D analysis. The whole length of the 1D simulation model here was set to 50m to reduce possible fluctuations in the numerical results (Figure 3-1). More importantly, the results achieved in 1D tests can be directly compared to the subsequent 2D tests with the same "well spacing". The porosity and permeability were homogeneous and set to 0.1 and 1 Darcy respectively, with an aim to reduce the pressure difference along the model (Yellig and Metcalfe, 1980; Khabibullin *et al.*, 2017).

3.2.2 2D areal models

Oil displacements by CO_2 under both immiscible and near-miscible conditions were simulated for unfavourable mobility ratios in 2D areal random correlated systems. Two heterogeneous permeability fields were generated based on Dykstra-Parsons (V_{DP}) coefficients (Dykstra and Parsons, 1950) and dimensionless correlation ranges (R_L). Model A which had a relatively short correlation length (0.1 of the system length) was generated to trigger possible fingering flow (Figure 3-2), while Model B had a longer correlation length (of the order of the system length), thus leading to channelling flow (Figure 3-3). The injector in these tests was set to inject pure CO_2 at a rate of 0.4 PV/d at reservoir conditions for 2.5 days (1PV in total) and the producer was controlled by setting the minimum bottom-hole pressure. Both wells were horizontal and were perforated along the width of the model. A set of parameters such as the residual oil saturation in representative cells and the oil and component recovery were compared between the 1D and 2D tests.

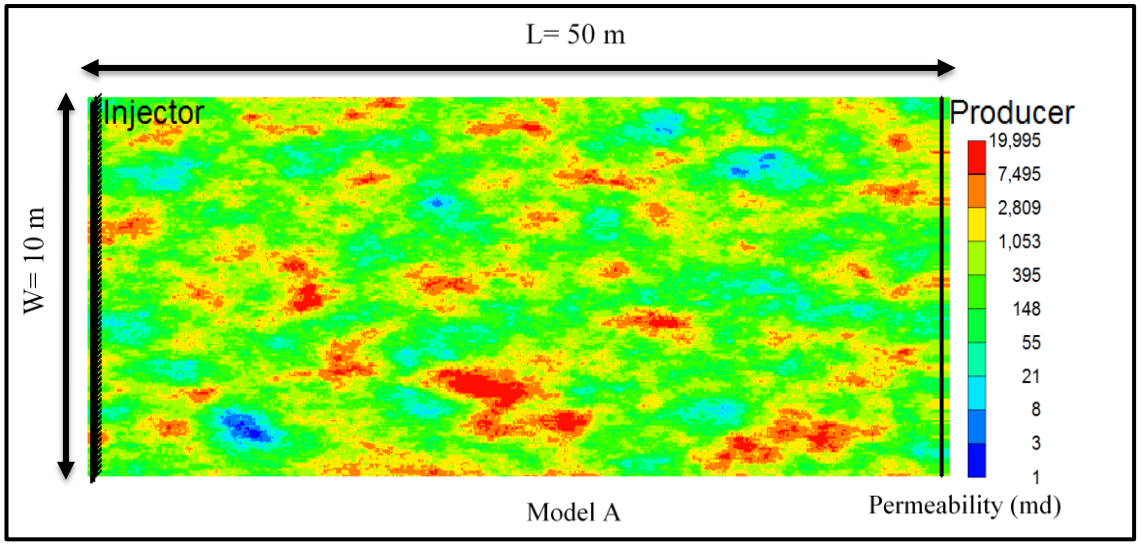

Figure 3-2 Permeability Field A (V_{DP}=0.7, R_L=0.1) used to trigger fingering flow.

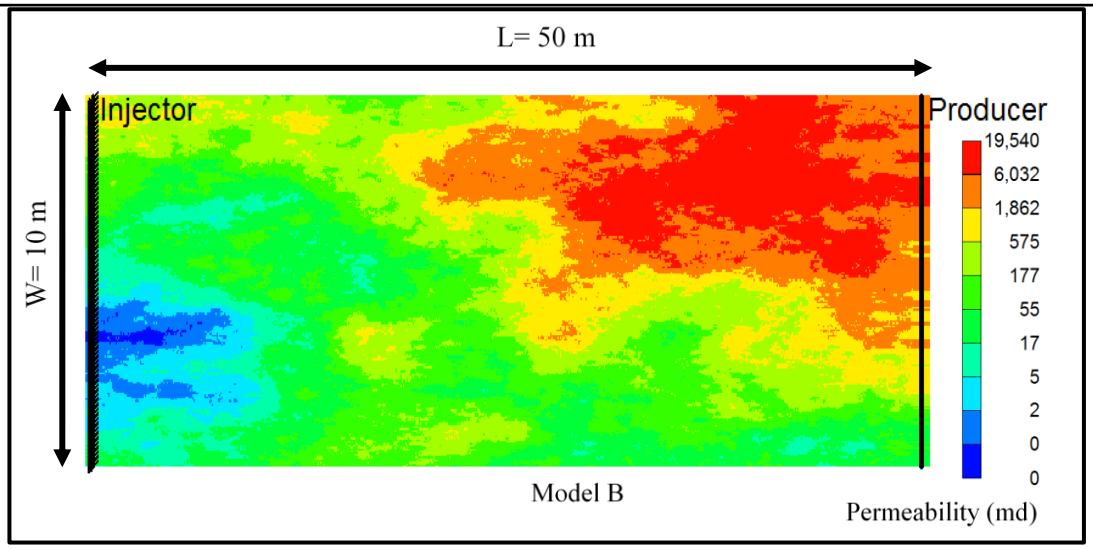

Figure 3-3 Permeability Field B (V_{DP}=0.7, R_L=1) used to trigger channeling flow.

3.2.3 Fluid model

Table 3-1 shows the data for a seven-component light oil (API ~ 35°) with a Minimum Miscibility Pressure (MMP) of 125 bar. This 7-component lumped oil was based on a 34-component oil (see Table-A1 in Appendix), which was provided to us by a sponsoring company. In fact, a typical lumping strategy consisting of 4 pseudo-components, such as CO_2, CH_4, C_{2-7} and C_{8+} has been tested to reduce the compositional cost (Orr, 2007). However, it was found that the 4-component system in this case is not able to properly reflect an important phenomenon, namely that, most of the oil can be stripped but heavy components (such as C20+) may be left behind in the 1D model during near-miscible CO_2 displacement (see Figure-A1 in Appendix). Therefore, a 7-component system is used here and the data given in Table 3-1 were applied to generate the PVT behaviour using the Peng-Robinson equation of state (EOS). Depending on the reservoir conditions, seven components may partition between two phases, i.e. a liquid hydrocarbon phase and a gaseous phase. The bubble point pressure was 38.5 bar at 53 °C (reservoir temperature). Oil viscosity was calculated using the Jossi, Stiel and Thodos' correlation with an initial value of 0.16 mPa·s. The relative permeability curves used here are shown in Figure 2-3. Note that a relatively high Sor (to immiscible gas) is chosen here (Sor=0.33) to give a higher target oil for stripping by compositional effects, and this emphasizes the magnitude of compositional effects on oil recovery. At this stage, neither hysteresis, capillary effects nor low-interfacial tension effects on the relative permeabilities are included in this chapter.

Equation of State							
Parameter, unit	CO_2	N_2 to CH_4	C_2 to C_4	C_5 to $C0_7$	C_8 to C_{12}	C_{13} to C_{19}	C_{20} to C_{30}
Mole fraction, %	1.2	11.7	19.5	22	28.2	9.4	8.1
Critical P, atm	72.8	45.2	41.9	31.3	23.9	17.2	11.9
Critical V, m^3/k-mol	0.094	0.099	0.206	0.333	0.458	0.766	1.260
Critical T, deg K	304.2	189.7	338.4	556.9	667.5	769.0	801.5
Acentric factor	0.225	0.008	0.148	0.249	0.328	0.567	0.942
Mw, gm/gmol	44.0	16.2	44.8	83.5	120.5	210.7	401.9
Volume shift	-0.082	-0.154	-0.085	-0.009	0.044	0.130	0.269
Parachor	78.0	76.5	150.5	248.5	344.9	570.1	905.7
Omega A	0.457	0.457	0.549	0.457	0.457	0.457	0.457
Omega B	0.078	0.078	0.093	0.078	0.078	0.078	0.078
$\delta_{CO2\text{-}i}$	0.000	0.104	0.124	0.129	0.150	0.080	0.130

Table 3-1 Equation-of-state parameters for different components used in the simulation study.

3.2.4 Numerical control

Here, an adaptive implicit mode, which can optimise both the computational cost and simulation stability, was used. This method entails switching from IMPES to a fully implicit formulation in the cells where the global mole fraction exceeds 0.15 (CMG, 2017). For the 1D model with a cell size of 0.001m in flow direction, the maximum time step was set to 5×10^{-6}day leading to a Courant number of 0.5. In addition, the maximum changes in global mole fraction were also specified during Newtonian iterations. If the change of global mole fraction of any component exceeds 0.5, the time-step size is reduced and the time-step is repeated. Note that refining the time step further or reducing the maximum change of global mole fraction made an insignificant change in the results and hence my simulations are essentially fully converged with this numerical control.

3.3 Results and Discussion

3.3.1 Component and phase distribution along the 1D model

In order to understand the details of component transfer, the component and phase distribution along the 1D model were compared between immiscible (70bar) and near-miscible (120bar) conditions. Two snapshots of the phase and component distributions

were taken at 0.6 PVI before CO_2 breakthrough and stacked together as seen in Figure 3-4.

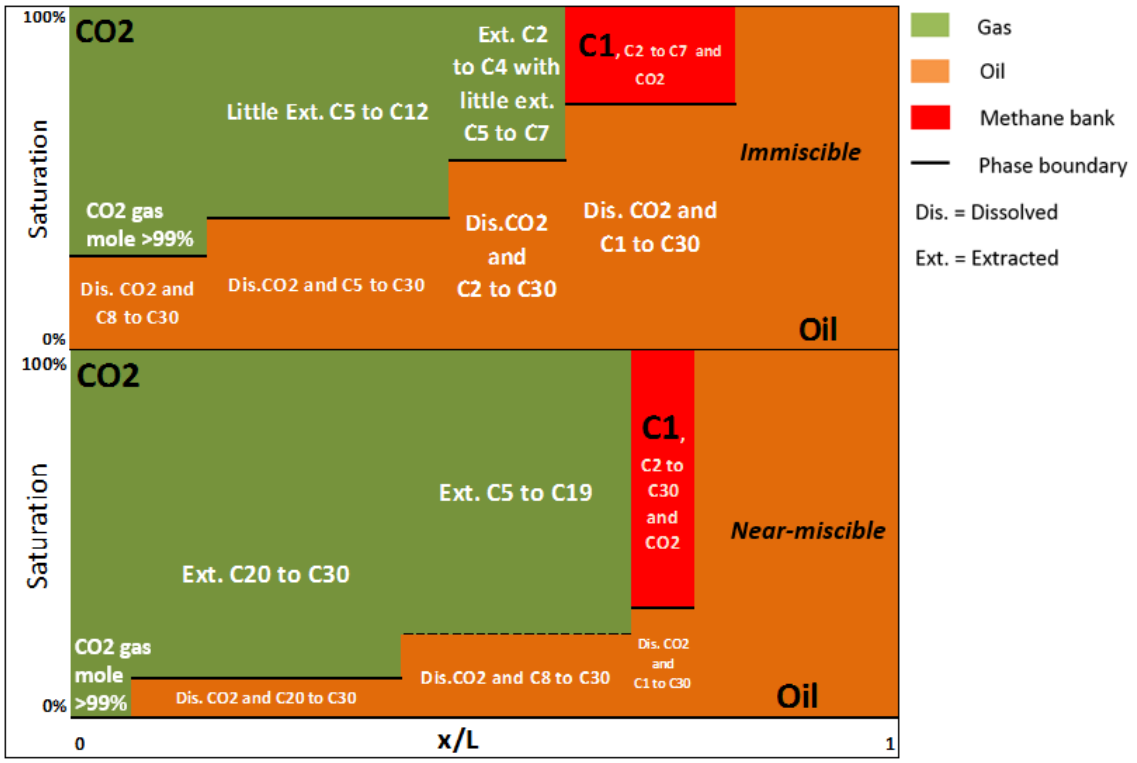

Figure 3-4 Component distribution along 1D model after 0.6 PVI at immiscible (top) and near-miscible (bottom) conditions.

At immiscible conditions, limited amounts of light and medium oil components are vaporised into the CO_2. A frontal dry gas bank (mainly methane) was found; this phenomenon, has been well analysed in previous studies (Holm and Josendal, 1974). The dry gas bank flows at a much lower viscosity and overtakes the oil at the front, and this may have an adverse effect on the sweep efficiency in reality. Compared with immiscible displacement, more vaporised oil components are present in the gas phase at near-miscible conditions. There is very little oil left behind the displacing front. The remaining oil mainly consists of heavy components (C20-C30 here) and the dissolved CO_2. In other words, the rest of the oil components have been stripped and recovered. In addition, the resulting gas saturation is much higher at near-miscible conditions due to the vaporized oil components. This effect might further aggravate the instability in multi-phase flow in realistic (multi-dimensional) simulations since the gas is much more mobile than the oil. Note that Figure 3-4 is presented here to qualitatively show the different level of mass transfer process between immiscible and near-miscible displacements rather than for detailed calculations. For this reason, the details such as the smearing-out of the displacing front are not included.

3.3.2 Composition path

In the previous section, I analysed the component distribution in all of the cells along the 1D model at one particular time. Here, the component constituents of a certain cell through the whole injection process was analysed in details. The aim of this part is to track the compositional variations of phases using ternary diagrams to evaluate the compositional effects. The dynamic fluid behaviour of CO_2 displacement with three pseudo components (CO_2, C1-7 and C8+) is presented. The compositional path for both oil and gas were investigated for a representative cell (15m from the injector), at both immiscible and near-miscible conditions. The representative cell selected here was designed to experience the full composition path during 1PV injection, but not to be dominated by CO_2 instantly.

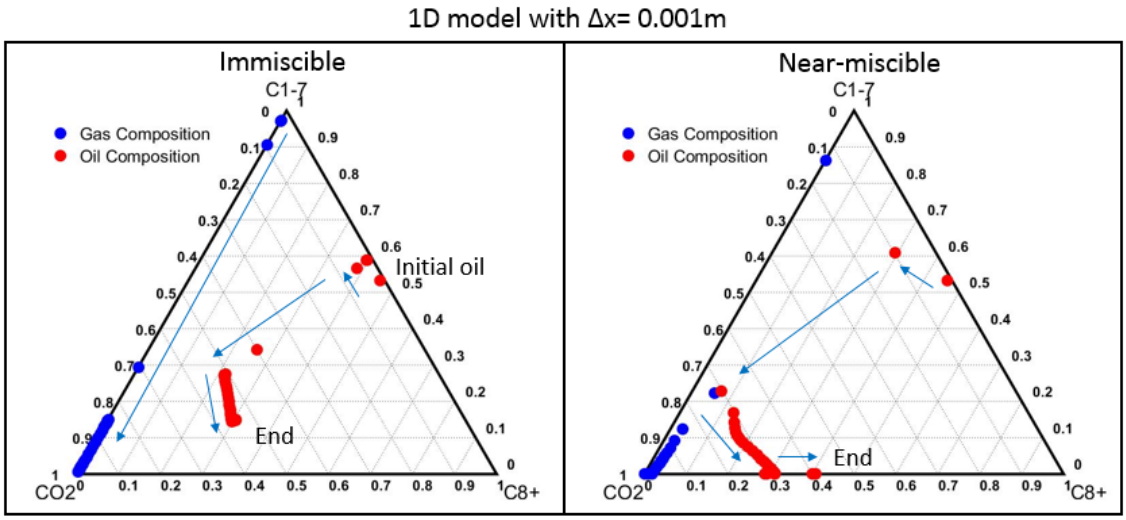

Figure 3-5 Oil and gas composition path of the representative cell in the 1D model at immiscible (left) and near-miscible conditions (right).

As seen in Figure 3-5 (right-hand diagram), the oil and gas composition can be very similar through multiple contacts during the process of mass transfer under near-miscible conditions. The oil composition then becomes heavier again with the process of mass transfer. This is because most of the oil components have been recovered leaving C20+ behind. On the other hand, the stripping effect of the oil components has very limited impact at immiscible conditions (left-hand diagram). It also explains why most of the medium-to-heavy components are left behind at immiscible conditions along the 1D model. At the same time, the amount of CO_2 dissolution is also limited through the whole injection process at immiscible conditions. At near-miscible conditions, a greater amount CO_2 dissolution occurs and CO_2 displacement is able to vaporize C1-7 from the oil phase almost completely after 1PVI. As expected, much higher local displacement efficiency

(remaining oil saturation close to 0 in this cell) can be achieved at near miscible conditions than at immiscible conditions (as seen in Figure 3-6).

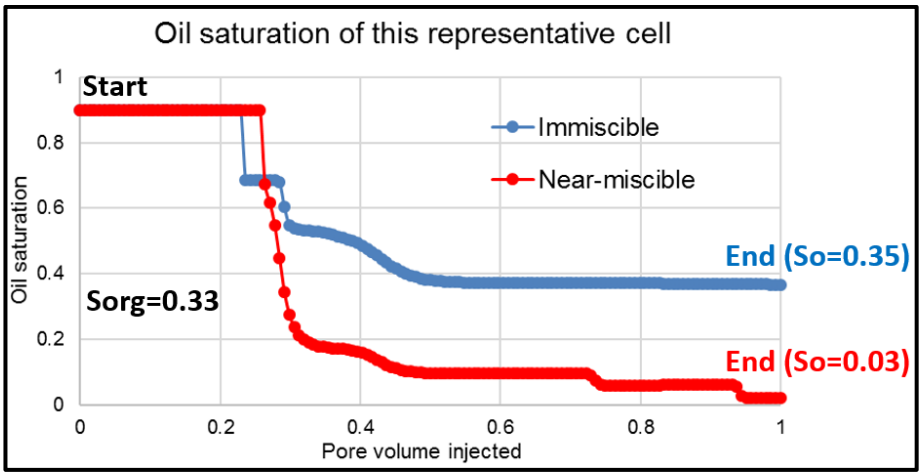

Figure 3-6 Remaining oil saturation of the representative cell at immiscible (blue) and near-miscible conditions (red) in the 1D model.

3.3.3 Dispersion in the model

In the previous section, the process of mass transfer (reflected by the composition path in a ternary diagram) has been investigated using a very fine-scale (essentially dispersion-free) 1D model. However, in reality, it is expected that some level of physical (dispersion-like) local mixing should exist in the system (Stalkup, 1983). According to Arya et al (1988) and Sorbie and Mackay (2000), the actual level of mixing in reservoirs should be 0.01m-2m at the scale of 10m-100m (50 m here). Here, a dispersitivity (α_L) of 0.025m was assumed and a tracer simulation (H2O* displacing H2O) was performed for various cell sizes, with the aim of using numerical dispersions to mimic the physical dispersions.

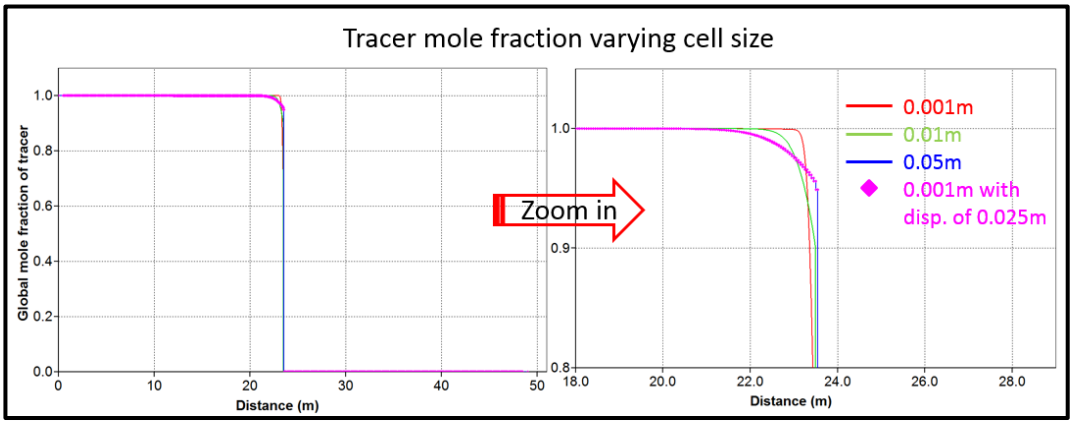

Figure 3-7 Snapshots of tracer mole fraction along the 1D model, with varying cell size taken at 0.4 PVI.

As seen in Figure 3-7, the results from our finest model (Δx=0.001m) with assumed dispersivity (0.025m) correctly converges with the coarser model (Δx=0.05 m) with no added dispersivity; recall that the dispersivity should be $\alpha = \Delta x/2$. Hence, the slightly coarser grid (Δx = 0.05m) will be used to mimic "realistic" (i.e. "reservoir-like") dispersivities for the subsequent 2D analysis. According to Jessen *et al.* (2004), the compositional effects can be very sensitive to dispersions, which will disrupt the shock structure and lead to lower levels of local stripping.

One of motivations of this study is to provide *input* for any potential upscaling methods considering mass transfers. That is, some of the effects modelled here which show the mixing and interaction between fluid flow and the changes in compositional paths should at least qualitatively, be as they occur in reality. Here, a comparison of displacement performance between models with the cell sizes of 0.001m and 0.05m respectively is presented in Figure 3-8.

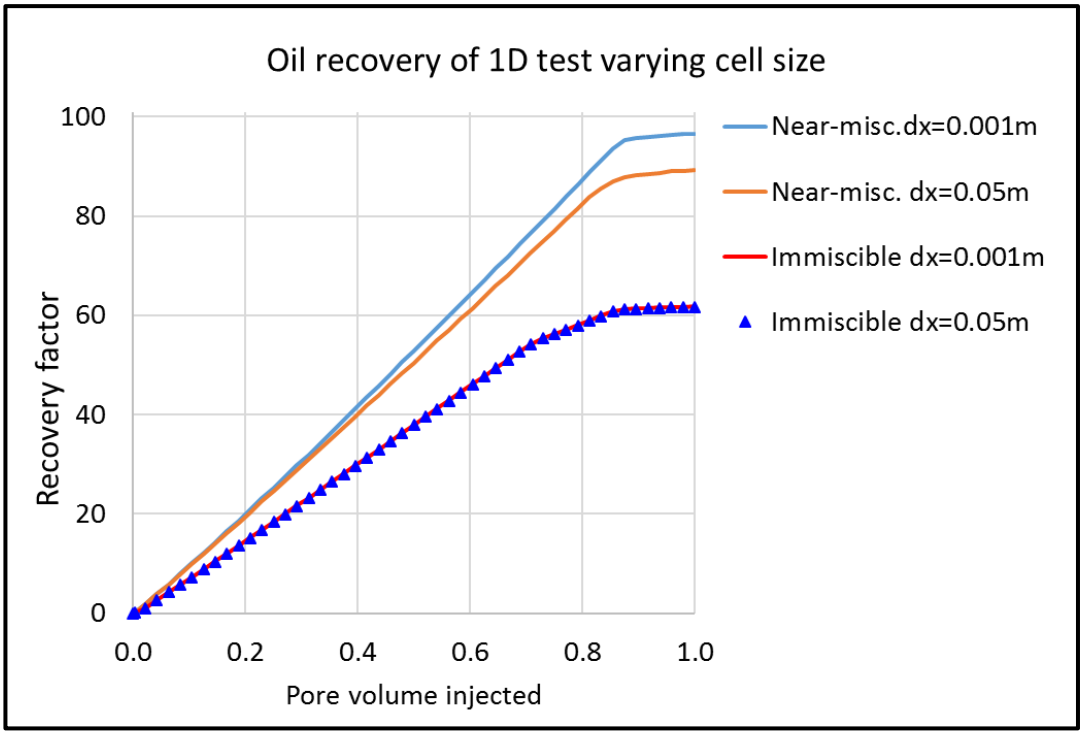

Figure 3-8 Oil recovery of 1D tests with PVI varying cell size in the flow direction (Δx).

As seen in Figure 3-8, the near-miscible displacement is more sensitive (as expected) than the immiscible displacement (discrepancy less than 1% between two immiscible curves). The oil recovery factor after 1PVI decreases from 96% to 89% under near-miscible conditions. Clearly, the displacement performance has been degraded due to the artificial dispersion. Such effects have been well analysed by Orr (2007), although they are highly

case-dependent on the oil composition. Here, the composition path of the model with a cell size of 0.05m is plotted, and this serves as a reference for the subsequent 2D heterogeneous models. As seen in Figure 3-5 (left) and Figure 3-9 (left), the composition path of immiscible displacement is almost identical for cell sizes of 0.001m and 0.05m. On the other hand, there is an observable discrepancy between the gas and oil composition of the coarser-grid model (Δx=0.05 m) and the finer model (Δx=0.001 m), particularly at the early contact of the displacement under near-miscible conditions, as seen in Figure 3-5 (right) and Figure 3-9 (right).

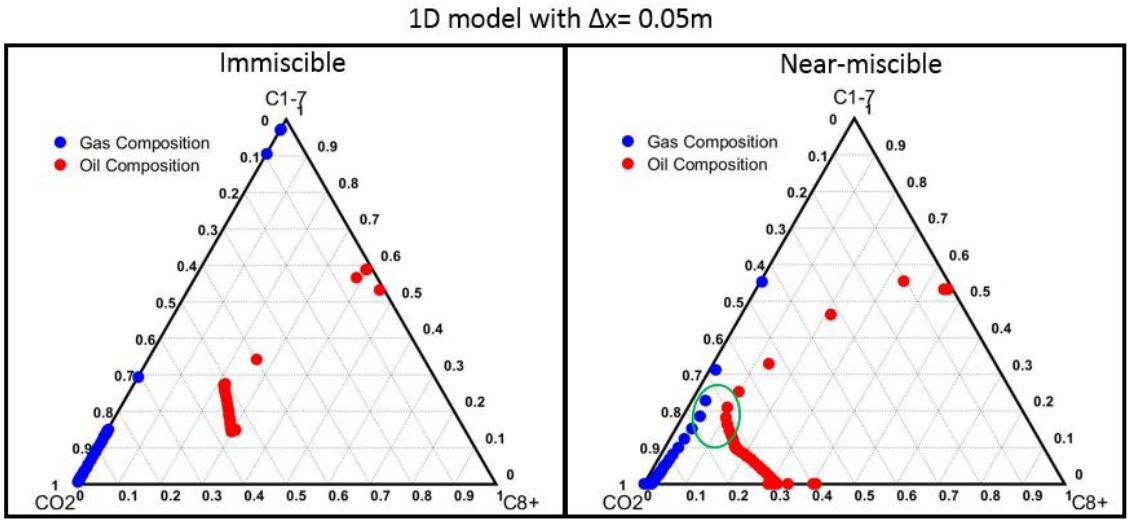

Figure 3-9 Oil and gas composition paths of the representative cell in the 1D model at immiscible (left) and near-miscible conditions (right) with the cell size of 0.05m.

3.4 Fingering flow regime

Keeping the previous points in mind, I now present results for flow simulations in our 2D "reservoir" system (50m x 10m) using heterogeneous correlated random permeability fields with short and long correlation lengths. The shorter-correlation-length system (5m here) leads to fingering flow whereas the longer-correlation-length (50m here) induces channelling flow, as described below. The results from model A (Figure 3-2), are presented first. Due to the unfavourable mobility ratios between gas and oil, typical fingering flow behaviour occurs for both immiscible and near-miscible flow. Note that a separate test with the unit mobility ratio on this permeability field presents stable front without any finger formation.

As seen in Figure 3-10, it is not surprising that the oil recoveries in our 2D tests are worse than the 1D test. As seen in Figure 3-11, multiple gas fingers (as expected) have been

developed under both immiscible and near-miscible conditions. However, the difference in the reduction of the oil recovery under immiscible/near-miscible conditions compared with the 1D tests deserves a further analysis. The lowered oil recovery under near-miscible conditions is more than double that under immiscible displacement. It was conjectured that the reduced recovery should be the result of a combination of differences in sweep efficiency associated with the viscous fingering and possible differences in local mixing that affect the composition path. In order to test this conjecture, two typical areas (i.e. in a non-preferential and a preferential route) were investigated using a similar methodology to the 1D tests. The composition path of 3 cells in a row (0.5m between each cell) in each streamline indicated by the black oval shapes is plotted in Figure 3-12.

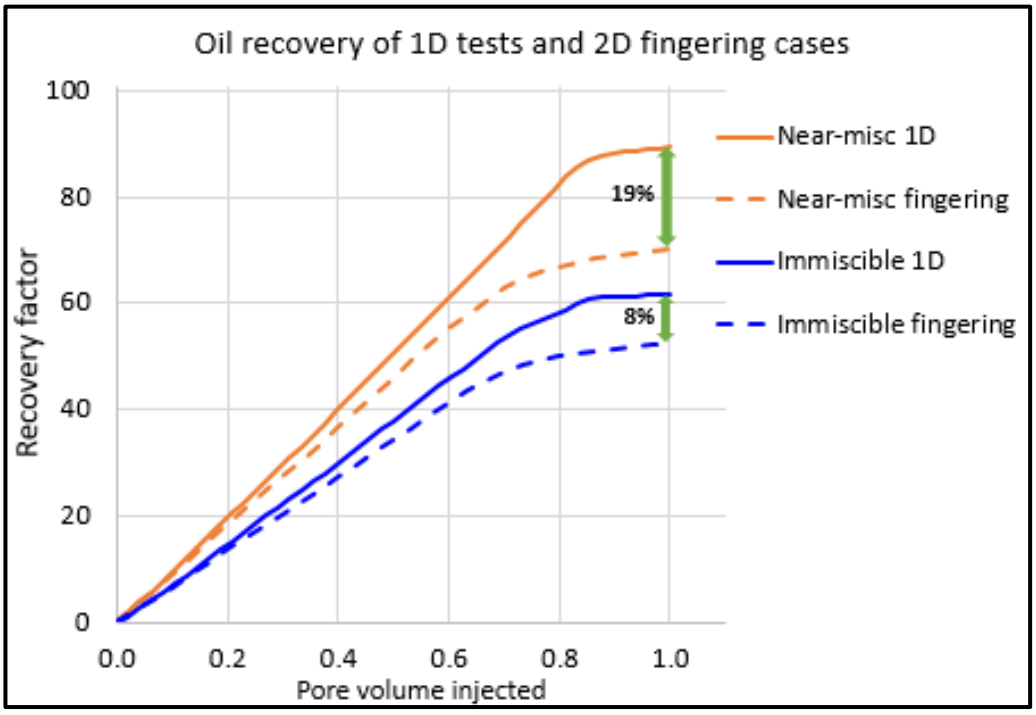

Figure 3-10 Oil recovery from 1D tests and fingering cases after 1 PVI under immiscible and near-miscible conditions.

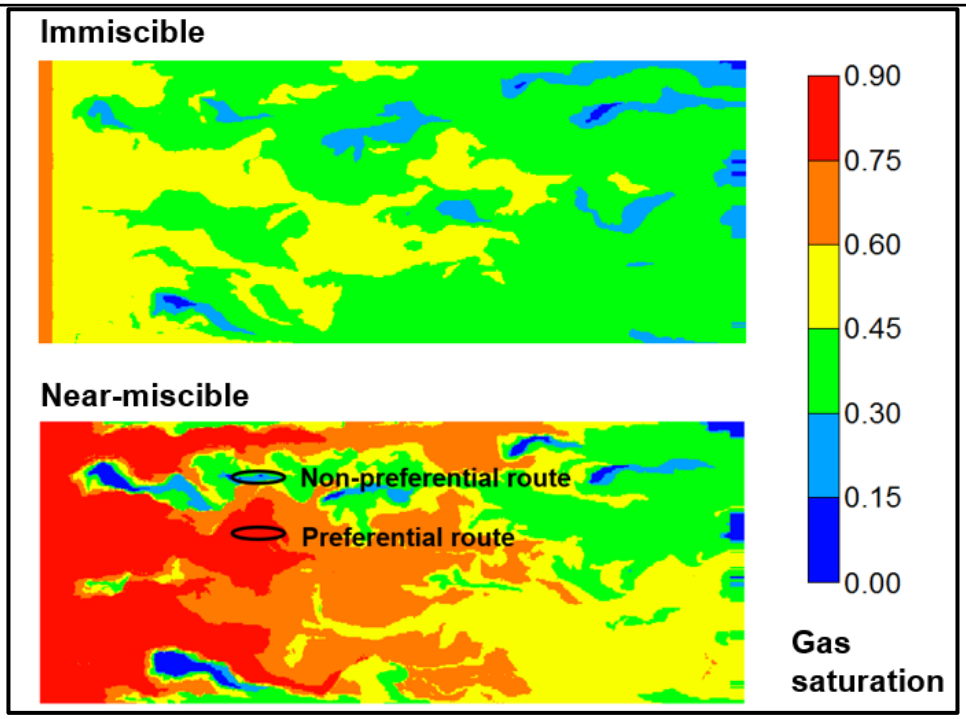

Figure 3-11 Snapshot of gas saturation after 1 PVI under immiscible (top) and near-miscible conditions (bottom).

As seen in Figure 3-12 (left), the compositional path of the selected preferential route is very similar to the 1D test with negligible discrepancy (Figure 3-9). On the other hand (Figure 3-12 right), the later stages of both the oil and the gas composition path are largely missing in the non-preferential route, which indicates that the journey along the composition path is not complete. In other words, the unstable phase flow determined by the underlying heterogeneity slows the flow in the unswept area and leads to unequal displacement performance between preferential and non-preferential routes. In fact, it is believed to be a typical example of how the phase flow interacts with compositional effects.

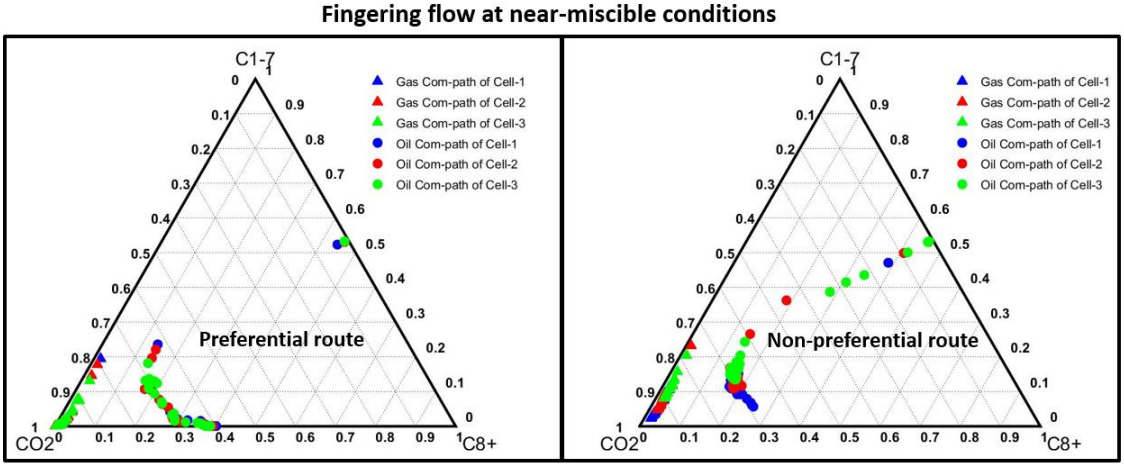

Figure 3-12 Comparisons of composition path between preferential (left) and non-preferential

route (right) in the 2D areal heterogeneous system.

The component recoveries for the 1D and 2D tests are shown in Figure 3-13 In the case of immiscible displacement, the reduction in recovery does not vary much with the components, from C5-7 and heavier. On the other hand, there is a greater reduction in the recovery of the heavier components in the near-miscible case. This is because near-miscible CO_2 displacement relies on a continuous process of mass transfer between gas and oil. Lighter components have moved preferentially in high gas saturation zones, and the heavier components left behind in slower flow zones have not been produced.

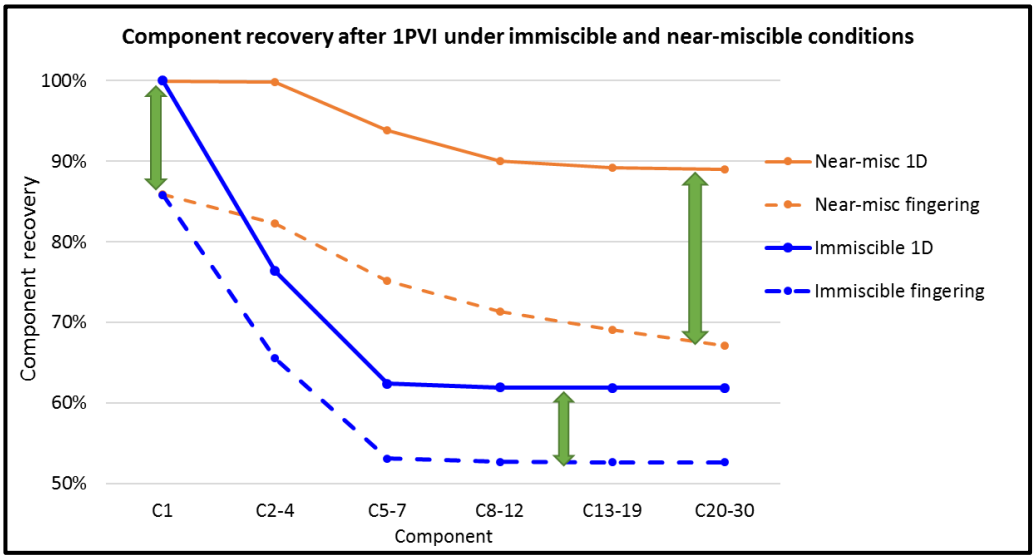

Figure 3-13 Comparisons of component recoveries between 1D tests and fingering cases under immiscible (blue) and near-miscible conditions (orange).

3.5 Channelling flow regime

Due to the dominant heterogeneity in the system with a longer correlation length, typical channelling flow occurs both in immiscible and near-miscible cases, as seen in Figure 3-14. The flow in such a system (dominant channel flow) is quite similar to the flow in a stratified formation. The presence of high-permeability area at the upper zone (Figure 3-3) leads to early CO_2 breakthrough occurs and very poor sweep efficiency. As a result, the oil recoveries after 1 PVI in the channelling cases are much lower than in the 1D tests under both conditions. Interestingly, the overall sweep of near-miscible displacement is rather worse than the immiscible displacement. This because the significant oil vaporization during near-miscible displacement increases the gas saturation and therefore leads to more severe channelling flow, which greatly suppresses the crossflow.

Therefore, the net result of the decreased sweep but improved local displacement efficiency leads to a very limited recovery improvement, as seen Figure 3-15.

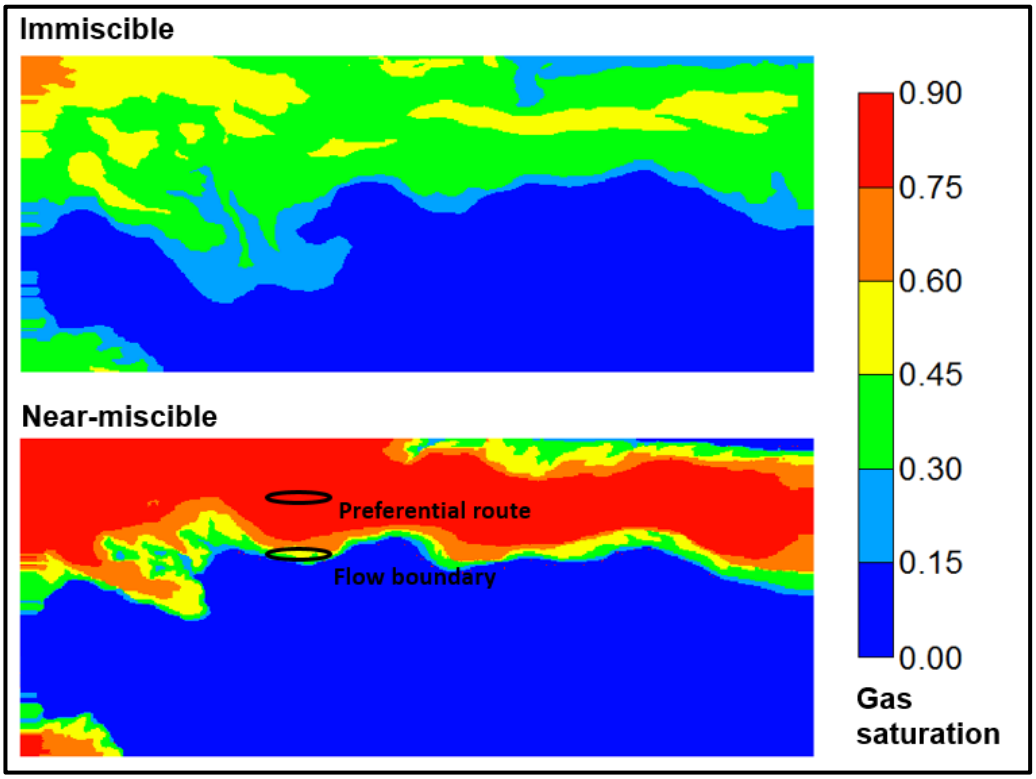

Figure 3-14 Snapshot gas saturation after 1 PVI under immiscible conditins (top) and near-miscible (bottom) conditions.

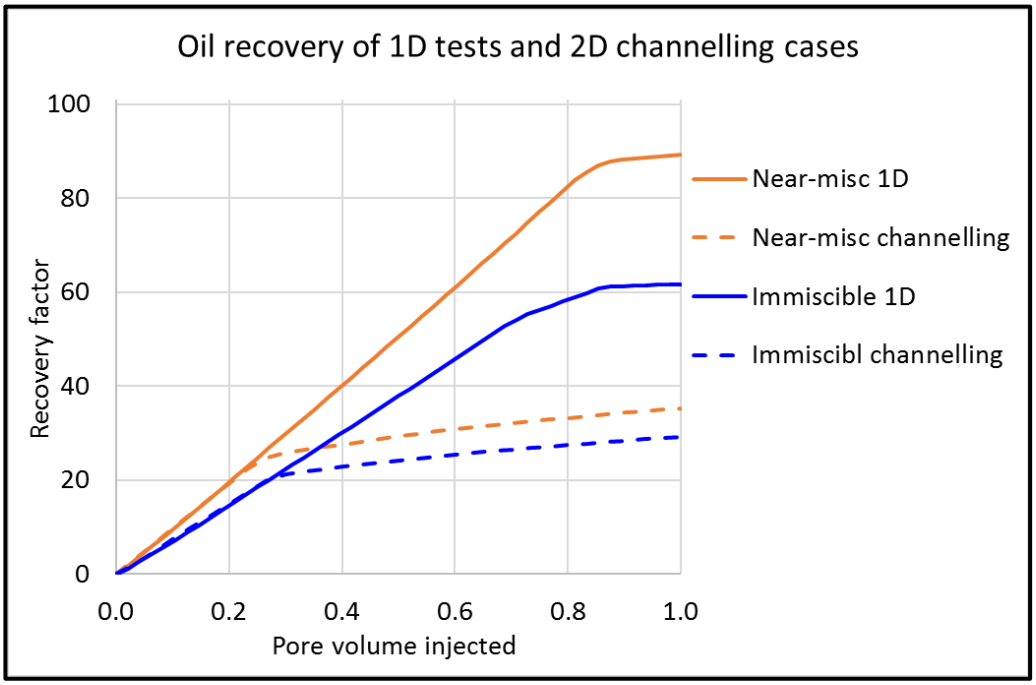

Figure 3-15 Oil recovery of 1D tests and channelling cases after 1 PVI under immiscible and near-miscible conditions.

Similar to the previous analysis of the fingering flow, I present the composition path of 3 cells in a row (0.5m between each cell) in two streamlines, indicated by black oval shapes, i.e. in a preferential route and at the flow boundary of the channel respectively (Figure 3-14). As expected, the composition path of the preferential route (Figure 3-16 left) is most similar to the 1D test whereas the one at the flow boundary (Figure 3-16 right) is much less complete. Unlike the fingering case, the medium-heavy component recovery is not reduced more than the lighter components (Figure 3-17). In other words, compositional effects are of less affected in the swept zone, where evident channelling flow occurs. Both the ultimate oil recovery and component recovery are significantly and about equally reduced, when the underlying heterogeneity is of dominant influence.

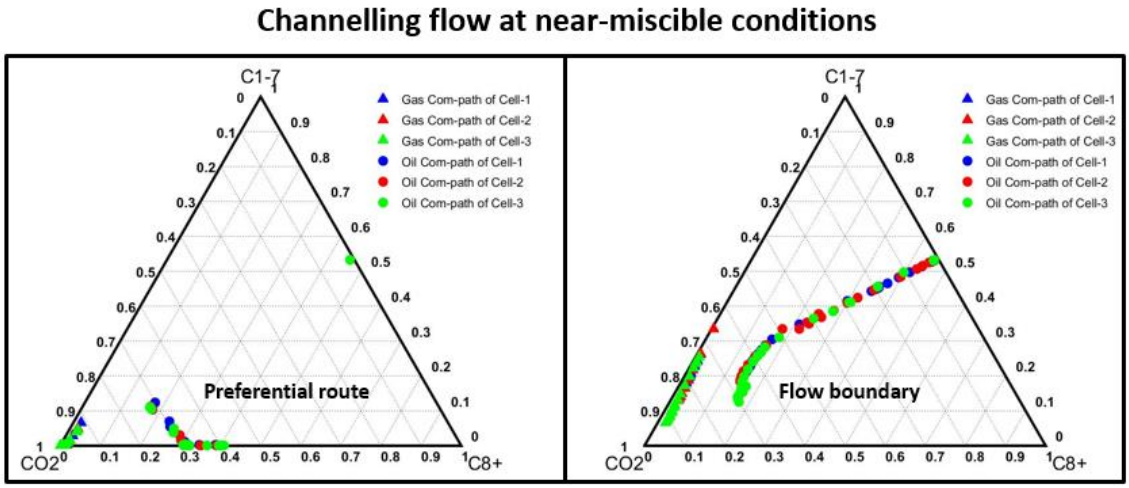

Figure 3-16 Comparisons of composition path between preferential (left) and flow boundary of the channel (right) in the 2D areal heterogeneous system.

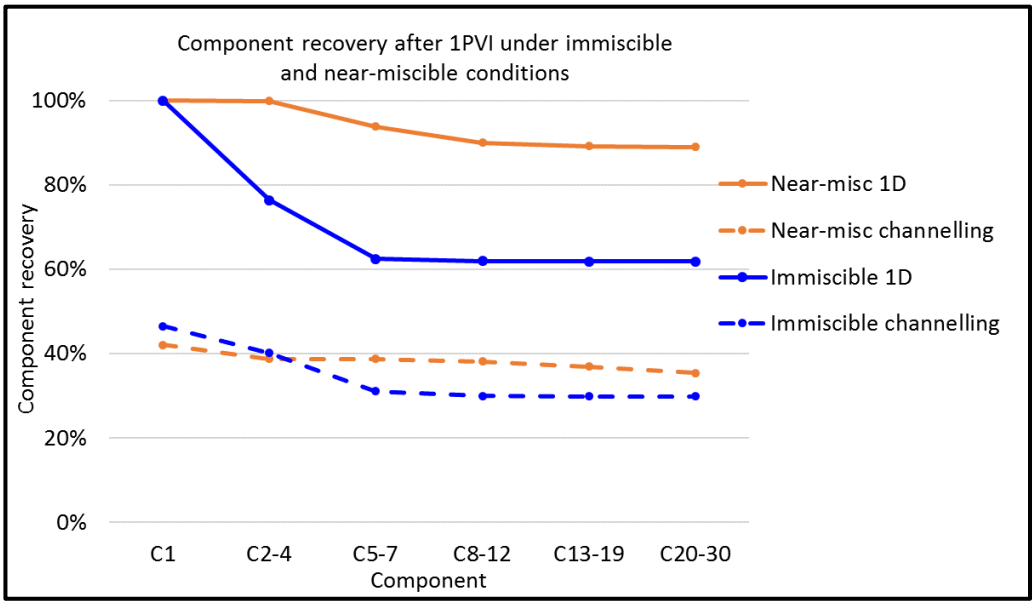

Figure 3-17 Comparisons of component recoveries between 1D tests and channelling cases.

3.6 Summary

The central intention of this chapter is to study how compositional effects contribute to oil displacement by CO_2, firstly in a 1D model and then in 2D areal heterogeneous models. We managed to correlate such discrepancies in the composition change (indicated by ternary diagrams) to the reductions in local displacement efficiency. In the absence of mixing (dispersion), certain shocks are known to occur in 1D multi-component near-miscible displacements of this type as extensively described by Orr (2007). However, in real systems there is always some level of mixing by various mechanisms e.g. dispersivity, heterogeneity and viscous fingering. This mixing will disrupt the shock structure, alter phase paths in a 1D model and consequently can reduce oil recovery by suppressing component stripping. In the models used in this work, I used very fine grids but with some level of mixing at a "realistic" reservoir scale (α_L = 0.025 m). This can be done by using a very small (50m x 10m) "reservoir" model. Indeed, the model is more like a medium sized single grid block and this allows us to use realistic levels of mixing (dispersivities). Using these models, the phase and component compositional paths observed for a typical grid block in a 1D calculation, can now be compared with those in 2D heterogeneous systems with different permeability structures that exhibit either fingering or channelling flow regimes. The cases of "composition only" in this study provide a baseline for any other mechanism to be superimposed, such as interfacial tension effects, gravity and hysteresis (if WAG is applied). Very importantly, the analysis of the dynamic compositional path and component recovery is effective to capture the potential discrepancies between the laboratory-scale phenomena and reservoir behaviour (or simply between different scales). This is especially relevant when both compositional effects and heterogeneity are important, such as in near-miscible CO_2 displacement. In the following chapters, this work will be extended to consider Water-Alternating-Gas (WAG) displacements including IFT (film flow) effects. Here, by comparing simulations of oil displacement by CO_2 in these different 2D systems, three aspects of how the compositional effects interact with the flow regimes are stated below.

1.The composition path in a 2D areal system does not follow the same composition path as in 1D tests, particularly in the later stages. Various types of mixing such as dispersivity (substituted by numerical dispersions here), heterogeneity and viscous fingering can slow the process of component stripping and thus lower the displacement efficiency. In

particular, recovery of heavier component is more likely to be affected in typical flow fingering regimes.

2.Compositional effects are of much less importance when channelling flow occurs. The strong oil vaporization can further aggravate the flow channel in cases considered here and therefore suppress crossflow. The net result of the decreased sweep but improved local displacement efficiency leads to a very limited recovery improvement. Due to the fact that heterogeneity is dominant in driving the channelling flow, subsequent analysis will be focused on the fingering flow regime, where both phase (i.e. compositional effects) and flow behaviour are important.

3.Assuming a certain level of mixing, a 1D test is able to represent a preferential flow route (well-swept area) in a multi-dimensional system regarding the local displacement efficiency for the same amount of injection. However, the overall displacement performance is highly dependent on the interaction of fingering/channelling flow, crossflow and compositional effects, which can be depicted using ternary diagrams.

Chapter 4 New Synthesis Incorporating Compositional and Interfacial Tension Effects

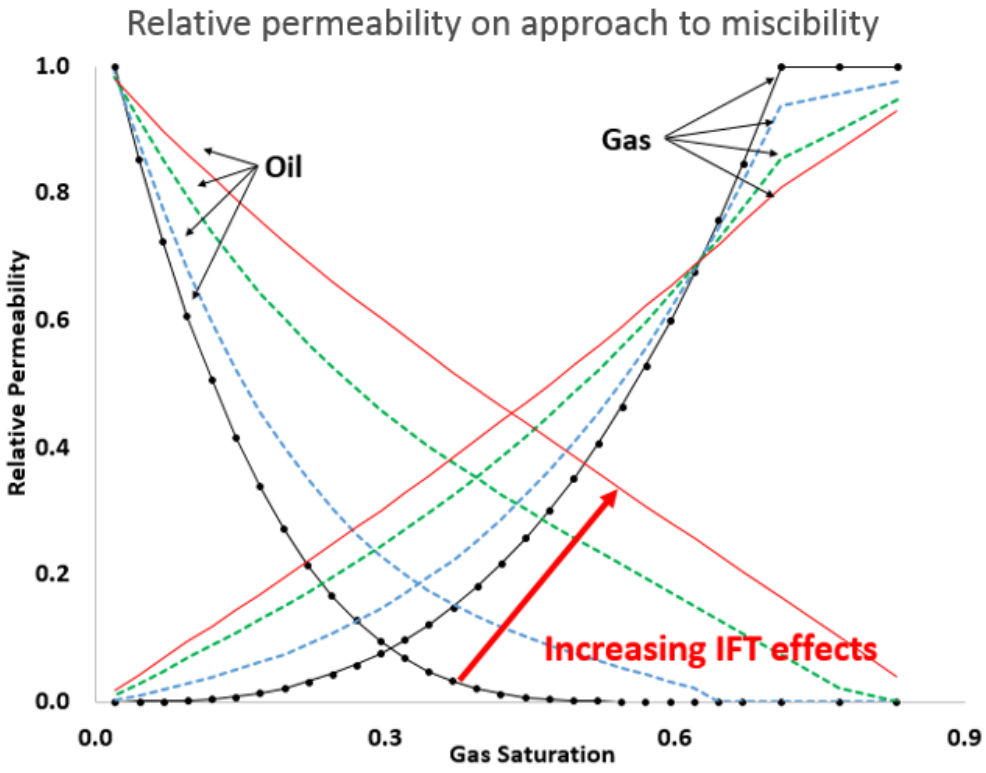

Publications:

Wang, G., Pickup, G., Sorbie, K., Mackay, E. and Skauge, A. (2020) 'Numerical Study of CO2 Injection and the Role of Viscous Crossflow in Near-miscible CO2-WAG', *Journal of Natural Gas Science and Engineering*, 74, p. 103112.

Wang, G., Pickup, G. E., Sorbie, K. S. and Mackay, E. J. (2019b) 'Detailed Assessment of Compositional and Interfacial Tension Effects on the Fluid Behaviour During Immiscible and Near-Miscible CO2 Continuous and WAG Displacements', *Transport in Porous Media*, 131(3), pp. 805-830.

4.1 Introduction

In the previous chapter, a comprehensive numerical study has been conducted on M_{CE} (compositional effects) and its influencing factors for this single mechanism acting alone; this may be described as applying conventional compositional simulation. In addition to M_{CE}, as the pressure increases and the system comes closer to miscibility (near miscible), another oil recovery mechanism involving enhanced oil layer flow occurs as a result of reduced gas/oil IFT (σ_{go}). Sorbie and van Dijke (2010) cited experimental observations and presented theoretical evidence that significant hydrocarbon film or layer flow occurs at σ_{go} above complete miscibility, i.e. $\sigma_{go} \sim 1 - 3$ mN/m. This is referred to as M_{IFT}, which is modelled here as an increase in hydrocarbon relative permeability under near-miscible conditions.

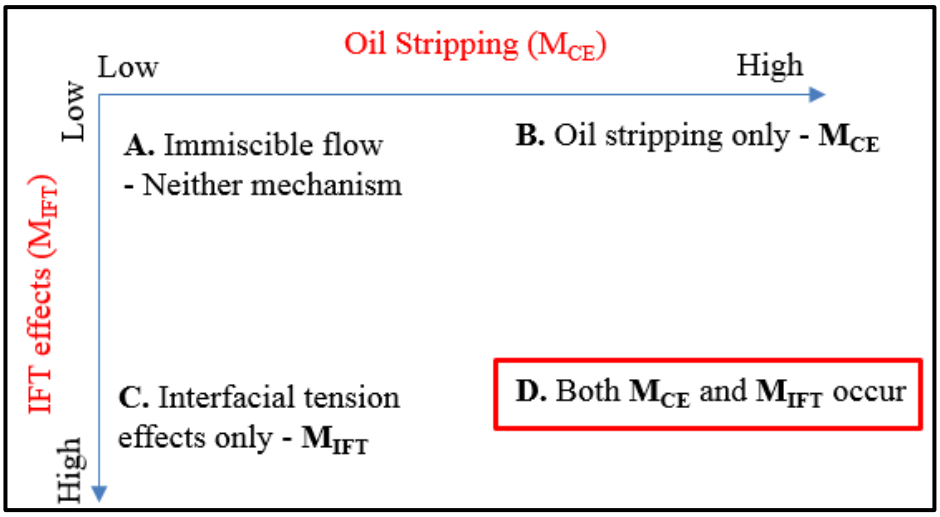

Figure 4-1 Schematic of the possible mechanistic processes that may occur in a CO_2 (gas) displacement process at immiscible and near-miscible conditions.

Figure 4-1 shows a schematic diagram with the range of possible combinations of mechanisms (M_{CE} and M_{IFT}) that can occur (at least theoretically) in CO_2 (or other gas) displacement processes. Given the importance of both M_{CE} and M_{IFT} during near-miscible displacement by which oil can be mobilised, this chapter shows how the M_{CE} and M_{IFT} mechanisms, separately and together, impose their effects on flow behaviour and oil recovery. In addition, a further motivation in this chapter is to analyse the overall outcome when these mechanisms are incorporated in the commonly used methods of IFT-dependent relative permeability, i.e. Coats (1980) and Betté et al. (1991). This detailed analysis of the modelling process of the oil displacement by CO_2 at near-miscible conditions within fine-scale models will lead to the development of more rigorous ways to simulate large-scale CO_2-EOR processes.

4.2 Model description

4.2.1 IFT-dependent models: Betté and modified Coats

Currently, there are two methods available in CMG/GEM (CMG, 2019) for modelling the effect of a change in IFT on relative permeabilities, i.e. Betté's model and Coats' model (modified version). Full details of equations used in these two models can be found in the section of 2.5.3. In fact, these two models entail using the same interpolation parameter f, which can be determined using Equation 2-36, i.e. $(\sigma_{go}/\ \sigma_{go}^{0})^{n}$. According to Coats (1980), the exponent "n" should be generally in the range of 0.1 to 0.5. A sensitivity analysis on the choice of n is included accordingly. To begin with, n is set to 0.5 as an example. Note that the differences between two models are twofold: they treat the residual oil and the relative permeabilities differently. Both models will be extensively tested and analysed in this chapter. The setup of the numerical models is the same as the cases previously presented in Chapter 3, with an aim to conduct a consistent analysis and guarantee that any change of flow behaviour results from the IFT effects here.

Before performing any simulations of oil displacement by CO_2 under IFT effects, a range of relative-permeability curves are firstly plotted varying the $(\sigma_{go}/\sigma_{go}^{0})$ ratio using both models, i.e. the Betté model and the Coats model. As seen in Figure 4-2, both models show that the relative permeabilities approach linearity with decreasing σ_{go} (as $\sigma_{go}/\sigma_{go}^{0}$ ratio decreases) and these two sets of curves are quite similar. However, there are discrepancies between oil relative permeability curves, which may have a significant impact on the flow behaviour. Here, I take the $(\sigma_{go}/\sigma_{go}^{0})$ ratio of 0.1 ($f = 0.32$ assuming the exponent of n as 0.5) as an example to be plotted in Figure 4-3 using semi-log scale to demonstrate these differences:

1. Based on the same initial input of immiscible relative permeabilities (Figure 2-3), the IFT-dependent oil relative permeability produced from the Coats model is generally lower than the one produced from the Betté model. This discrepancy increases with gas saturation (i.e. decreasing oil saturation). In addition, the gas relative permeability from the Coats model was slightly lower than that from the Betté model.
2. It was also found that the residual oil saturation in the Coats model is proportional to the $(\sigma_{go}/\sigma_{go}^{0})$ ratio, as seen in Equation 2-39. On the other hand, the residual oil saturation in the Betté model goes immediately to zero under IFT effects. In other

words, oil is always mobile (K_{ro}>0) as long as the IFT effects are triggered (i.e. $\sigma_{go} < \sigma_{go}^{0}$). This is because of the nature of the method used for modelling IFT effects in the Betté model (Equation 2-41 and Equation 2-42). This method has no further treatment of the residual oil saturation. Because of the contribution of the non-zero gas relative permeability to K_{rh}, the consequent oil relative permeability is therefore not zero, although it may often have a very low value (e.g. 0.001-0.05).

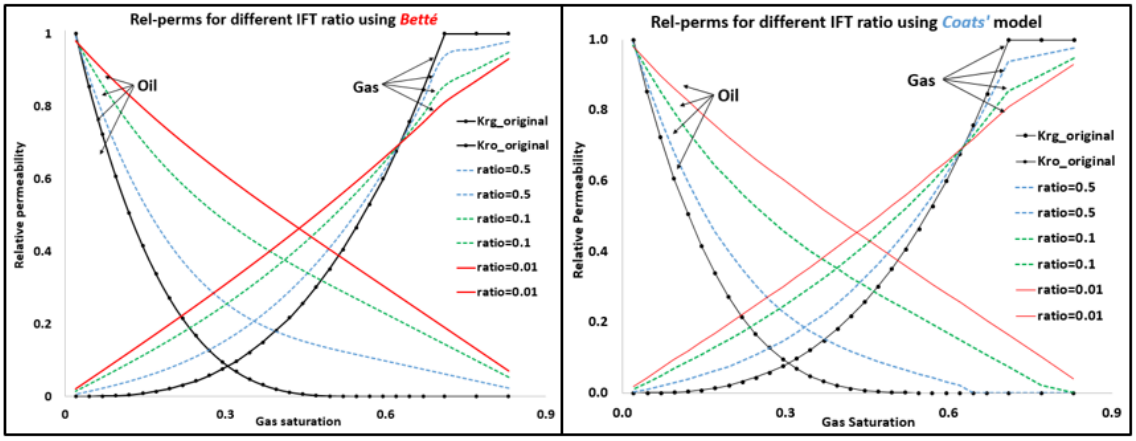

Figure 4-2 Relative gas and oil permeability of an example with varying ($\sigma_{go}/\sigma_{go}^{0}$) ratio, Betté model (left) and Coats model (right).

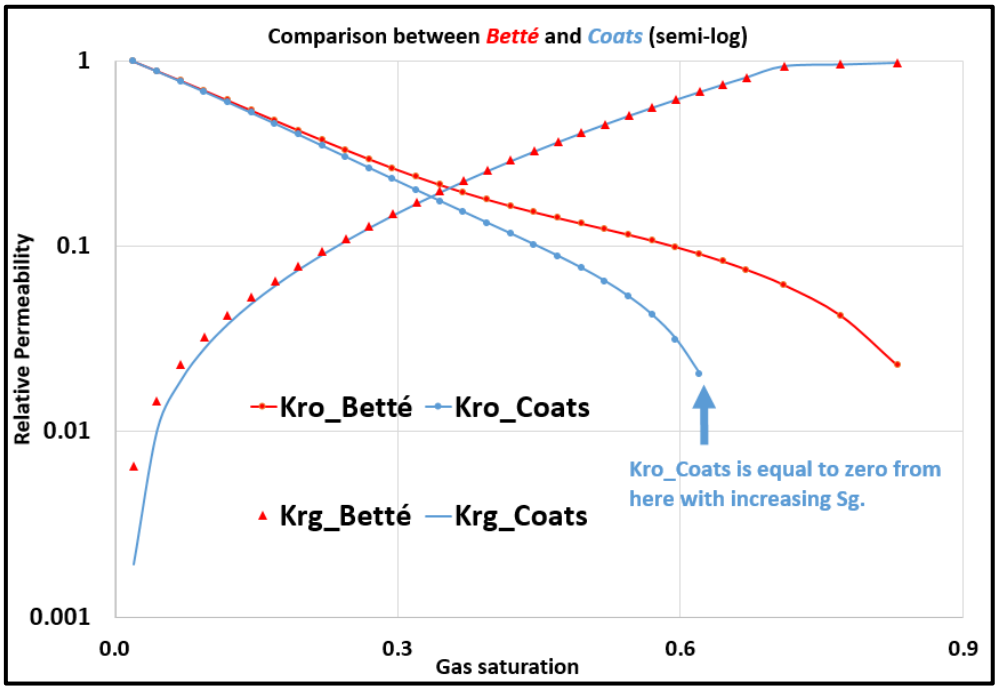

Figure 4-3 An example of relative permeabilities with a $\sigma_{go}/\sigma_{go}^{0}$ ratio of 0.1.

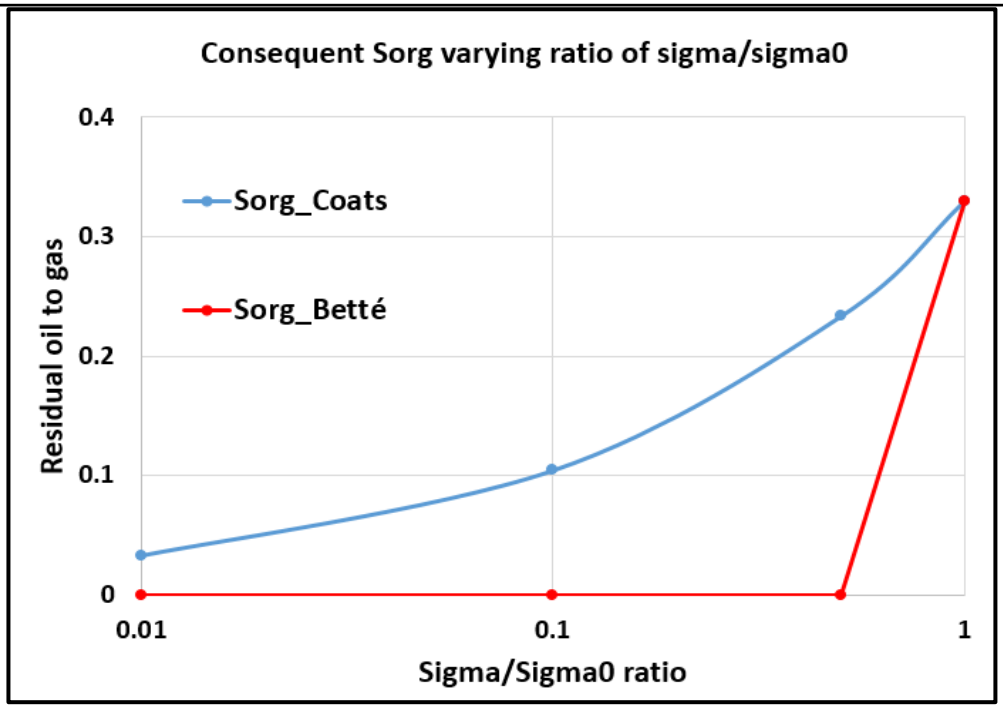

Figure 4-4 Residual oil to gas as a function of $\sigma_{go}/\sigma_{go}^{0}$ ratio.

In fact, such M_{IFT}-induced features of relative permeabilities can be easily masked by the dominant compositional effects (M_{CE}), i.e. oil stripping, which is able to extract oil further below the residual saturation under certain conditions. Results will be presented from a series of numerical simulations to assess and differentiate the impacts of the M_{CE} and M_{IFT} mechanisms on the flow behaviour during CO_2 injection. The possible discrepancy of the simulation results were investigated between these two models, i.e. Betté et al. (1991) and Coats (1980), in order to improve the modelling of the transition from immiscible to miscible oil displacement by CO_2.

4.2.2 Injection strategy

As shown in the Section 3.4, the displacing front is unstable (as expected) during the continuous injection of CO_2, which leads to a great amount of bypassed oil. In order to achieve a better displacement performance, WAG injection, which is commonly applied in practice to improve the mobility control when fingering flow occurs, has been tested and analysed using the injection strategy shown in Table 4-1. Note the aim of this thesis is not to optimise the injection scenario to maximise the oil recovery. For this reason, a typical injection strategy is applied throughout the rest of the analysis in this thesis. In addition, only the fingering flow regime (triggered by Model A shown in Figure 3-2) will be the focus in the following chapters. This is because the regime of channelling flow is dominantly driven by the permeability field rather than the key physics of interest.

Continuous 1PVI	1 PVI continuous CO_2 injection at reservoir conditions				
WAG	1st water cycle	1st gas cycle	2nd water cycle	2nd gas cycle	3rd water cycle
2PVI	0.4 PVI water	0.4 PVI CO_2	0.4 PVI water	0.4 PVI CO_2	0.4 PVI water

Table 4-1 Injection strategy.

4.3 Pseudo tracer analysis

The tracer analysis is not directly available with our simulator when performing compositional simulations (CMG, 2019). Therefore, a pseudo tracer simulation was carried out to demonstrate some of the mechanistic flow features in our 2D models. Specifically, when it was suspected from our original simulations that viscous crossflow (Zapata and Lake, 1981; Sorbie and Skauge, 2019) may be an important mechanism in near-miscible WAG process, we wished to test this hypothesis directly by labelling the bypassed oil after the first gas flood. This analysis involved injecting a certain amount of tracer oil, which had same EOS data as initial oil. The "C_8 to C_{12}" (the component with the most mole fraction) was renamed as C8* and served as a tracking target. All the other simulation parameters were the same as the ones in previous simulations. The main details of the design of the tracer simulations are as follows:

1. All EOS parameters of this tracer oil (C8*) were exactly same as the initial oil, thus the oil phase behaviour was identical.
2. The tracer oil was injected into a chosen position in a ***non-preferential*** (bypassed) flow route (identified from 2D simulations without injecting tracer first), with the aim of tracking the flow behaviour in the bypassed zone.
3. Tracer was ***not*** injected at the start of the WAG floods (at t =0) in order to minimize the impacts from the initial water cycle, where the stable displacing front can greatly distribute the tracer and therefore complicate the investigation the IFT effects. A very small amount of tracer was injected into the chosen bypassed grid block at a rate of 1/12000 PV/hour for 2 hours (1/6000 PV in total). Such injection was conducted either at the beginning of the simulation for the CO_2 continuous injection floods (i.e. at t= 0) or the beginning of the first gas cycle during WAG (i.e. at t =0.4 PV). We found that such a slow and small amount of tracer injection had a negligible impact on the overall flow pattern, compared with the simulations with no tracer.
4. The whole tracer injection process was designed to avoid any contacts with CO_2 to guarantee C8* only exists in the oil phase before the injected CO_2 arrives.

Results will now be presented from a series of numerical simulations to assess and differentiate the impacts of the M_{CE} and M_{IFT} mechanisms on the flow behaviour and oil displacement characteristics during CO_2 injection. We investigate any possible differences in simulation results from the two models which describe the M_{IFT} mechanism, i.e. Betté et al. (1991) and Coats (1980), in order to improve the modelling the transition from immiscible to miscible oil displacement by CO_2. To follow the structure and logic of these tests, the results are presented in seven steps/sections outlined in Table 4-2.

Section	Model dimension	Injection scheme & Mechanisms included	Objective
4.4.1	1D	Continuous CO_2 injection: 1. Neither M_{CE} nor M_{IFT} 2. M_{IFT} acting only (non-physical)	To assess the impact of M_{IFT} on the oil recovery in a typical 1D model during immiscible continuous injection.
4.4.2	2D areal	Continuous CO_2 injection: 1. Neither M_{CE} nor M_{IFT} 2. M_{IFT} acting only (non-physical)	To investigate the impact of M_{IFT} on the oil recovery during immiscible continuous injection.
4.4.3	1D	Continuous CO_2 injection: 1. M_{CE} acting only 2. Both M_{CE} and M_{IFT}	To determine the threshold value of interfacial tension for modelling IFT effects.
4.4.4	2D areal	Continuous CO_2 injection: 1. M_{CE} acting only 2. Both M_{CE} and M_{IFT}	To investigate the combined impact of M_{CE} and M_{IFT} on the oil recovery during near-miscible continuous injection.
4.4.5	2D areal	CO_2-WAG 1. M_{CE} acting only 2. Both M_{CE} and M_{IFT}	To investigate the combined impact of M_{CE} and M_{IFT} on the oil recovery during near-miscible WAG displacement.
4.4.6	Tracer analysis (2D)	Continuous and CO_2-WAG 1. M_{CE} acting only 2. Both M_{CE} and M_{IFT}	To investigate the role of viscous crossflow in the recovery of bypassed oil.
4.4.7	Sensitivity analysis (2D)	CO_2-WAG 1. M_{CE} acting only 2. Both M_{CE} and M_{IFT}	To investigate the impact of 3-phase relative permeability models on the predictions of oil recovery.

Table 4-2 Outline of numerical tests performed and objectives of each stage for this chapter.

4.4 Results and Discussion

4.4.1 Preliminary 1D test on IFT effects at immiscible conditions (non-physical)

The first set of simulations studied IFT effects (M_{IFT}), in the absence of compositional effects (M_{CE}). This is an artificial scenario, but is useful for gaining an understanding of IFT effects. The simulations were performed at a pressure of 70 bar, which was below the minimum miscibility pressure (MMP). In order to determine a suitable threshold value of σ_{go}^{0} to use when modelling IFT effects to reflect the "film flow" mechanism (M_{IFT}), a representative cell (3/10 of the 1D system length from the slim-tube injector) was selected to track its IFT throughout the whole process of immiscible displacement. The choice of the threshold value used in this study is based on results by. As shown in Figure 4-5, IFT first decreases from 7 mN/m to 3 mN/m and then increases again up to about 5 mN/m (because of CO_2 dissolution and minor stripping). Therefore, to illustrate the effects of the IFT only in this immiscible displacement, a range of threshold values (from 5 mN/m and 10 mN/m) has been tested to analyse their effects on the oil recovery. In addition, the threshold was set to 100 mN/m, in order to examine an extreme (non-physical) case where the IFT effect is "switched on" throughout the displacement rather than only in the notional "near-miscible" region. Here, I simulated the immiscible displacement to minimize the compositional effects, but emphasize the IFT effects through testing a set of larger threshold values. This (unrealistic) case would be case C (M_{IFT} only) in the schematic phase diagram in Figure 4-1.

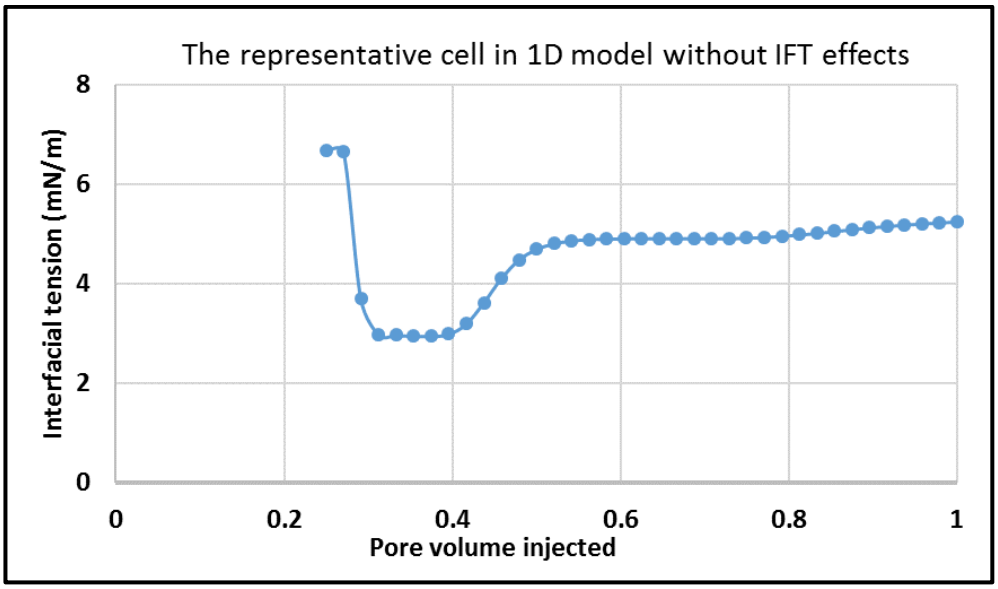

Figure 4-5 IFT in the representative cell at immiscible conditions.

The results in Figure 4-6 show that, as expected, for this M_{IFT} only case, the greater the value of σ_{go}^0, the better the ultimate oil recovery is achieved in both models. At the same time, the discrepancy between the two models also decreases with threshold IFT value. This is because the residual oil saturation in the Coats model is getting closer to 0 with increasing σ_{go}^0 (i.e. decreasing $\sigma_{go}/\sigma_{go}^0$ ratio). Very importantly, it is found that even with the threshold value of 100 mN/m (the IFT effects act under all conditions in the displacement), the oil recovery is 76%, which is much less efficient than a typical near-miscible 1D test (close to 90%).

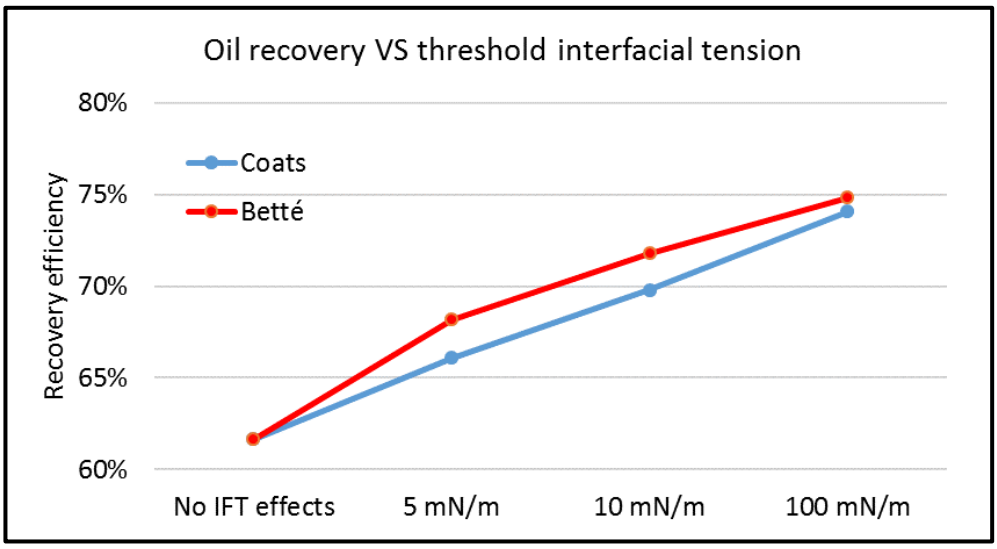

Figure 4-6 Recovery factor using various threshold value, σ_{go}^0.

On the other hand, it is rather surprising that there is only a limited difference in the oil recovery (no more than 3%) between the two models. It was conjectured that this small difference in recovery is probably due to the fact that the oil relative permeability caused by IFT effects is too small to enable oil to flow through this 50m-long 1D model. In order to test this conjecture, I extended the 1D simulations to reach 2PV and then even 10PV of CO_2 injection with a σ_{go}^0 value of 10 mN/m. This tests the case where the two models could possibly make significantly different predications. As seen in Figure 4-7, the discrepancy increases quite significantly with injected pore volume and reaches about 10% after 10PV of CO_2 injected. It therefore can be concluded here that, the two models generally agree with each other when a system is highly miscible, i.e. very small $\sigma_{go}/\sigma_{go}^0$ ratio (e.g. 0.001 in a first-contact miscible system), with limited CO_2 injection. However, such a discrepancy can be amplified by the increasing injected pore volume, particularly during the transition from immiscibility to miscibility, i.e. $\sigma_{go}/\sigma_{go}^0$ ratio at a magnitude of 0.01-0.1 in a near-miscible system. This is because the different treatment of oil

relative permeability between two models is mainly focused on the control of the residual oil zone, where the oil relative permeability is very low and can only be detected through high PV of gas injection.

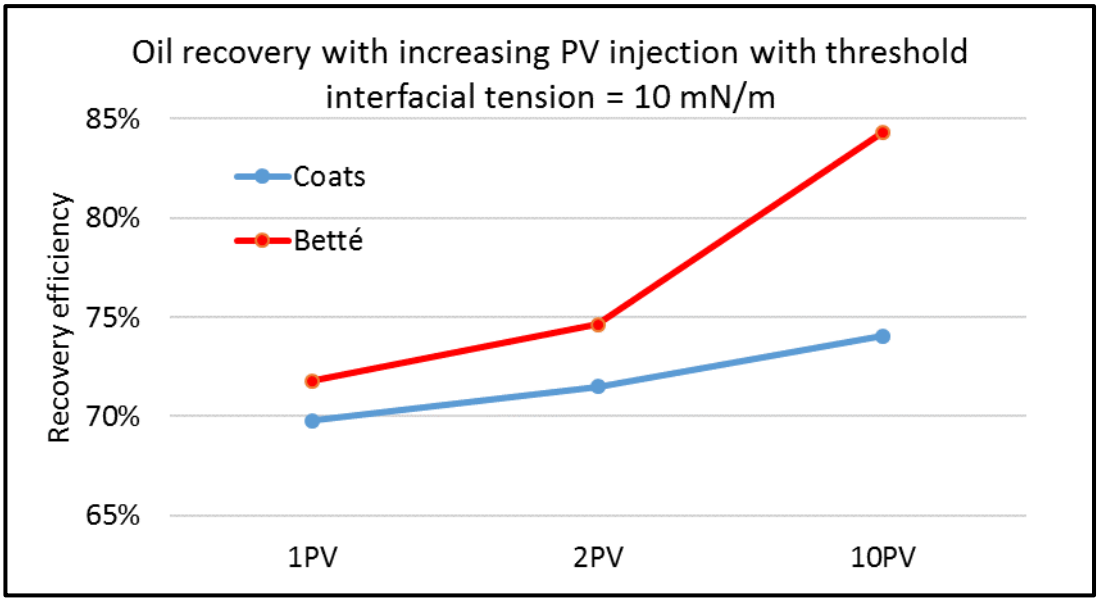

Figure 4-7 Recovery factor from cases varying injected pore volume with fixed value of σ_{go}^{0}=10 mN/m.

In order to evaluate the significance of IFT effects using both models when viscous instability and heterogeneity are involved, σ_{go}^{0} was set to 10 for the subsequent 2D areal immiscible CO_2 displacement. Therefore the smallest ratios of $\sigma_{go}/\sigma_{go}^{0}$ is about 0.3 leading to a residual oil saturation of 0.18 using Coats model. Note that σ_{go} is not constant throughout the injection process due to component mass transfer, which is very weak at immiscible conditions but strong at near-miscible conditions.

4.4.2 Impact of M_{IFT} on the oil recovery during continuous injection at immiscible conditions (non-physical)

Figure 4-8 shows the fluid distributions after 0.5PV of CO_2 injection under purely immiscible conditions (no IFT), and with IFT effects for the value of σ_{go}^{0}= 10 mN/m. As expected, fingering flow occurs in the system due to the unfavourable mobility ratio. For the same amount of CO_2 injection at reservoir conditions, cases with IFT effects show slightly decreased macroscopic sweep efficiencies. This is because the oil mobilized by IFT effects can then be recovered allowing more gas to flow into these regions. The consequent higher gas saturation leads to more aggressive gas fingers and therefore aggravates the imbalance of the fluid flow between preferential routes in the gas fingers (as indicated by oval shapes in Figure 4-8) and the non-preferential bypassed routes. As

a consequence, the results in Figure 4-9 show that the oil in the non-preferential routes is even more poorly recovered (i.e. bypassed) than the base case (no IFT effects), whereas the oil in the preferential routes can be more efficiently produced.

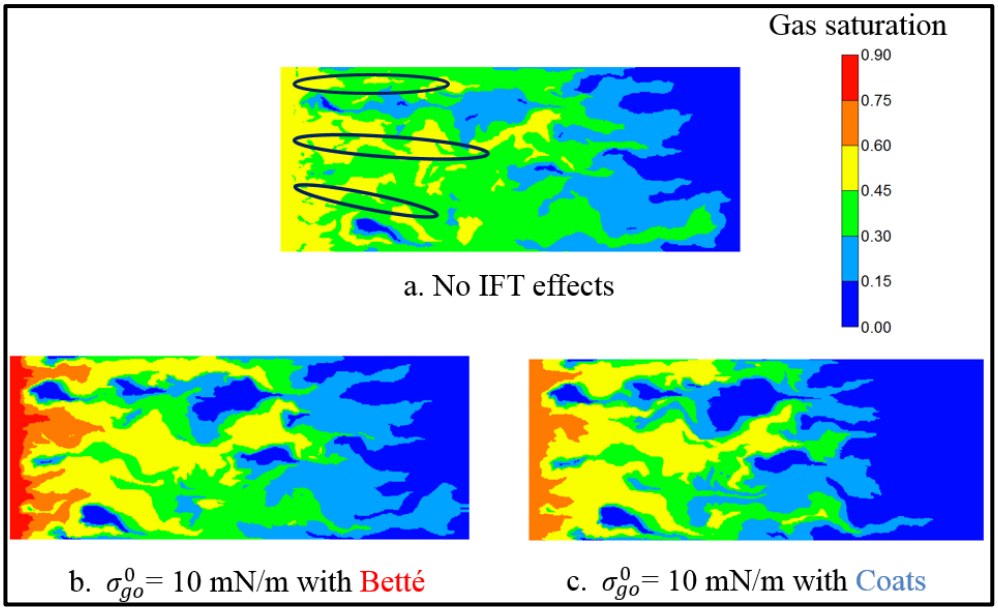

Figure 4-8 Snapshots of gas saturation with 0.5PVI of CO_2 at immiscible conditions.

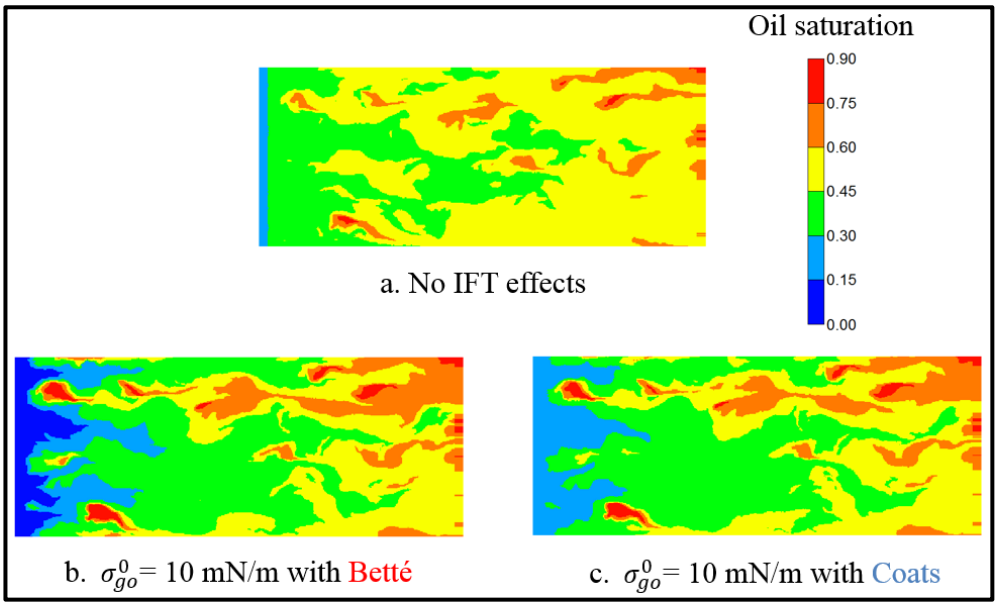

Figure 4-9 Snapshots of oil saturation with 1PVI of CO_2 at immiscible conditions.

As seen in Figure 4-10, the combined IFT effects of poorer sweep but lower remaining oil in the preferential paths lead to a very limited improved oil recovery compared to the base case without IFT effects (Betté: 4.1%, Coats: 2.9%). In addition, the local displacement efficiency in the preferential routes near the injector is slightly better based on the Betté model than on the Coats model. This is simply because of the different

treatment of residual oil saturation between two models and matches our observations made in the previous slim-tube section. However, this discrepancy does not make much difference in the oil recovery between the two models after 1 PVI, which is a typical volume for continuous CO_2 injection in laboratory (Betté *et al.*, 1991). This is because, even with the Betté model, the newly mobilized oil is still of very low permeability and therefore not sufficient to be recovered with a certain amount of continuous CO_2 injection (see Figure 4-10).

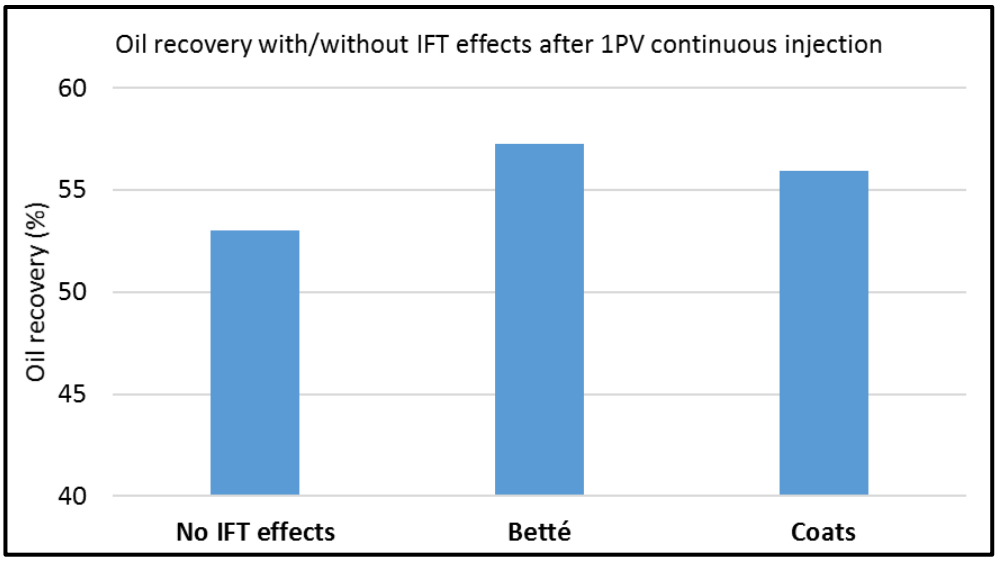

Figure 4-10 Oil recovery with/without IFT effects at immiscible conditions after 1PV CO_2 continuous injection.

4.4.3 Determination of threshold value for modelling IFT effects at near-miscible conditions

Simulations that minimized the oil-stripping effects (M_{CE}) but included and exaggerated the IFT effects (M_{IFT}) on the flow behaviour in a fingering flow regime have been presented in the previous section. This provided a better understanding of the magnitude of the impact, which IFT effects might have on flow behaviour. Now, the near-miscible displacement (P = 120 bar) is simulated with various levels of IFT effects to investigate the combined outcome from both mechanisms (M_{CE} & M_{IFT} shown in Figure 4-1). Figure 4-11 shows the calculated grid block IFT throughout the 1D simulations in a representative cell for the near miscible displacement; the immiscible IFT values from Figure 4-5 are also shown for comparison.

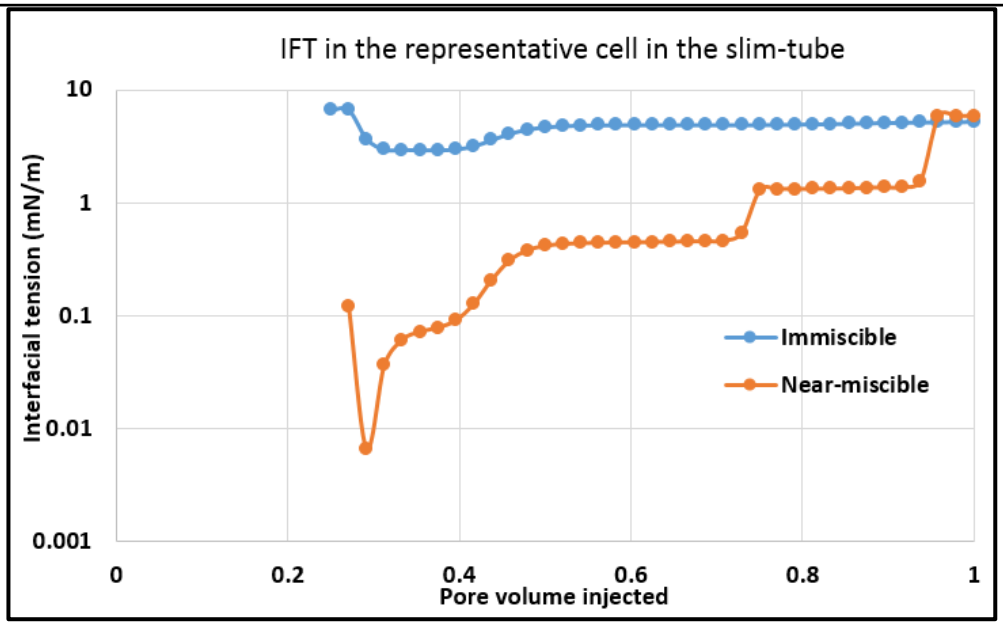

Figure 4-11 IFT in the representative cell at near-miscible conditions.

The results in Figure 4-11 (orange line) show that or the near-miscible flooding case clearly lead to a much wider range of IFT values during the whole process (from 0.01 to 7 mN/m). In the early stages of the displacement, CO_2 and oil are approaching miscibility through the mass transfer process, and IFT sharply decreases. In fact, the lowest IFT occurs at the point where gas and oil composition are most similar. In other words, this moment corresponds to the point that gas and oil composition are closest to each other in the ternary diagram, as shown in Figure 3-9 (green oval). With further contacts between CO_2 and oil, σ_{go} again increases and the fluids become immiscible. This is because the light-medium oil components have been mostly vaporized leaving the remaining oil consisting mainly of heavy components. This phenomenon has been extensively described in Chapter 3. The lowering of the IFT, which is a consequence of the compositional effects (M_{CE}), also leads to an increased oil relative permeability (M_{IFT},) as soon as $\sigma_{go} < \sigma_{go}^{0}$. In addition, these effects impose a further complexity as they must also interact with the flow behaviour in heterogeneous systems in the preferential and non-preferential flow paths. It has been clearly demonstrated that "***different mechanisms work in different places for different processes***".

Again, a range of σ_{go}^{0} values was tested to analyse the role of M_{IFT} mechanism on the ultimate oil recovery in the near-miscible 1D oil displacements by continuous CO_2 injection. As shown in Figure 4-12, the IFT effects on the near-miscible displacement in the 1D model were found to be minor regarding the oil recovery. This is simply because the oil-stripping effects (M_{CE}) have already been able to recover most of the oil in the 1D

system and therefore leaving little target oil saturation for IFT effects (M_{IFT}) to work on. Therefore, the discrepancy between the two models under near-miscible conditions is also negligible. What should also be highlighted here is that the remaining oil saturation mostly consists of the heavy components (higher viscosity) with very poor mobility (which also leads to the increasing IFT as the flood progresses). This will further hinder the oil phase flow (poor mobility), leading to a fairly limited incremental oil recovery. In other words, the oil stripping effects (M_{CE}) have greatly masked and restricted IFT effects (M_{IFT}) and are therefore dominant during the oil displacement by CO_2 (continuous injection) in 1D tests under near-miscible conditions. It was noted above that Betté et al. (1991) had already described this effect. However, given the findings below, they did not point out that 1D experiments are actually a very poor way of examining the IFT effects (the M_{IFT} mechanism) in continuous gas injection; worse still, such experiments actually ***miss*** these effects.

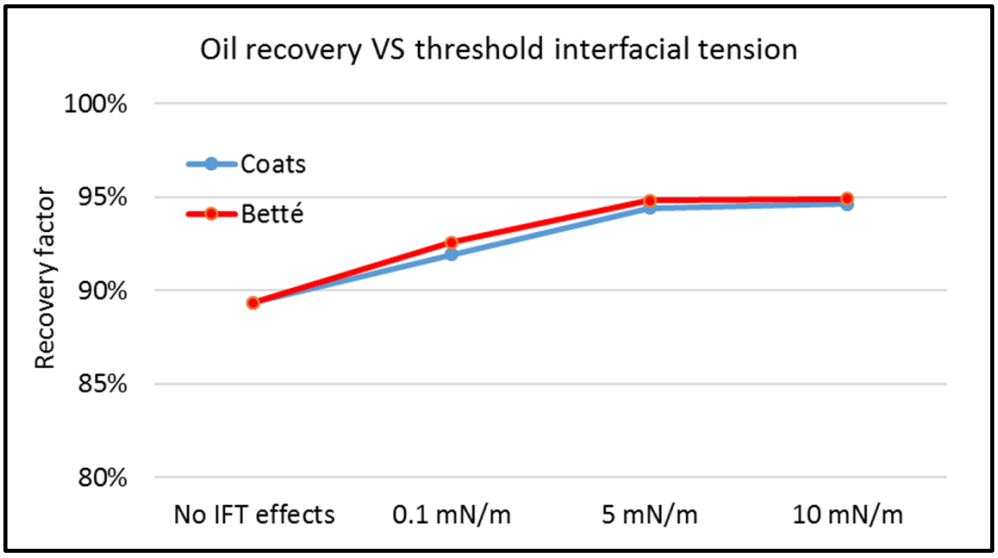

Figure 4-12 Recovery factor vs time for various values of σ_{go}^{0}.

4.4.4 Combined impact of M_{CE} and M_{IFT} on the oil recovery during continuous injection

In fact, IFT effects are commonly either ignored or simulated with a very low value of threshold, such as 0.001 mN/m (fully miscible conditions). However, according to Sohrabi et al. (2004) and Sorbie and van Dijke (2010), oil layer flow is an important flow mechanism during near-miscible gas displacement. They found that although gas-oil interfacial tension is not ultra-low (e.g. at a level of σ_{go}~ 1-3 mN/m), significant oil flow can still be observed through oil layer drainage. In order to reflect their theory and

evaluate the significance of such effects, the threshold IFT, σ_{go}^{0} in our simulations is set to 5 mN/m for the following 2D areal near-miscible CO_2 displacements. That is to investigate the effect of combined mechanisms (M_{CE} and M_{IFT}) on the flow behaviour, when viscous instability and heterogeneity are involved.

Figure 4-13 shows a snapshot of the gas distribution in the system after 0.5 PV of CO_2 injection and Figure 4-14 shows the remaining oil distribution after 1PV of CO_2 injection; the cases shown are for the near-miscible case (fixed M_{CE}) with/without IFT effects (with/without M_{IFT}). A comparison of Figure 4-8a and Figure 4-13a shows how the oil-stripping mechanism affects flow behaviour. For the same pore volume of CO_2 injected, the gas saturation is much higher in the near-miscible case than in the immiscible case in the preferential routes (as indicated by the oval shapes). Under near-miscible conditions, the oil components have been mostly vaporized into the CO_2 and thus flow in the gas phase. As a result, the greatly increased gas saturation will form more aggressive gas fingers under near-miscible conditions than under immiscible conditions. More interestingly, IFT effects mobilize some oil, which leads to a slightly worse macroscopic sweep efficiency. Both mechanisms are working in tandem to recover the oil in the preferential routes (as indicated by the oval shapes) but forming more severe gas fingers at the same time, as seen in Figure 4-13 (a-c). As a result, the oil in the preferential routes can be more efficiently produced, whereas the oil in the non-preferential routes is even more poorly recovered than in the base (Figure 4-15). The results in Figure 4-15 show that the oil recovery after 1PVI has been modestly increased by the IFT effects (3 - 4%), but only by a very limited amount due to viscous instability forming dominant gas fingers. As expected, there is a minor dicrepancy regarding the ultimate oil recovery between Betté and Coats, due to the dominant stripping effecects (oil components flow in gas phase). Both of them are showing that there is a significant amount of bypassed oil in the non-preferential routes.

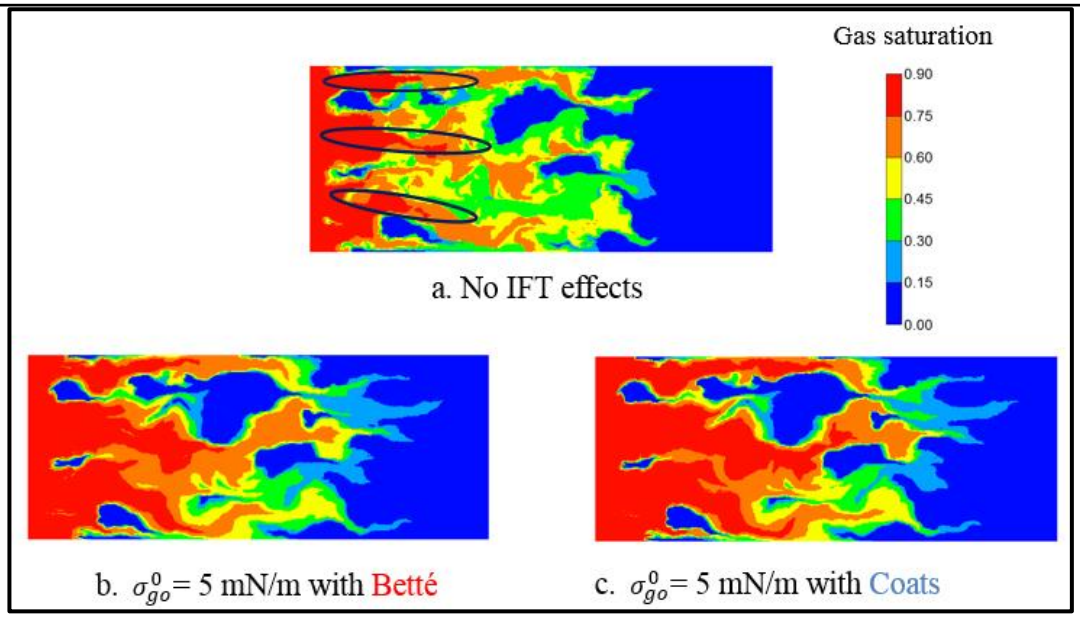

Figure 4-13 Snapshots of gas saturation with 0.5PVI of CO_2 under near-miscible conditions.

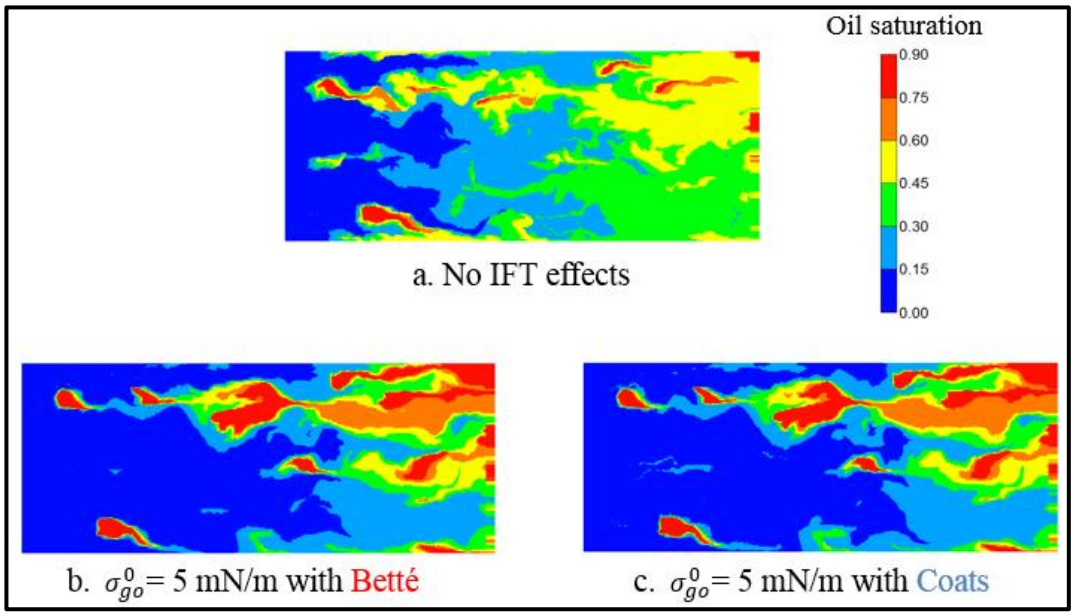

Figure 4-14 Snapshots of oil saturation after 1PVI CO_2 under near-miscible conditions.

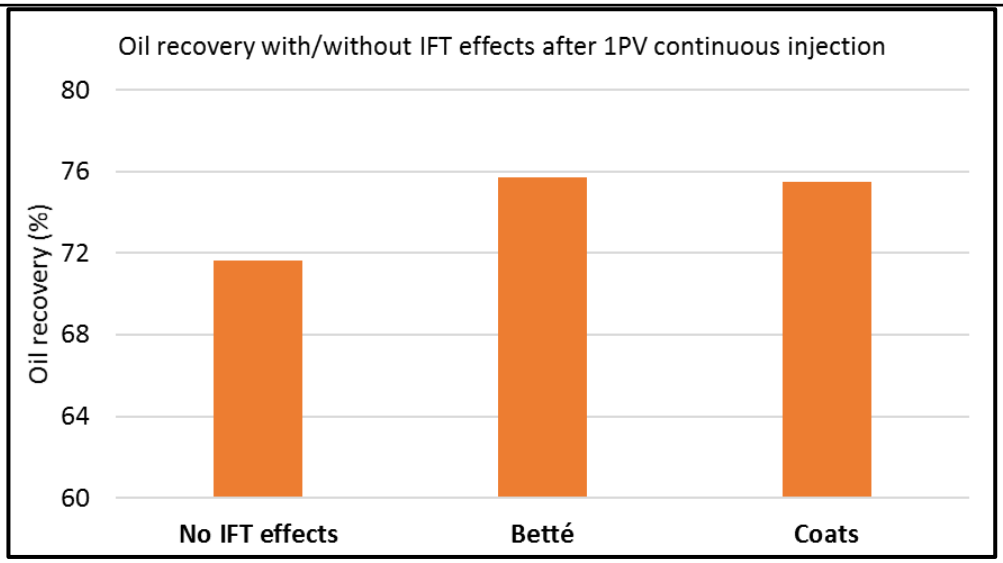

Figure 4-15 Oil recovery after 1PV continuous CO_2 injection with/without the account of IFT effects (σ_{go}^{0}= 5 mN/m).

The issue of the oil left in the non-preferential routes is resulted from the dominant gas fingers. The analysis of these interactions between oil stripping/compositional effects (M_{CE}) and IFT effects (M_{IFT}) has led me to consider WAG injection, which is expected to improve the stability of the displacing front. Therefore, a range of numerical simulations of near-miscible WAG displacement with the aforementioned injection strategy (Table 4-1) was conducted with/without IFT effects as shown below.

4.4.5 Combined impact of M_{CE} and M_{IFT} on the oil recovery during CO_2-WAG injection

At this stage, the Stone 2 model was used to model the oil relative permeability serving as a base case. Other typical 3PRP models, such as Stone 1 and Baker saturation weighted method, were tested to avoid the possible biased results due to the choice of 3PRP models. The analysis of this sensitivity test is presented in section 4.4.7.

Figure 4-16 (Betté) and Figure 4-17 (Coats) show the remaining oil saturation at various stages of the WAG simulations comparing near-miscible cases (always with M_{CE} acting) both with and without the IFT effects (M_{IFT}) included. The figures on the left (a-d) show the results without IFT effects (M_{CE} only), and those on the right (e-h) with IFT effects (combined M_{CE} and M_{IFT}). As expected, WAG is able to efficiently improve macroscopic sweep with/without IFT effects. Very importantly, both the Betté and the Coats model give the same prediction that the overall displacement performance is significantly enhanced through the IFT effects (M_{IFT}). In contrast to the case of continuous injection, the local displacement efficiency, particularly in the non-preferential routes, can be very

effectively improved in the case of WAG displacement. As seen in Figure 4-18 and Figure 4-19, it was also found that the recovery from the second water and second gas injection cycle have been instantly and greatly improved due to the additional IFT effects (M_{IFT}). Note that a range of threshold values of interfacial tension (0.1~5mN/m, denoted as T in figures below) and the exponent value (0.1~0.5, denoted as E in figures below) for the calculation were tested to assess the possible impacts of the enhanced oil relative permeability on the oil recovery. Taken the threshold value of 5 mN/m and exponent value of 0.5 as an example, the improvement due to the M_{IFT} mechanism in the oil recovery is up to approximately 14% as shown in Figure 4-20.

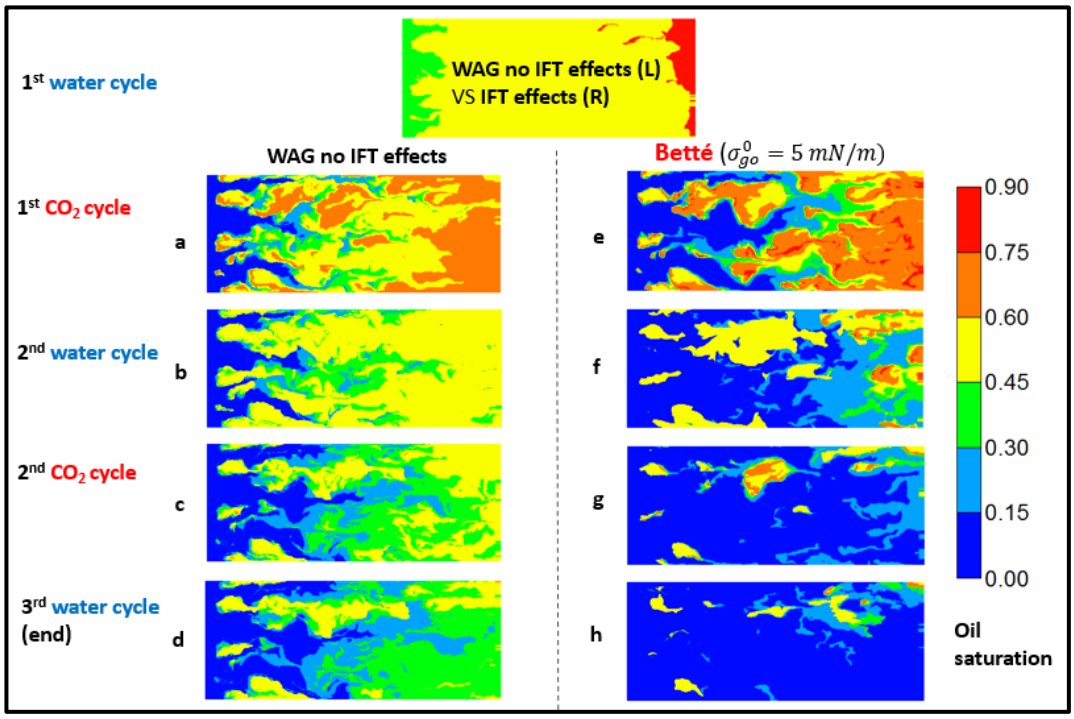

Figure 4-16 Track of remaining oil saturation throughout the 2PVI of WAG based on Betté model.

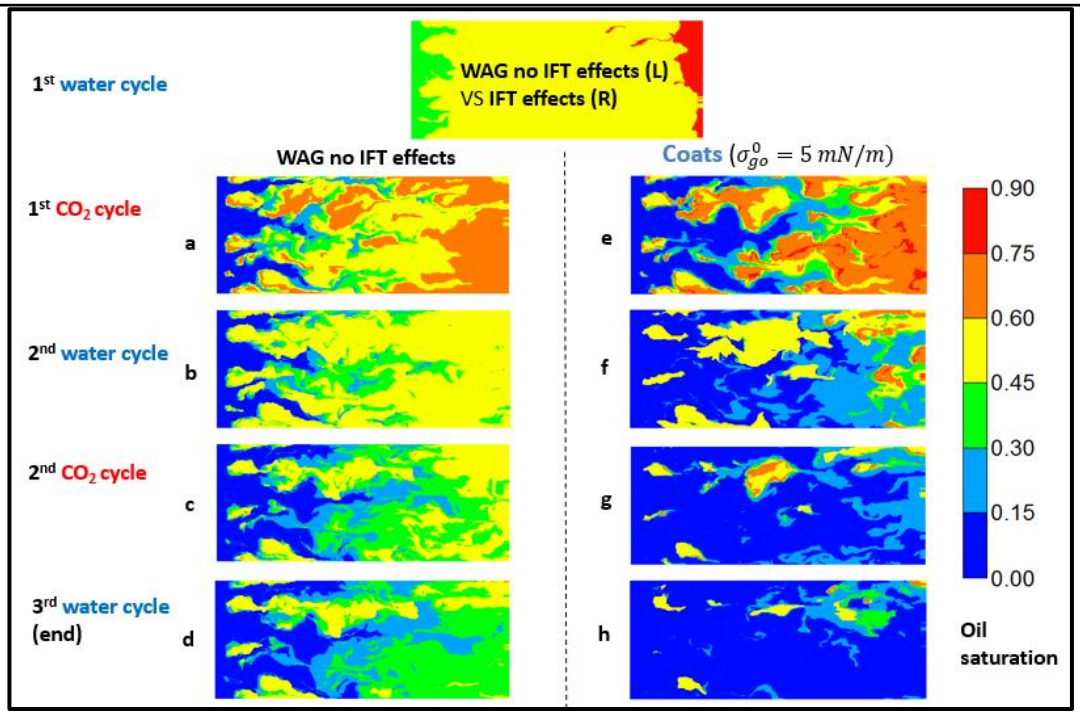

Figure 4-17 Track of remaining oil saturation throughout the 2PVI of WAG based on Coats model.

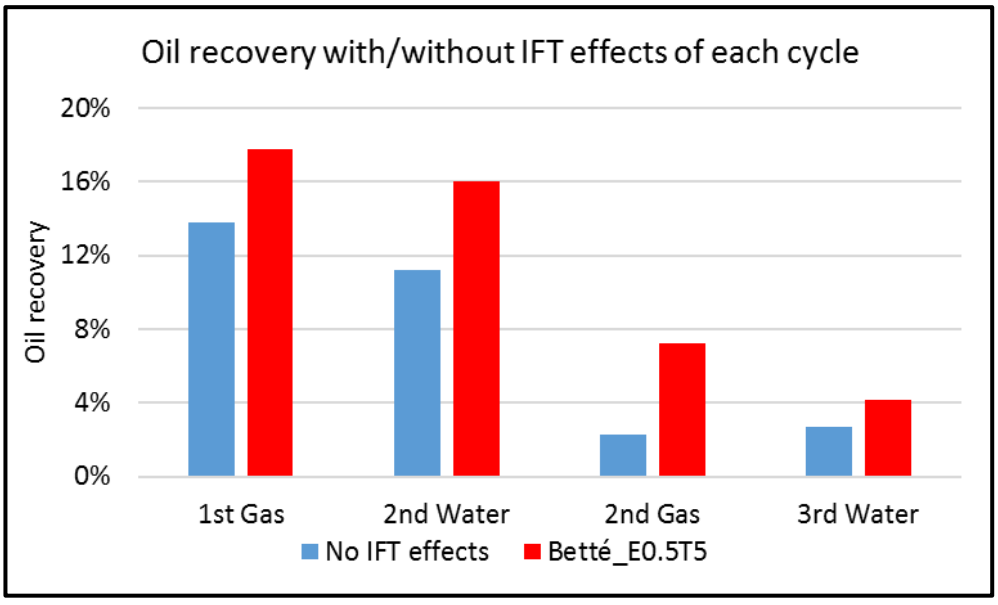

Figure 4-18 Incremental oil recovery of each cycle due to IFT effects based on Betté model.

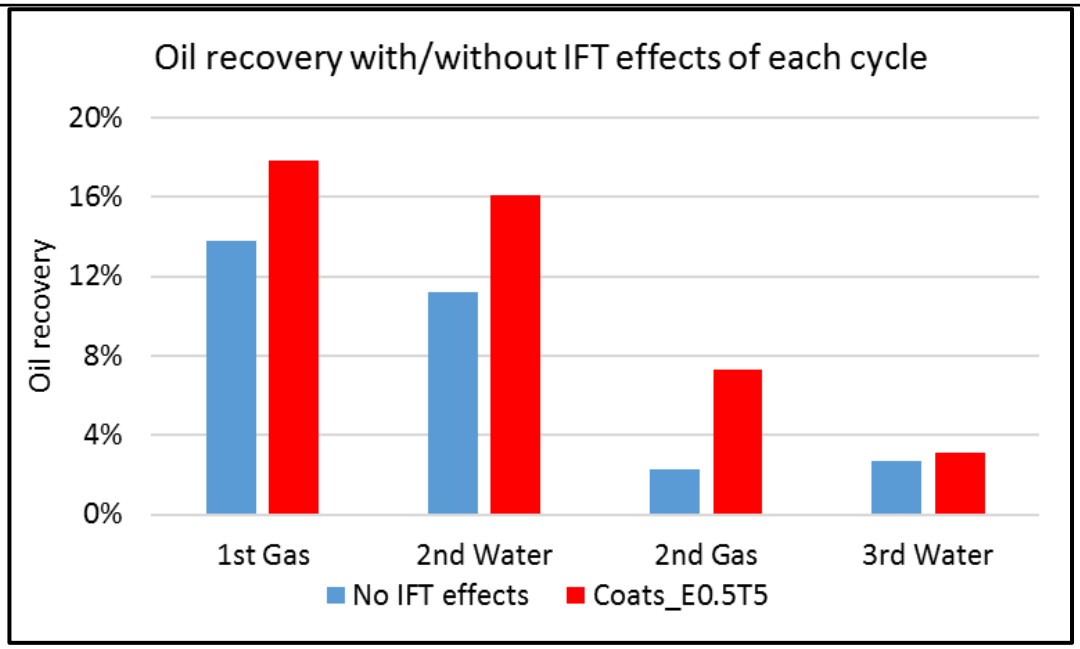

Figure 4-19 Incremental oil recovery of each cycle due to IFT effects based on Coats model.

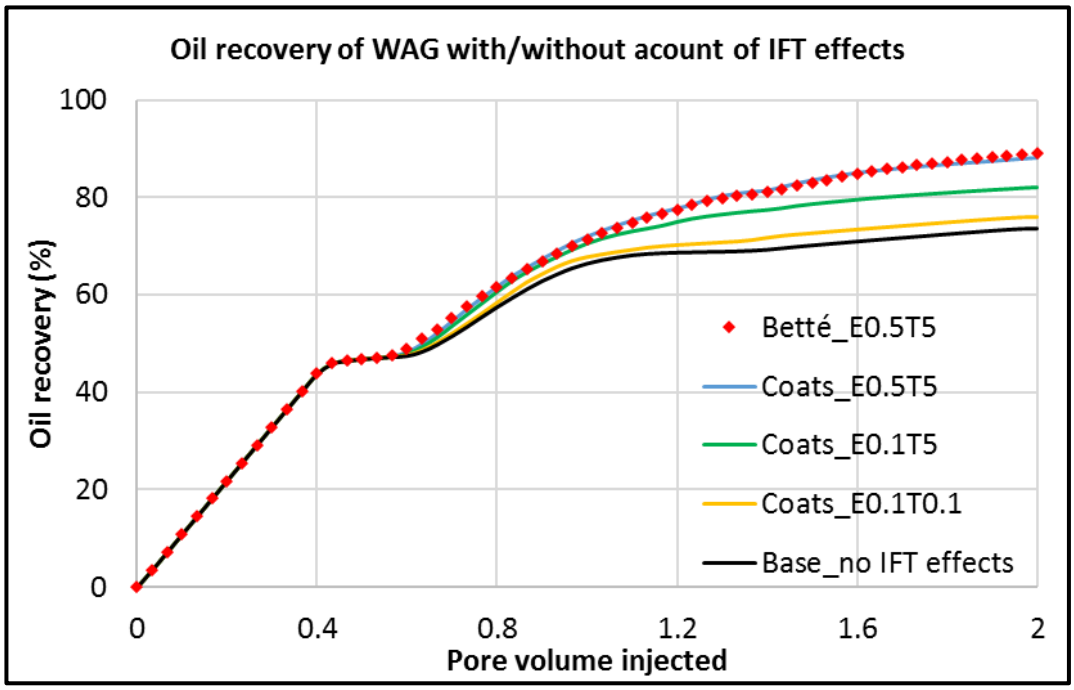

Figure 4-20 Oil recovery with/without the account of IFT effects with varius values of exponent (E) and threshold IFT (T).

Now the question is how do IFT effects significantly improve the displacement performance in non-preferential routes? To answer this question, I select two representative cells (3/10 of the system length from the injector) shown in Figure 4-21, one in a preferential route (indicated as a square shape) and the other in a non-preferential route (indicated as a triangular shape). The parameters of phase flow velocity and interfacial tension were tracked throughout the whole injection process for these two cells (several pairs of cells were studied but results for just one typical pair is presented here).

The investigation of IFT effects is based on the Coats model with an exponent (E) of 0.5 and threshold value of 5 mN/m.

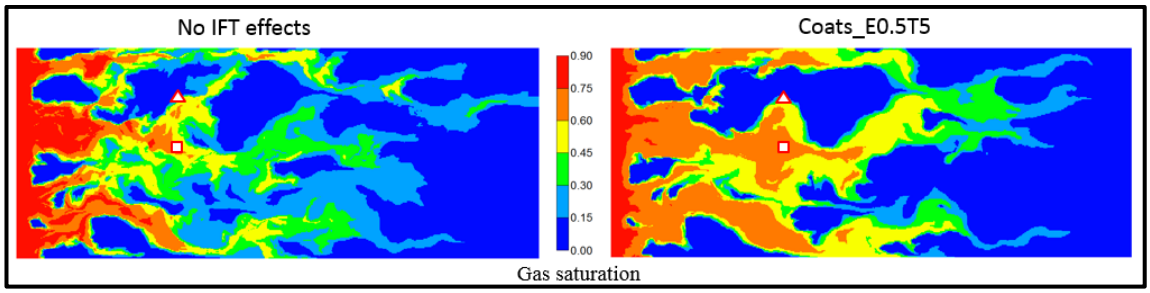

Figure 4-21 Gas saturation at the end of first gas injection cycle: No IFT effects (L) & with IFT effects (R).

As seen in Figure 4-22, the oil velocity out of the cell in the non-preferential route has been greatly increased by the IFT effects during the second water cycle (0.8-1.2 PVI). In contrast to the oil-stripping effects (M_{CE}), the IFT effect (M_{IFT}) is not dependent on continuous contact between oil and CO_2. Instead, the remaining oil is mobilised by IFT relative-permeability effects and can be efficiently produced by the subsequent water injection. Moreover, there has been no increase in the gas velocity in the cell in the non-preferential route, which further indicates that the improved oil displacement performance has be resulted from the IFT effects (M_{IFT}) rather than stripping effects (M_{CE}). Note that the water velocity is lower than that of oil velocity but not as much as an order of magnitude. In the next section, I will demonstrate that this improvement in oil recovery from the non-preferential paths is due to a local viscous crossflow mechanism, which is prevalent during the water cycle following the gas cycle.

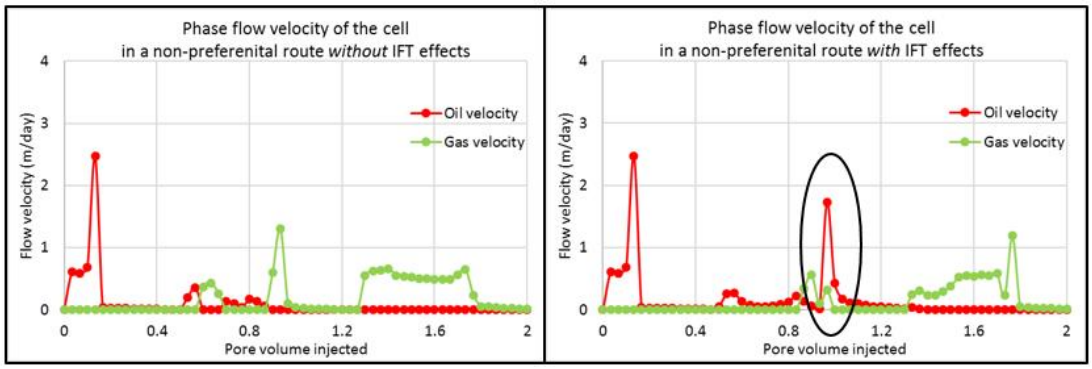

Figure 4-22 Phase velocity of the cell in a non-preferential route: No IFT effects (L) and with IFT effects (R) based on Coats model.

It was also found that the magnitude of σ_{go} in the preferential route was generally greater than in the non-preferential route. This is because of the fact that the two cells are at

unequal stages of oil stripping effects, i.e. the preferential route is at a later stage than the non-preferential route (Figure 4-23). For this reason, the incremental oil mobility due to IFT effects is much less in the preferential route than in the non-preferential route. Besides that, the local displacement performance is already very efficient in the preferential route even without the IFT effects. As seen in Figure 4-24, there has been very limited change in the oil velocity during the first gas cycle (0.4-0.8 PVI) and no increase during the rest of the injection. Therefore, I conclude that IFT effects have presented very limited impact in the preferential routes, particularly when oil-stripping effects are dominant. This further demonstrates why continuous gas injection without WAG is less efficient than applying near-miscible WAG.

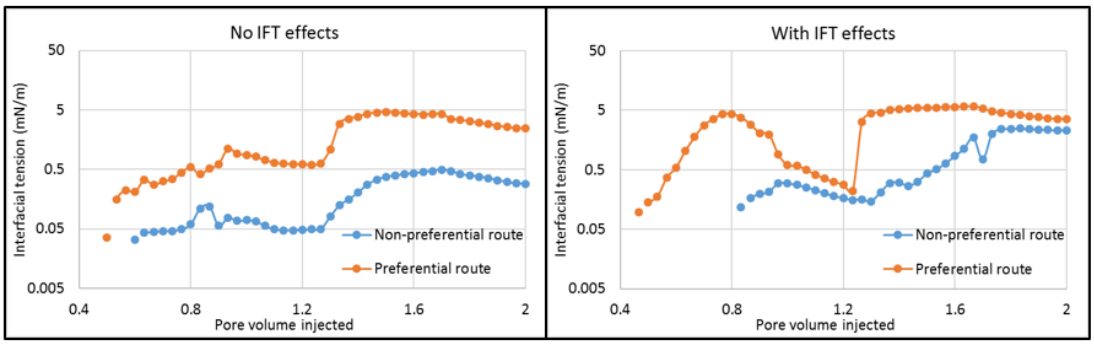

Figure 4-23 Comparison of the interfacial tension of representative cells: No IFT effects (L) and with IFT effects (R) based on Coats model.

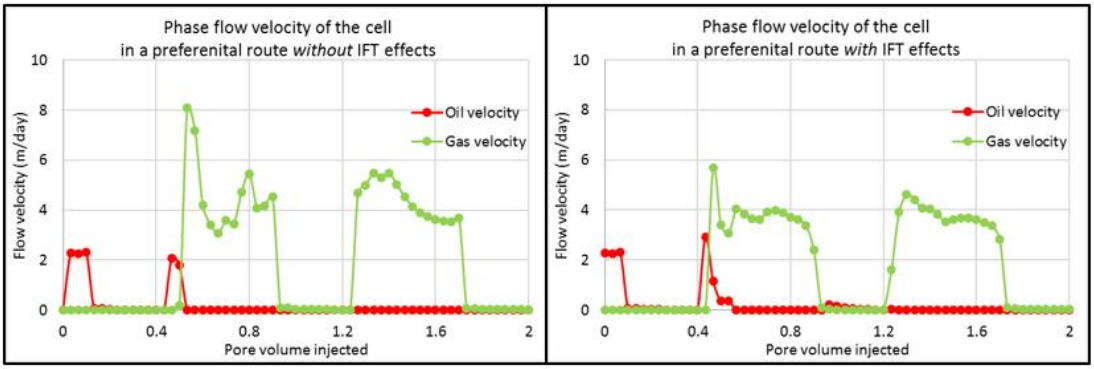

Figure 4-24 Phase velocity of the cell in a preferential route: No IFT effects (L) and with IFT effects (R) based on Coats model.

The significance of the IFT effects (M_{IFT}) during near-miscible CO_2-WAG injection has been clearly identified so far. Now it is important to address the question of: how can M_{IFT} effectively change the flow pattern during WAG displacement but have much reduced impact on the flow behaviour during the continuous CO_2 displacement in my case? The reason to address this issue explicitly is that, although oil can be mobilized by IFT effects and be displaced by a stable displacing front, the consequent oil relative permeability (near the zone of residual oil) is still very low. Therefore, I might expect

that it should take a long time (or much injection) to be extracted; but this is evidently not the case.

As seen in Figure 4-18 to Figure 4-20, both models give the same prediction that M_{IFT} can have an immediate effect and the oil recovery has been quickly and efficiently enhanced during the second water cycle (0.8PV-1.2PV) and second gas cycle (1.2PV-1.6PV). This implies that there must be some other flow features triggered/amplified by IFT effects in our 2D heterogeneous models. In fact, it was conjectured that this very efficient recovery mechanism looked rather like viscous crossflow. To test this hypothesis, a tracer analysis was performed using the method stated previously to investigate the flow trajectory of the oil in the non-preferential routes (i.e. the bypassed oil). Since there was negligible difference in the WAG results between Betté and Coats models, the tracer analysis was only performed on Coats model.

4.4.6 Tracer analysis for near-miscible displacement

As seen in Figure 4-25, a very small amount of tracer was injected into an arbitrary position in a pre-identified non-preferential route under near-miscible conditions (strong M_{CE}). In the case of continuous injection, the tracer oil with C8* was injected at the beginning of the simulation. On the other hand, the tracer oil with C8* was injected at the beginning of the first gas cycle during WAG (i.e. right after the first water cycle). Delaying the tracer injection was to minimize the impacts from the initial water cycle, where the stable displacing front can greatly distribute the tracer and therefore add difficulty in investigating the IFT effects. The tracer injection lasted for 2 hours at the rate of 1/12000 PV/hour (1/6000 PV in total). Apart from that, all the other simulation parameters are same as the ones in previous simulations.

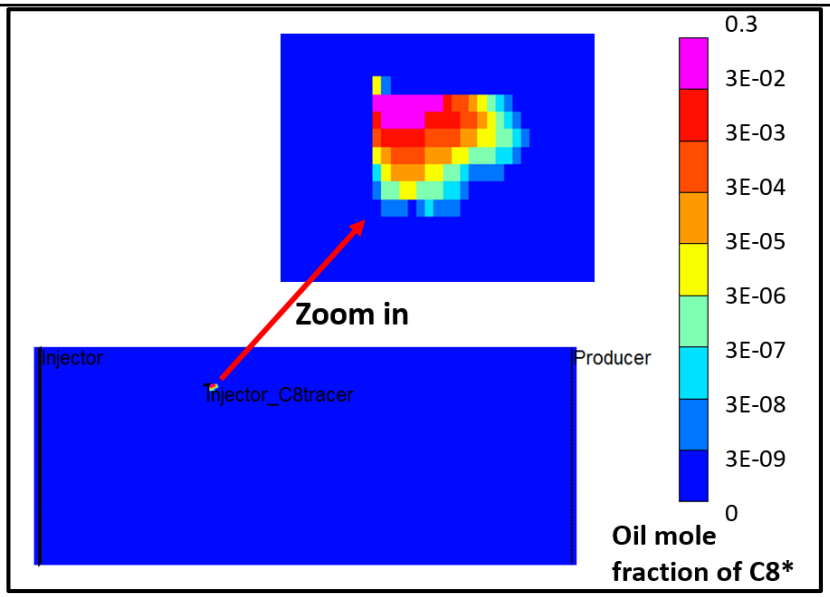

Figure 4-25 The snapshots at the end of tracer injection.

As seen in Figure 4-26 a - d, the snapshots of the tracer distribution were captured after a certain amount of injection in four cases, i.e. at the end of continuous injection (a & b) and at the end of second gas cycle of WAG injection (c & d). All of them show that the tracer migration is strongly affected by crossflow. Very importantly, the case of near-miscible WAG displacement with IFT effects has by far the most extensive tracer migration and therefore the greatest crossflow. Here, three sets of comparisons are conducted and are commented on regarding the flow behaviour.

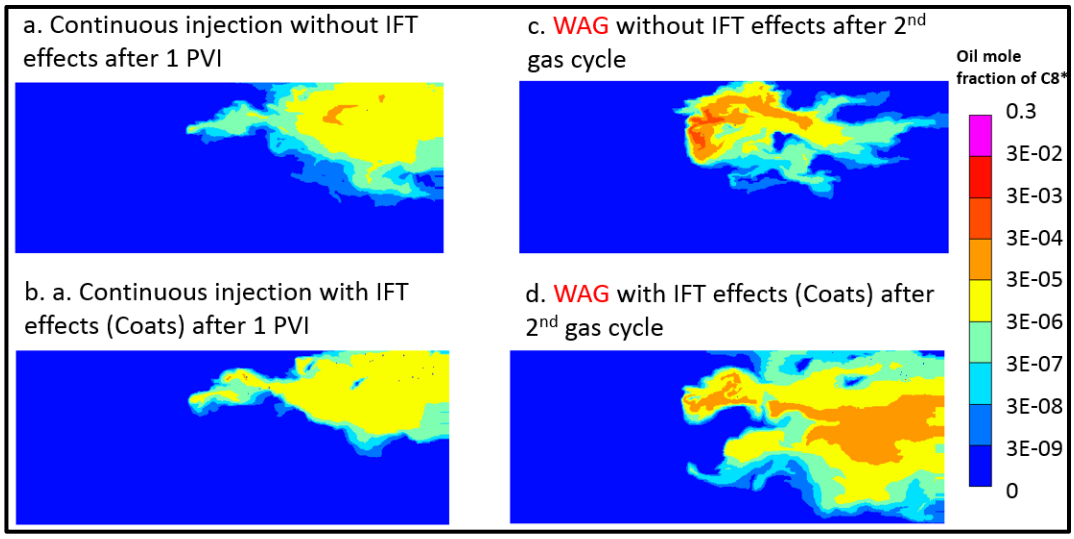

Figure 4-26 The snapshot of oil mole fraction of tracer (C8*) based on Coats model (E0.5T5).

1. Comparison between Figure 4-26 **a** and **b** (near-miscible continuous CO_2 injection with/without IFT effects)

IFT effects have fairly limited impact on the oil crossflow during the continuous CO_2 displacement with a certain amount of CO_2 injection (1PV here). The improved oil relative permeability is still not sufficient to compete with the dominant gas fingers (as a result of strong stripping of oil, M_{CE}). For this reason, a significant amount of remaining oil can still be found between gas fingers, i.e. in the non-preferential routes, no matter whether we include or exclude IFT effects (M_{IFT}) during the continuous CO_2 injection.

2. Comparison between Figure 4-26 **a** and **c** (near-miscible CO_2 continuous/WAG injection without IFT effects)

Without IFT effects, neither the case of continuous injection nor WAG injection has a wide distribution of tracer. This explains why the local displacement efficiency in the non-preferential routes is still of great potential even after WAG. As seen in Figure 4-16 a-d and Figure 4-17 a-d, the remaining oil in the non-preferential routes has been mostly under the control of S_{orw} (0.44 here). Therefore, a stable displacing front is a necessary but not sufficient condition for maximizing the displacing performance in the zone of bypassed oil.

3. Comparison between Figure 4-26 **c** and **d** (near-miscible WAG injection with/without IFT effects)

It can clearly be seen that the extent of crossflow has been significantly enhanced/amplified by the IFT effects during WAG displacement. The oil mobilized by IFT effects (even with very low permeability) from the non-preferential routes "finds" its way by crossflow into the neighbouring preferential routes (much shorter distance than directly flowing to the producer). Note that such a process is highly dependent on a relatively stable displacing front in order to amplify the crossflow. Then the oil component will be stripped by the compositional effects (M_{CE}) and subsequently recovered in gas the phase, which is of much higher mobility and can lead to an instant increase in the oil recovery. This explains why IFT effects can greatly modify the displacement performance and rapidly improve the oil recovery in the case of near-miscible WAG with IFT effects but have a minor impact in the rest of the cases.

In addition, it is now clear why there is only negligible discrepancy between the Betté and Coats models when simulating near-miscible WAG. This is because the interfacial tension effects in the non-preferential routes can be very strong due to the fact that the remaining oil is still at the early stage of IFT cycle as indicted in Figure 4-11. In other

words, σ_{go} is sufficiently low to make the residual oil close to zero (based on Coats) and thus make the two models produce almost the same results.

4.4.7 Sensitivity analysis of the 3PRP models for WAG displacement

It is well known that the result of a WAG injection can be greatly influenced by the choice of 3PRP model. As mentioned previously, a sensitivity analysis of three of the most widely-used 3PRP models was performed, namely: Stone 1, Stone 2 and Baker's saturation weighted method. Figure 4-27 (a-c) shows the distribution of remaining oil saturation after 2PV near-miscible WAG displacement in the absence of IFT effects. As indicated by the red oval in Figure 4-27, the only observable differences are mainly in the area of non-preferential routes. There is less remaining oil in the area indicated by the red oval with the Stone 1 model than with the other two models.

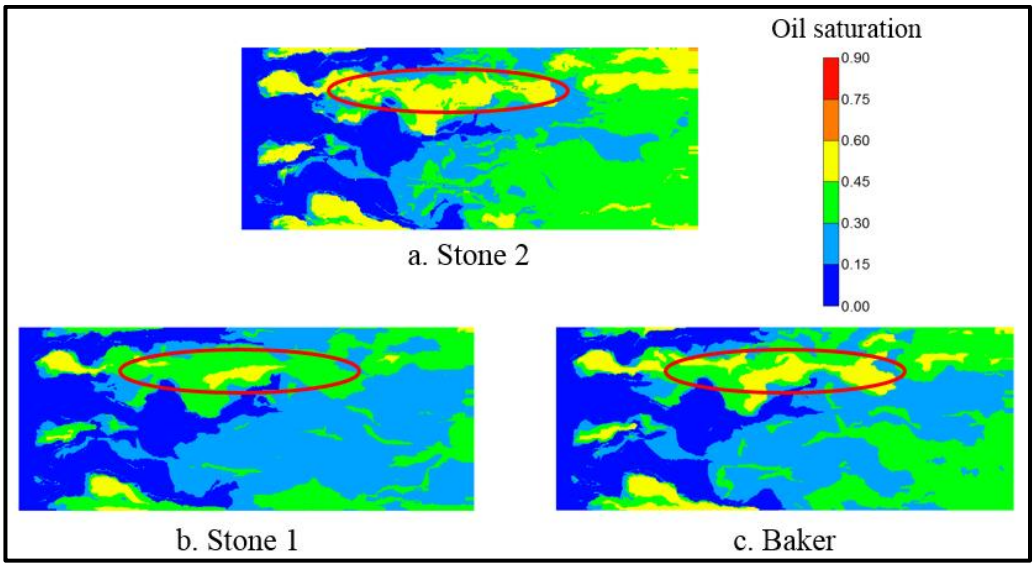

Figure 4-27 Remaining oil saturation varying 3PRP methods without IFT effects.

Figure 4-28 (a-c) presents three sets of oil isoperms produced from each of these methods. The main differences between these models are in the region approaching residual oil saturation (as expected). Stone 2 has the largest area of residual oil saturation, whereas Stone 1 has the smallest. As a result, Stone 2 gives the most pessimistic prediction in terms of oil recovery whereas Stone 1 gives the most optimistic prediction, although these differences are relatively modest as shown in Figure 4-29. Clearly, the Stone 2 recovery result is not a "prediction", it is essentially "input", as no simulation needs to be done to reach this conclusion. However, the residual oil saturation in this ternary diagram can be significantly overcome by compositional effects in near-miscible gas injection to achieve a much lower remaining oil saturation. In other words, oil components can be vaporized

into CO_2 and produced in the "gas" phase (supercritical fluid, in fact, but using gas relative permeability for flow velocity), particularly from the preferential routes where oil stripping effects can be dominant. This is also the reason why there are only observable discrepancies in the non-preferential routes when using different 3PRP models.

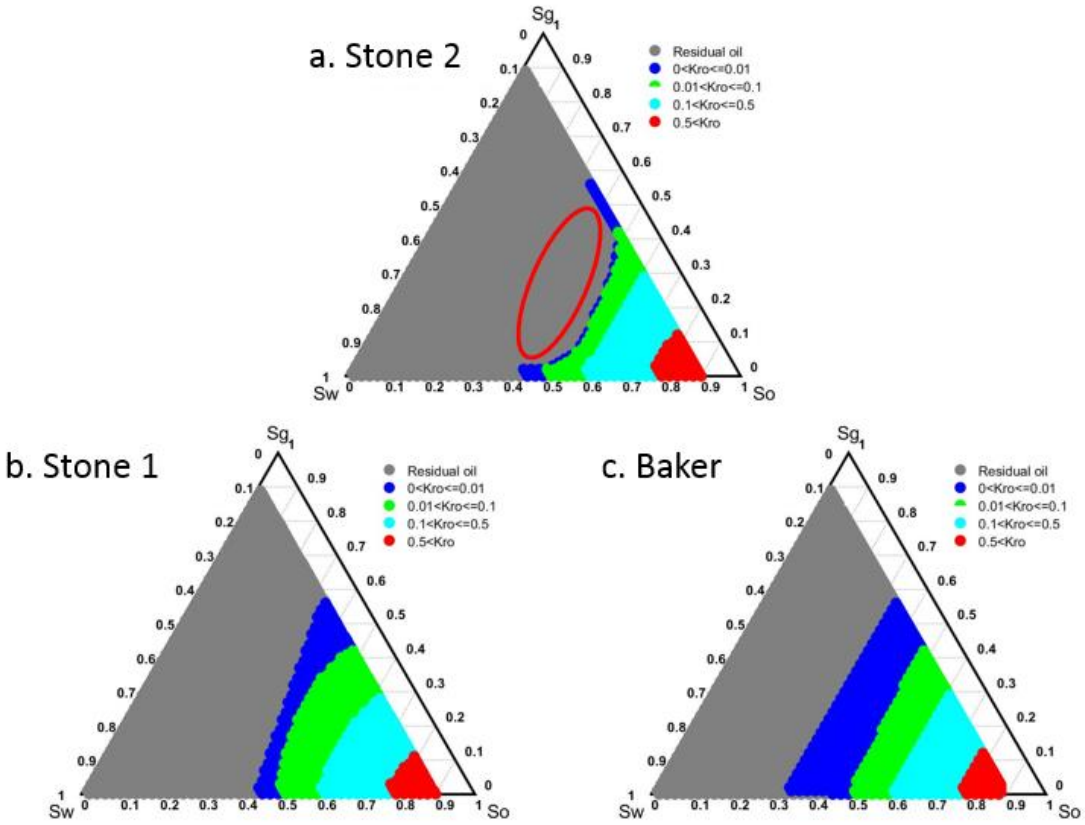

Figure 4-28 Oil isoperm varying 3PRP methods: a. Stone2, b. Stone1 and c. Baker.

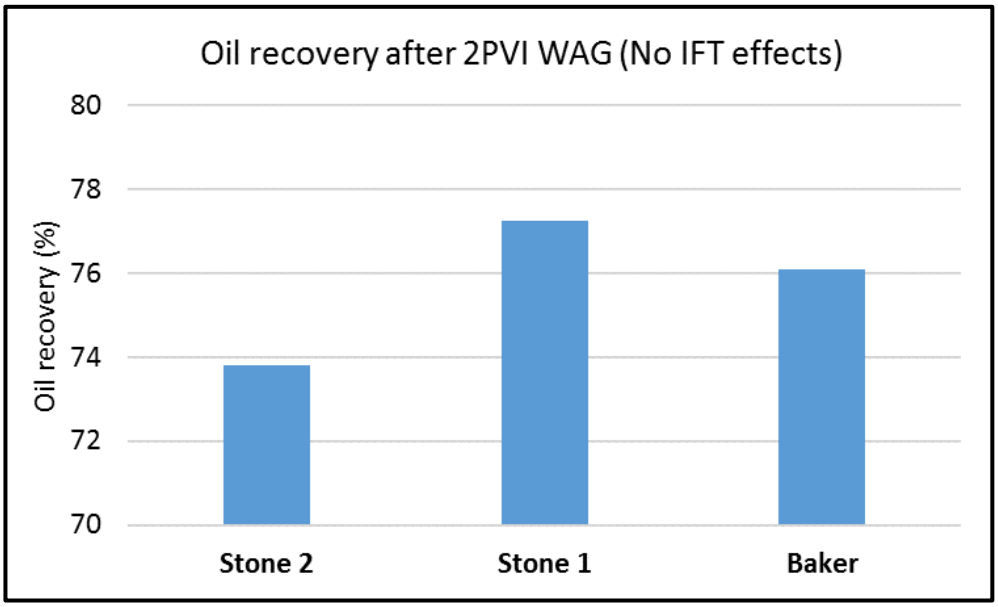

Figure 4-29 Ultimate oil recovery varying 3PRP methods without IFT effects.

The results in Figure 4-30 now show the distributions of remaining oil saturation after 2PV near-miscible WAG displacement *including* IFT effects modelled based on Coats model (n = 0.5, σ_{go}^{0} = 5mN/m). Interestingly, these results show that the discrepancies are much reduced and almost negligible.

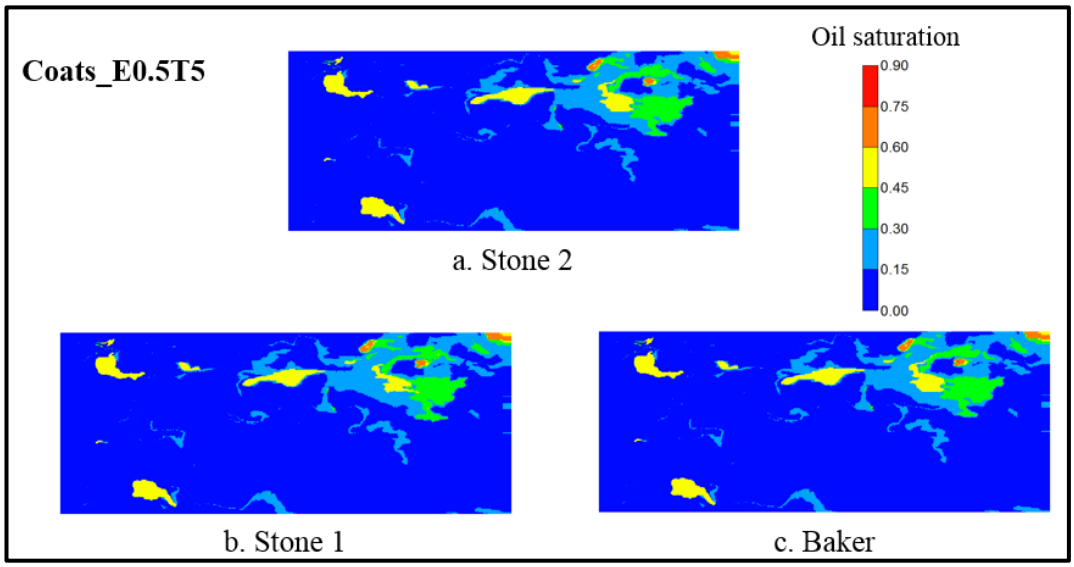

Figure 4-30 Remaining oil saturation varying 3PRP methods with IFT effects using Coats model.

Interestingly, IFT effects reduce the discrepancies in the results when varying 3PRP methods. Here, I present two examples of relative permeability varying the ratio of σ_{go} (3 mN/m and 0.1 mN/m) and threshold value (σ_{go}^{0}=5 mN/m). As seen in Figure 4-31, the oil isoperm diagrams are becoming much more similar with decreasing σ_{go}. This is because of the nature of the method used for modelling IFT effects which have been applied (Equation 2-41 to Equation 2-45). This method entails an interpolation between immiscible (initial) and miscible relative (K_{rh}) permeabilities, under the control of a weighting factor (f). The lower σ_{go}, the lower the contribution that the initial 3PRP can make to the final oil relative permeability. In other words, the oil relative permeability should be almost the same regardless of the modelling method at certain local values of σ_{go}, such as at the ultra-low level (0.001 mN/m). As expected, the results in Figure 4-32 show that there is hardly any difference in the prediction of the ultimate oil recovery.

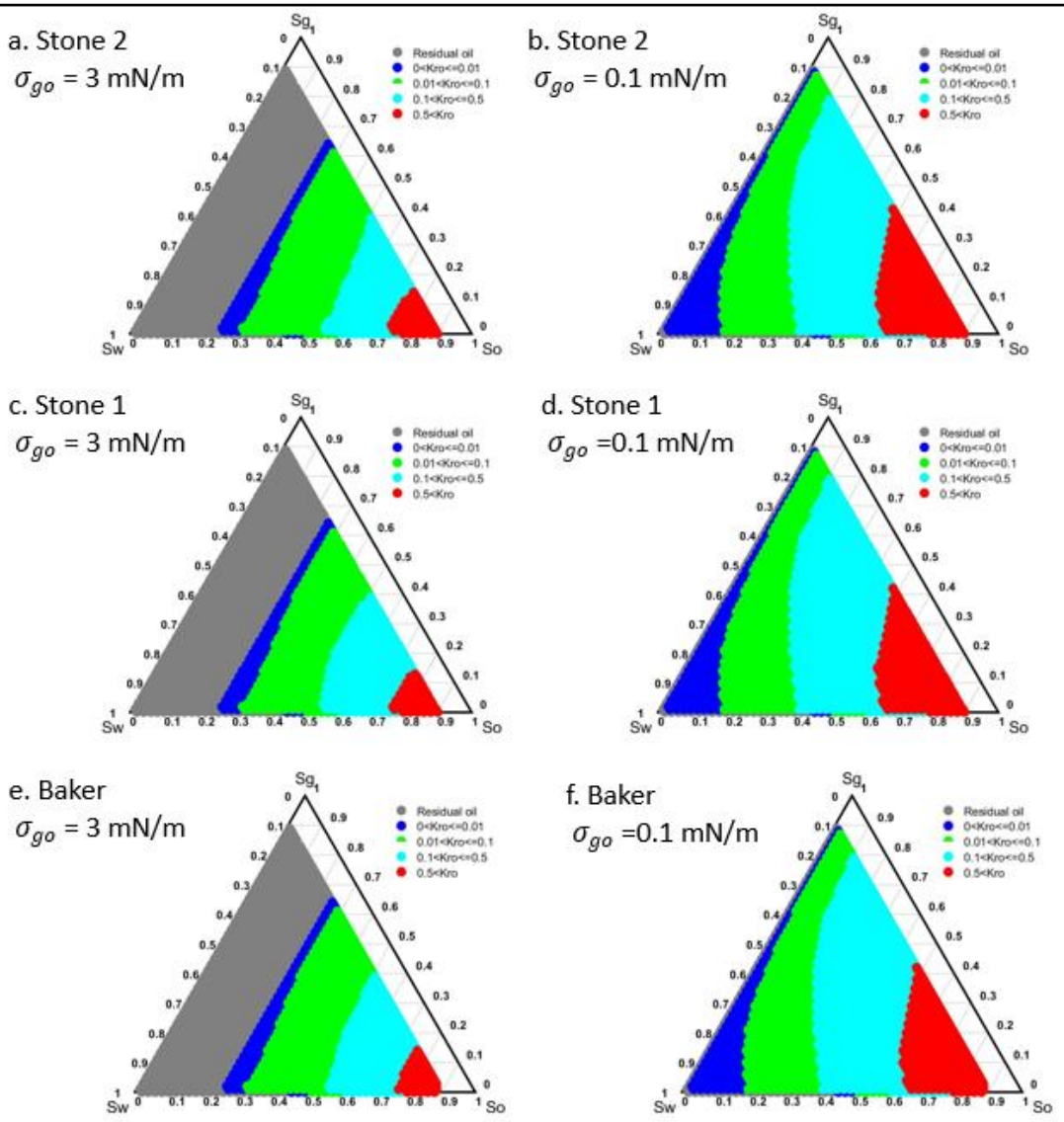

Figure 4-31 Oil isoperm varying 3PRP methods: a&b. Stone2, c&d. Stone1 and e&f. Baker with IFT effects.

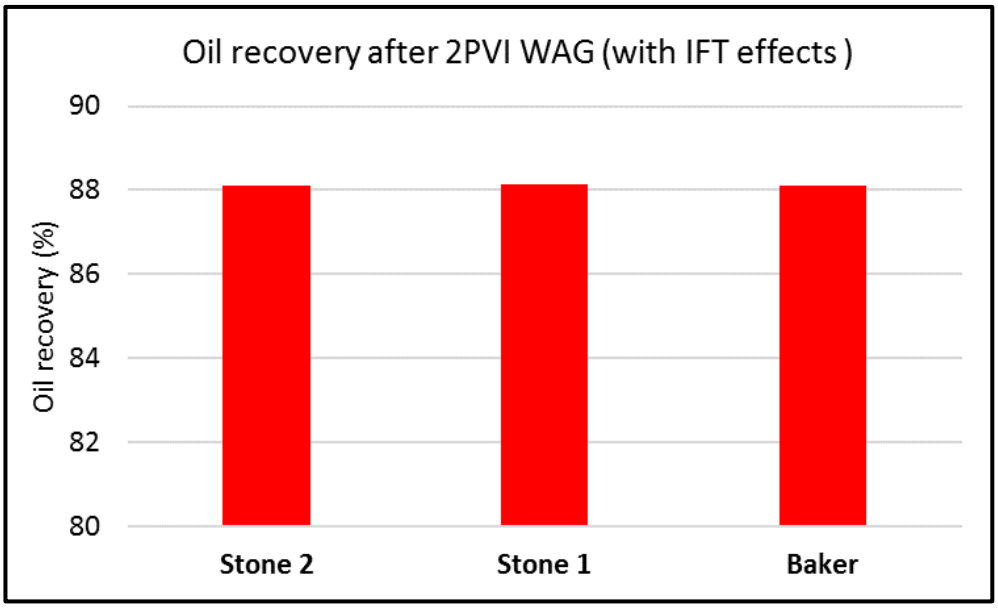

Figure 4-32 Oil recovery varying 3PRP methods with σ_{go}^{0}=5mN/m using Coats model.

4.5 Summary

The central objective of this chapter is to study the balance and interactions of the different mechanistic contributions to the physics occurring during oil displacement by CO_2 (both continuous and WAG). Mechanism 1 (M_{CE}) is the oil stripping/compositional effect and Mechanism 2 (M_{IFT}) is the near-miscible IFT effect on oil relative permeability. Based on sufficiently fine-scale models, it is now clear how these mechanisms interact with each other and affect the sweep and local displacement efficiency in the fingering flow regime. In addition to the model (Figure 3-2) on which the main work developed here, other realisations of models were also constructed and tested to avoid biased conclusions (see Figure-A3 and Figure-A4 in Appendix). The efforts of studying the key processes separately leads to a greater insight into the physics of CO_2 displacement. From the point of view of modelling, the key discrepancy between Coats and Betté models was recognised and analysed with an aim to provide insight into the simulation of the transition from immiscible to near-miscible systems. Here are four key observations from the range of numerical simulations, which have been presented here.

1.Incremental oil recovery is insensitive to IFT effects (M_{IFT}) during continuous CO_2 injection. This is because both M_{CE} (oil stripping effects) and M_{IFT} (IFT effects) are working in tandem to recover the oil in the preferential routes, but forming more severe gas fingers at the same time leading to more imbalanced flow paths. The final result of the competing IFT effects of poorer sweep but lower residual oil in the preferential paths leads to a very limited increased oil recovery.

2.Unlike stripping effects (M_{CE}), IFT effects (M_{IFT}) are not dependent on continuous contacts between CO_2 and oil. Instead, the remaining oil in the non-preferential routes could be mobilised by IFT effects and be efficiently recovered by the subsequent cycles through a viscous crossflow mechanism.

3.The very rapid improvement in oil recovery during the second water and gas cycles in WAG is because of the enhanced/amplified viscous crossflow as a result of IFT effects (M_{IFT}). With a stable displacing front during WAG, the oil mobilized by IFT effects in the non-preferential routes "finds" its way to the neighboring preferential routes and is then recovered relatively rapidly by strong compositional effects (M_{CE}). Our simulations confirm that WAG is able to make very efficient use of the combined

M_{CE} and M_{IFT} mechanisms in heterogeneous system, particularly in the non-preferential flow routes.

4.Coat's model takes account of the variation of residual oil with the reduction in IFT, whereas the th Betté model does not. Therefore, Coats model is of mechanistically better treatment on the residual oil than the Betté's model. Therefore Coats model is prefered for the modelling of near-miscible WAG processes and is applied for the rest of analysis.

5.It has been demonstrated how the ***different mechanisms*** (oil stripping, M_{CE} and IFT effects, M_{IFT}) work in ***different places*** (preferential and non-preferential routes) for ***different processes*** (continuous CO_2 injection and WAG) under ***different conditions*** (immiscible/near miscible).

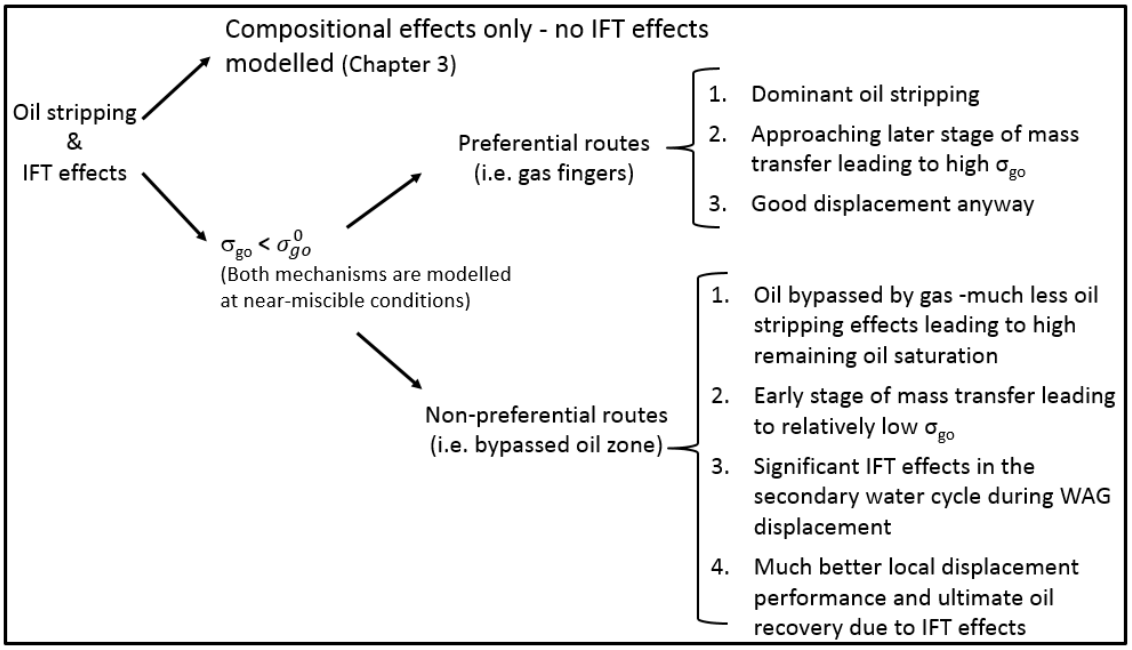

Figure 4-33 Summary map of the main findings from this chapter.

Chapter 5 Extension of Additional Physical Processes Occurring during WAG Displacement

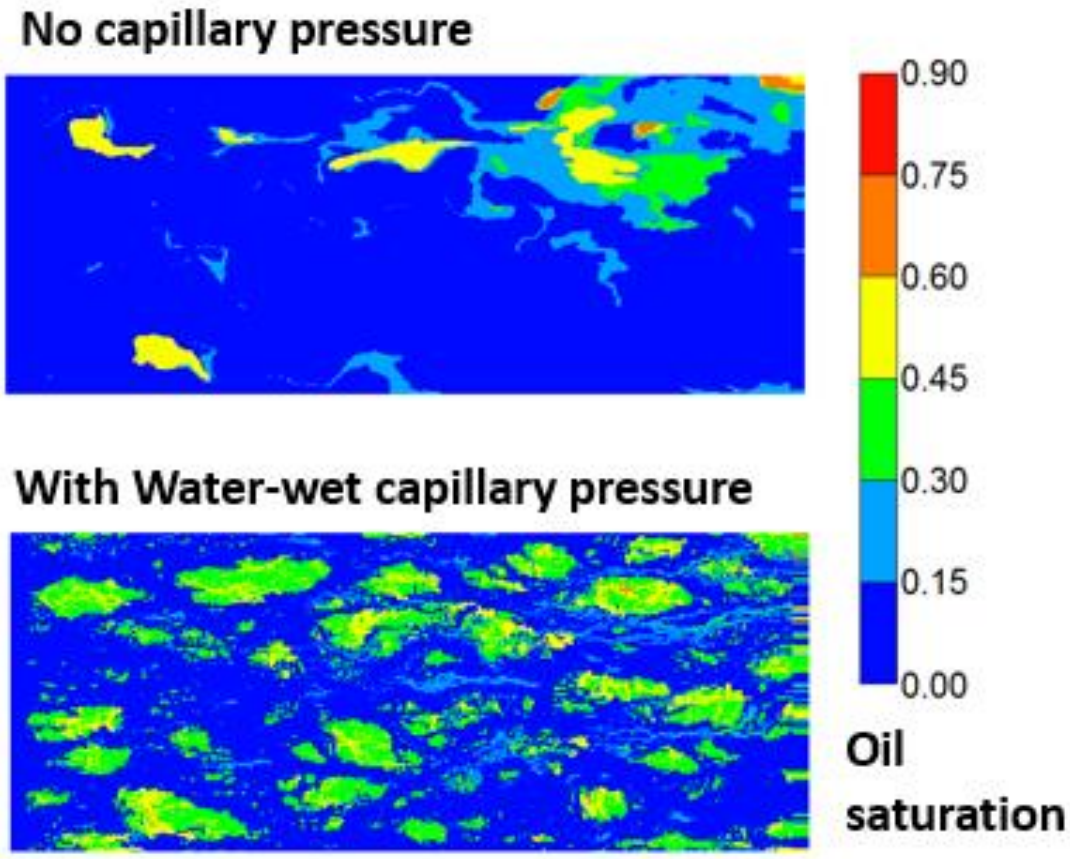

Distribution of remaining oil in the cases with/without capillary pressure

In preparation:

Wang, G., Pickup, G., Sorbie, K., Mackay, E. and Skauge, A. (2020) 'Impacts of gas trapping and capillarity on oil recovery by near-miscible CO_2-WAG'.

5.1 Introduction

Two major mechanisms of oil mobilisation (M_{CE} and M_{IFT}) occurring at near-miscible conditions have been extensively analysed in Chapter 3 and Chapter 4, respectively. Very importantly, the viscous crossflow amplified by M_{IFT} in WAG injection is the key to recover the oil previously bypassed by gas fingers in non-preferential routes. Strictly speaking, the near-miscible displacement is a special type of immiscible displacement, where the interface between phases still exists. Hence, typical multiphase flow physics, which commonly occur in WAG displacements, cannot be ignored. Therefore, the current study is extended to another three important multiphase flow physical processes, i.e. gas trapping, water hysteresis and capillary force. In addition, the gravity effect was briefly investigated with 2D vertical simulations to test the robustness of the newly developed synthesis.

Note that the aim of this chapter is not to history match experimental data or to propose modifications of these models. Instead, the research interest is to understand how these physical processes interact with the mechanisms of oil mobilizations (M_{CE} and M_{IFT}) under near-miscible conditions. Based on the cases formulated in Chapter 4, a sensitivity analysis was conducted to investigate the impact of each physical process of interest on oil recovery in near-miscible WAG processes.

5.2 Model description

In order to investigate those multiphase flow physics occurring in WAG processes, a range of commonly used models available in CMG/GEM was selected to incorporate with the new synthesis (M_{CE} and M_{IFT}) developed in the section Chapter 4. The corresponding modelling methods of three flow features (gas trapping, water hysteresis and capillary force) are summarised in Table 5-1. The full details of these models, such as the formulae and the underlying theories, can be found in sections 2.5.4 and 2.5.5. The choice of input values for flow simulations is explained below.

Flow feature	**Model**
Gas trapping	Trapping model developed by Carlson (1981) Trapping model developed by CMG (2019)

Water hysteresis	Permeability hysteresis model developed by Larsen and Skauge (1998)
Capillary force	J-function proposed by Leverett (1941)

Table 5-1 Models used for multiphase flow physics occuring in WAG.

5.2.1 Models of Carlson and CMG

According to Land (1971), gas is disconnected in the form of ganglia leading to a reduced mobility when strong flow reversals occur. The greater the gas saturation, the more the trapped gas fraction. In order to reflect this flow feature, two widely used models, which were developed by Carlson (1981) and CMG (2017) respectively, are applied to analyse impacts of gas trapping on the displacement performance. Full details of these methods can be found in section of 2.5.4.1. According to Carlson (1981), the trapped gas saturation is in a range of 0.2-0.4 with a historical maximum gas saturation of 0.4-0.9. Therefore, C in Land's model (Equation 2-46) is set to 1.39, which leads to a maximum trapped gas saturation (S_{grmax}) of 0.4 here.

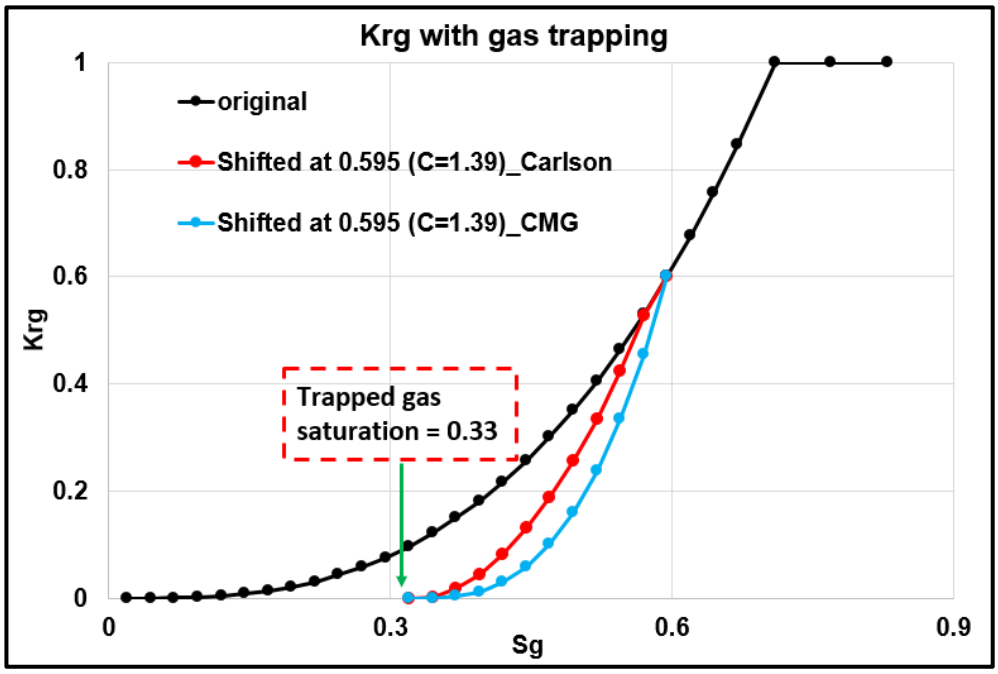

Figure 5-1 Examples of treatment of gas relative permeability using models developed by Carlson (red) and CMG (blue) respectively.

Figure 5-1 shows how the two models manipulate the gas relative permeabilities when taking account of the trapping mechanism. Assuming the system process shifts from gas

displacement to water displacement at a gas saturation of 0.595, both models give a same value of trapped gas saturation (S_{grh}), which is equal to 0.33. This is because both models utilise the same correlation between the trapped gas saturation and the gas saturation at the shift point, i.e. Land's model. It can be also seen that the model of Carlson (1981) gives a range of slightly greater values of K_{rg} than CMG's method for the succeeding imbibition process. Input values for WAG modelling taking into account of gas trapping are summarized in Table 5-2.

	Model	Key parameter
3-phase relative permeability	Stone1/Stone2	N/A
IFT effects	Coats	$n = 0.5;\ \sigma_{go}^{0} = 5mN/m$ (E0.5T5)
Gas trapping	Carlson/CMG	C = 1.39

Table 5-2 Models invovled in the analysis section of gas trapping (5.3.1).

5.2.2 Model of Larsen and Skauge

It has been reported that water may also present the permeability hysteresis in a WAG process, such as in a non-strongly water-wet system (Wang, 1988). Therefore, Larsen and Skauge (1998) proposed a hysteresis model based on Carlson's model (for gas trapping) to reflect the hysteresis effects of water. One of the key features of this model is connecting the water relative permeability to the gas saturation at the start of the process. This widely used model is applied here to investigate water hysteresis on the oil recovery by near-miscible WAG displacements.

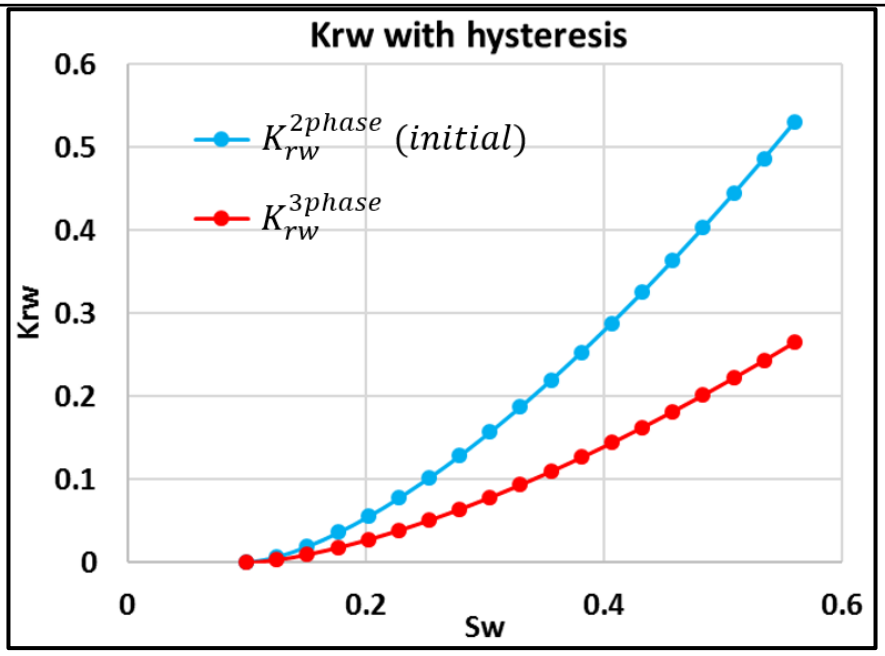

Figure 5-2 Relative permeabilities of water in a WAG process.

This model entails using saturation-interpolated scanning curves to determine water relative permeability. A secondary water relative permeability curve (denoted as K_{rw}^{3phase}) is introduced to serve as the lower boundary of the scanning curves for the interpolation, whereas the initial permeability curve (K_{rw}^{2phase}) is the upper boundary. The water relative permeability is extrapolated between these two boundary curves, depending on the gas saturation. According to Larsen and Skauge (1998) and Egermann *et al.* (2000), K_{rw}^{3phase} is assumed to be half of K_{rw}^{2phase}, as plotted in Figure 5-2. Although there is some debate on the wettability order of phases, it has been never reported that gas is the most wetting phase. Therefore, the effect of gas trapping is also taken into account in this section. Note that the effect of gas trapping can be only modelled by Carlson's method when utilising the Larson and Skauge's model. Full details of this model can be found in section of 2.5.4.2. The key input values for the flow simulations are summarized in Table 5-3.

	Model	Key parameter
3-phase relative permeability	Stone1/Stone2	N/A
IFT effects	Coats	$n = 0.5$; $\sigma_{go}^{0} = 5mN/m$ (E0.5T5)

Gas trapping	Carlson	C = 1.39
Hysteresis of K_{rw}	Larson and Skauge	K_{rw}^{3phase} =0.5 $*K_{rw}^{2phase}$

Table 5-3 Models invovled in the analysis section of water hysteresis (5.3.2).

5.2.3 Leverett J-function

The capillary effect is considered as an another important mechanism in driving the multiphase flow behaviour (Hassanizadeh and Gray, 1993). The Leverett J-function is a commonly used method to extrapolate capillary pressure data varying with permeability, porosity (homogeneously set to 0.1 here), interfacial tension and contact angle. According to Berg (1975) and Shen *et al.* (2005), the interfacial tension of water and crude oil is generally at a level of 20-50 mN/m. In this study, the interfacial tension of water and crude oil was set to 45 mN/m. As seen in Figure 5-3, a set of capillary curves for a drainage process was generated using the J-function (Leverett, 1941). The contact angle (θ) was assumed to be 30° and 150° to represent a water (blue) and oil wet (red) system respectively. Since the interfacial tension of oil and gas under near-miscible conditions (0.01-8 mN/m as seen in Figure 4-11) is much smaller than the assumed interfacial tension between oil and water (45 mN/m), the capillary pressure of gas and oil is ignored here. In other words, the pressure of oil and gas are assumed equal, as shown in Figure 5-4.

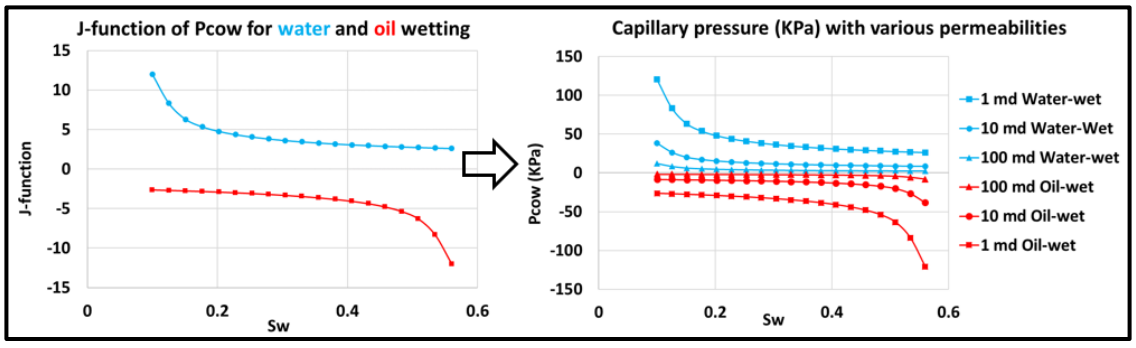

Figure 5-3 J-function (left) and the capillary forces (right) used in this section.

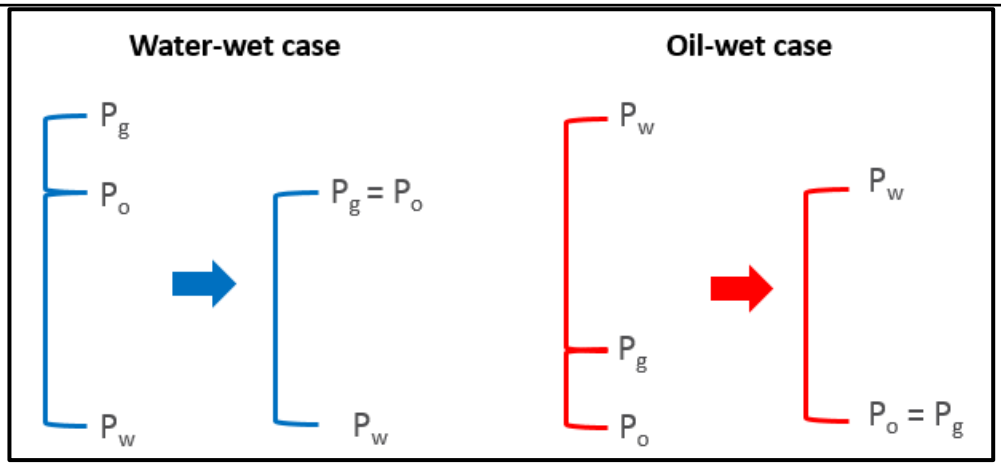

Figure 5-4 Schematic of phase pressure

What should be highlighted here is that the injection rate was varied to test different conditions of balance between the viscous force and capillary force. As stated in Table 4-1, the injection rate was initially set to 0.4 PV/d (flow velocity of injection = 2 m/d). In the section concerning the capillary force (5.3.3), an additional scenario with an injection rate of 0.1 PV/d (reduced by four times) was simulated as a comparison to the original case. Note that such a reduction in injection rate has a negligible impact on the fluid behaviour and oil recovery in cases, which do not take into account the capillary force, i.e. the simulation results discussed in Chapter 4 (see Figure-A2 in Appendix). The hysteresis effect of capillary pressure was not taken into account for simplicity. Key parameters of flow simulations conducted in this section are summarized in Table 5-4.

	Model	Key parameter
3-phase relative permeability	Stone2	N/A
IFT effects	Coats	$n = 0.5$; $\sigma_{go}^{0} = 5mN/m$ (E0.5T5)
Capillary force	J-function	$\theta = 30°$ (water-wet) and 150° (oil-wet); $\sigma_{ow} = 45\ mN/m$

Table 5-4 Models invovled in the analysis section of capillarity effects (5.3.3).

5.2.4 2D vertical model

It has been well reported that the gravity effect could be another key influencing factor (positive and negative) during the process of WAG displacement (Sanchez, 1999; Faisal

et al., 2009). This is because the density difference between the three phases (water, oil and gas) may lead to severe gravity segregation. Although this issue has been extensively analysed in the literature, it is worthwhile to conduct a brief test based on 2D vertical models, with a particular aim to ascertain the necessity and the robustness of the newly developed synthesis (M_{CE} and M_{IFT}). In other words, the question is whether the gravity effect will dominantly eliminate the benefits led by the combined M_{CE} and M_{IFT} during the near-miscible WAG displacement. Therefore, sample simulations of near-miscible WAG process in 2D vertical models were performed.

To keep the permeability structure consistent between the vertical and areal models, the 2D vertical model was constructing by rotating the 2D areal model (Figure 3-2), i.e. the orientation was changed from the x-y to the x-z plane. Since gravity segregation is not the central focus of this study, the vertical to horizontal permeability ratio (k_v/ k_h) was set to 0.1 and 1, homogeneously, to simplify the question. The initial densities of the injected CO_2 and in-situ oil were approximately 500 kg/m^3 and 700 kg/m^3, which were determined through calculations of EOS in the simulator (CMG, 2019). The initial water density was input as 1000 kg/m^3. Key parameters of flow simulations conducted in this section are summarized in Table 5-5.

	Model	Key parameter
3-phase relative permeability	Stone2	N/A
IFT effects	Coats	$n = 0.5$; $\sigma_{go}^{0} = 5mN/m$ (E0.5T5)
K_v/K_h	N/A	0.1 and 1

Table 5-5 Models invovled in the analysis section of gravity effect (5.3.4).

5.3 Results and discussion

5.3.1 Effect of gas trapping

Two-pore volumes of WAG displacement under near-miscible conditions was simulated taking account of gas trapping in addition to M_{CE} and M_{IFT}. According to CMG (2019), the determination of oil and gas permeability consists of three steps with the following

sequence: 3-phase model (e.g. Stone 2), gas trapping (e.g. Carlson) and IFT effects (e.g. Coats). Figure 5-5 was plotted to show the remaining oil saturation at the end of WAG injection. All four cases show, almost equally, that the overall displacement performance is degraded due to the effect of gas trapping, compared to the case only taking into account M_{CE} and M_{IFT} (Figure 4-30 a). The region where there is the most remaining oil is in the largest non-preferential route, i.e. the yellow zone where oil saturation is 0.45-0.6. Interestingly, the oil in the preferential routes could still be efficiently recovered and was hardly affected by the effect of gas trapping. As seen in Figure 5-6, the effect of trapped gas has led to a modest reduction in the oil recovery (approximately 3 ~ 4%).

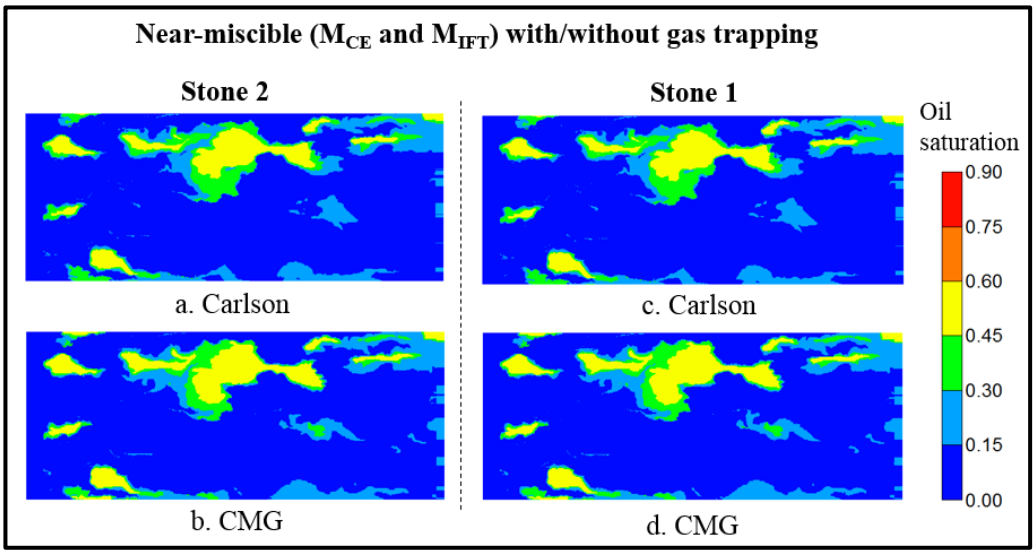

Figure 5-5 Oil saturation after 2PV of near-miscible WAG using Stone 2/Stone 1: a. Stone 2 & Carlson; (b) Stone 2 & CMG; (c) Stone 1 & Calson; (d) Stone 1 & CMG.

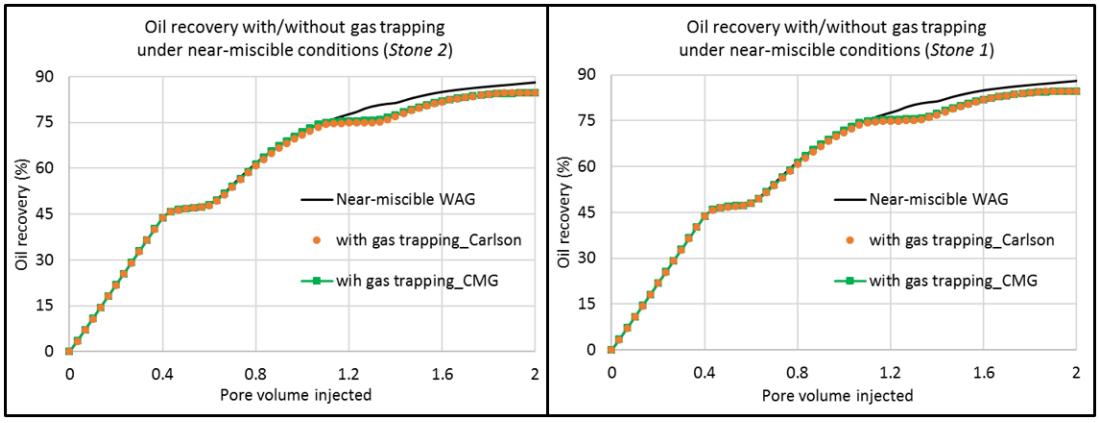

Figure 5-6 Oil recovery based on Stone 2 (L) and Stone 1 (R) with/without the effect of gas-trapping after 2PV of WAG under near-miscible conditions.

Additional simulations were carried out in order to investigate the reason for the lower recovery in the non-preferential routes. Figure 5-7 shows the oil recovery of each cycle

when the effects of gas trapping are included. Interestingly, the reduction in oil recovery is mostly from the second water cycle. Since the degraded displacement performance mainly occurs in a non-preferential route, it was conjectured that the viscous flow might be affected. Therefore, a separate pseudo-tracer analysis was conducted using the same method as the one in 4.4.6. Since there is negligible difference among these results which take account of gas trapping, this tracer analysis was only conducted with Stone 2 and Carlson.

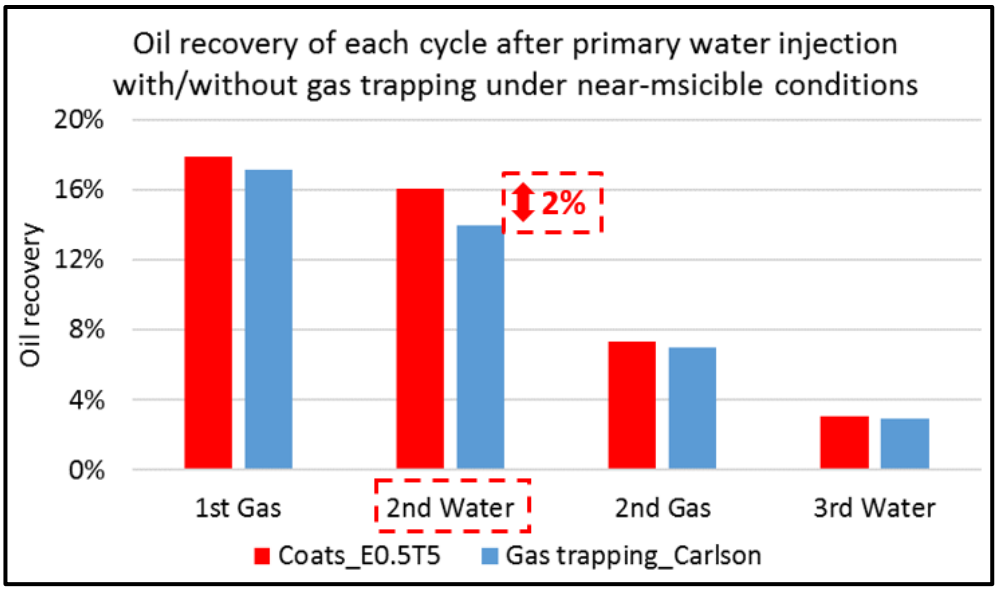

Figure 5-7 Oil recovery of each cycle based on Stone 2 without (red) and with (blue) the account of gas-trapping during near-miscible WAG displacement.

As seen in Figure 5-8, the tracer distribution, which indicates the extent of oil crossflow, has been moderately restricted by the trapped gas saturation. The reasons are twofold. Firstly, the effect of gas trapping has restricted the redistribution of gas into non-preferential routes during the second water cycle (1.2-1.6PV). For this reason, the overall amount of oil that can be mobilised by M_{IFT} is reduced. Another aspect is that the IFT-triggered K_{rot} (total oil relative permeability) is positively correlated with K_{rg} (Equation 2-43 and Equation 2-44). In other words, the smaller K_{rg} is, the smaller K_{rot} is. Therefore, the relative permeability of the oil under M_{IFT} is also negatively affected when the effect of gas trapping is included. As seen in Figure 5-9, the oil velocity of a representative cell in a non-preferential route is significantly reduced at the second water cycle, where the viscous crossflow is the key flow mechanism to recover the oil in these zones. Since the trapped gas is re-mobilized when the gas saturation increases again, the oil in the preferential routes can still be well recovered through the compositional effects.

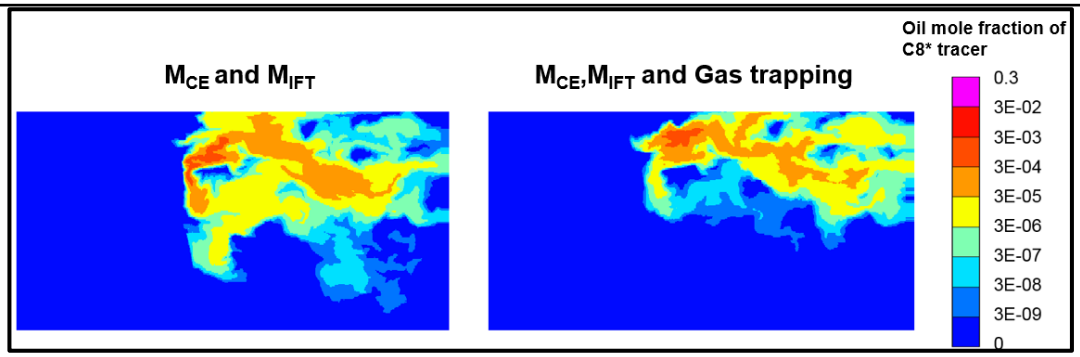

Figure 5-8 The snapshot of oil mole fraction of tracer (C8*) based on Stone 2 without (L) and with (R) the account of gas-trapping at the end of second water cycle.

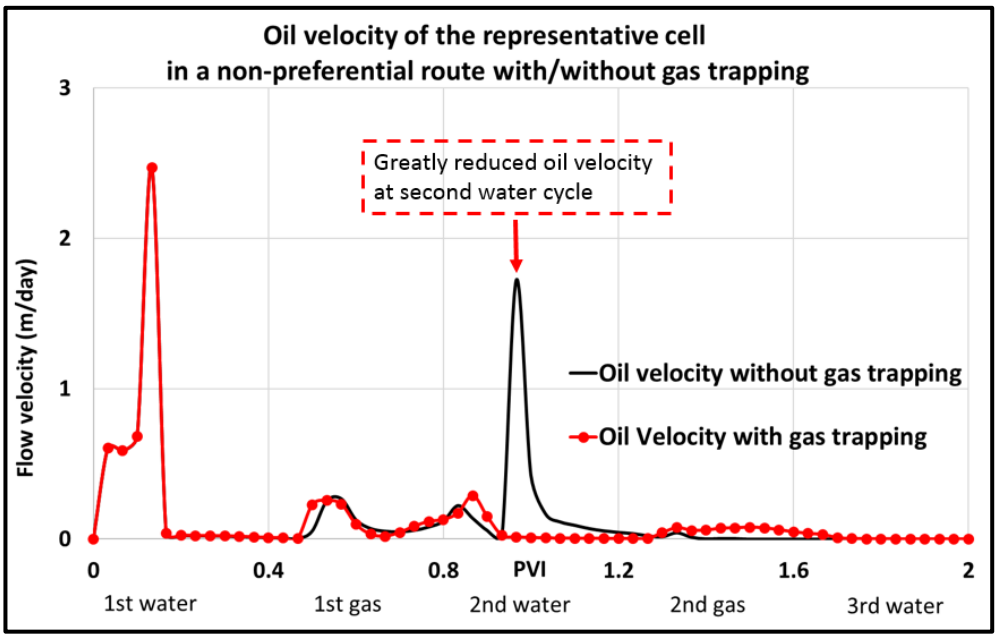

Figure 5-9 Oil velocity of the representative cell in a non-preferential route with (blue) and without (red) the effect of gas trapping.

5.3.2 Effect of water hysteresis

In the last section, the impacts of gas trapping on the oil recovery were investigated in a near-miscible WAG process. Due to the reduced mobility of both gas and oil, the extent of viscous crossflow is slightly degraded leading to a modest reduction in the oil recovery. In this section, the simulation of 2D near-miscible WAG was conducted taking account of permeability hysteresis both water and gas. Figure 5-10 shows the distribution of remaining oil saturation after 2PV WAG injection. As seen in Figure 5-11, the oil recovery is slightly increased compared to the initial base case (M_{CE} and M_{IFT}) and the case taking into account of gas trapping. In particular, water hysteresis has slightly improved the displacement performance during the second and the third water cycle (Figure 5-12). This is because the gas saturation at the start of the second and third water cycle in preferential routes is much higher than that in non-preferential routes. For this

reason, the water mobility in the preferential routes is even more reduced than that in non-preferential routes. This should force more water to flow into non-preferential routes and therefore slightly improve the oil recovery.

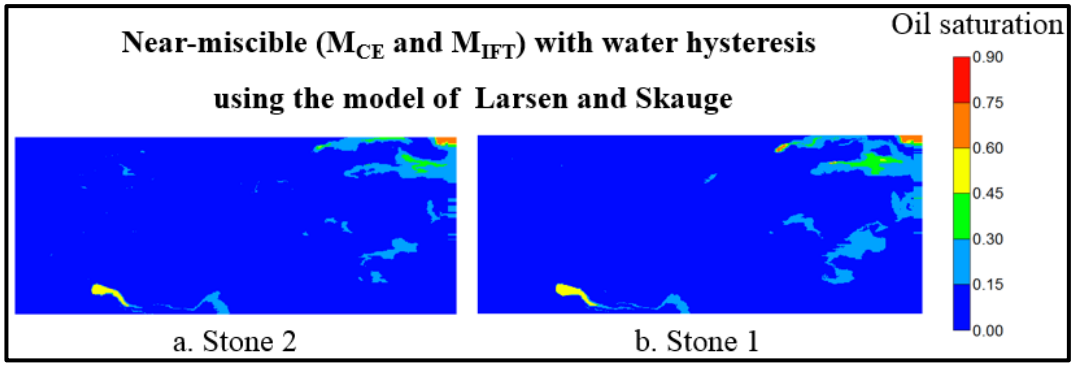

Figure 5-10 Oil saturation after 2PV of near-miscible using 3-phase hysteresis model developed by Larson and Skauge: Stone 2 (left) and Stone 1 (right).

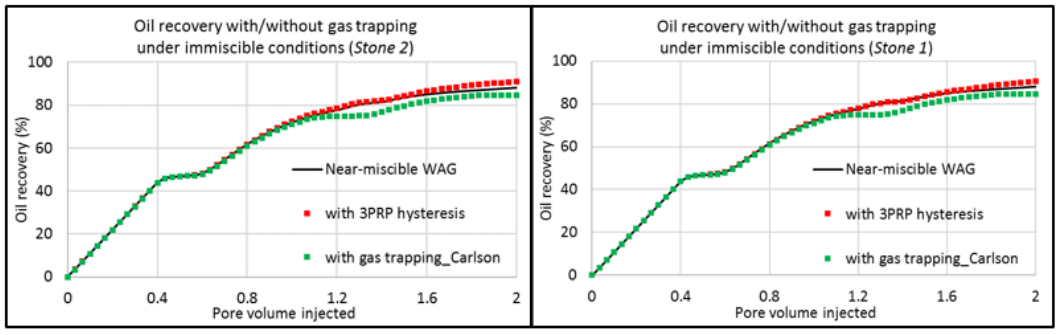

Figure 5-11 Oil recovery based on Stone 2 (L) and Stone 1 (R) with/without hysteresis after 2PV of WAG under near-miscible conditions.

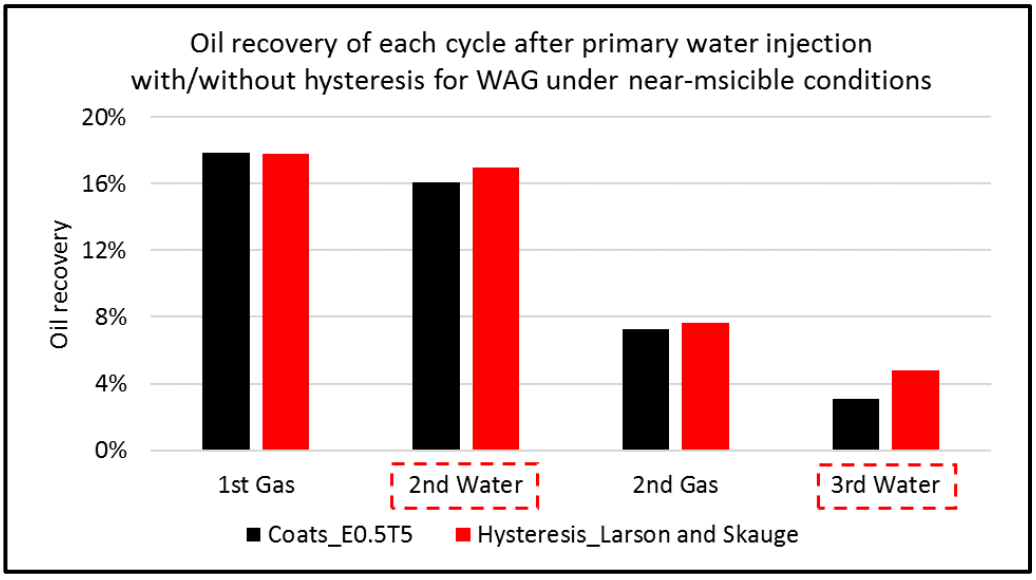

Figure 5-12 Oil recovery of each cycle based on Stone 2 without (red) and with (blue) the account of 3-phase hysteresis during near-miscible WAG displacement using Stone 2.

Another interesting finding is that there is negligible discrepancy between Stone 2 and Stone 1 in terms of the oil recovery. According to Equation 2-55, the hysteresis model developed by Larsen and Skauge (1998) entails a separate correlation between the residual oil saturation (S_{om}) and the trapped gas saturation. In other words, the residual oil saturation is further reduced if Stone 1 is used. Clearly, it has negligible impact on the oil recovery in simulations demonstrated above. This is because, in the preferential routes, the dominant oil stripping (M_{CE}) has recovered the most of the oil in these zones. As for the non-preferential routes of gas flow, the trapped gas saturation is much lower than that in the preferential routes. Therefore, the positive impact of trapped gas saturation on the residual oil saturation is trivial in the non-preferential routes and completely masked by the IFT effects. In fact, Larsen and Skauge's model was developed based on a purely immiscible study. In other words, neither the compositional effects nor the IFT effects were considered in their study. It is interesting that the treatment of the residual oil saturation in their method presents a very different level of impact on the oil recovery during near-miscible WAG process.

5.3.3 Effects of capillary force

Typically, capillary forces are considered to be of secondary importance in field-scale flow simulations (Ringrose *et al.*, 1993). This is simply because cell sizes (Δx= 50m~1000m) commonly used in field-scale reservoir simulations are too coarse to resolve the impact of capillary pressure on flow behaviour. With the use of very fine-scale simulations (Δx= 0.05m), the significance of the capillarity is ascertained as shown in the results below.

5.3.3.1 Water-wet system

Two scenarios, one with the initial injection rate (a) and the other with the reduced injection rate (b), were both simulated. Figure 5-13 shows the remaining oil saturation after 2PV WAG displacement in a water-wet system. It can be seen that the included water-wet capillary pressure has caused a negative impact on the displacement performance. Multiple oil zones have been bypassed at the end of the WAG injection. The sweep efficiency has been much degraded by the capillary force. Very importantly, such effects are greatly amplified when the injection rate is reduced by four times (Figure 5-13 b), where the viscous force (i.e. pressure gradient) is much lower. Figure 5-14 is plotted to track the oil recovery throughout the injection process. Compared with the initial case without capillarity (M_{CE} and M_{IFT}), the oil recovery is reduced by capillarity

by approximately 2 % in the case with the initial injection rate (Case a) and 7% in the case with the reduced injection rate (Case b), respectively.

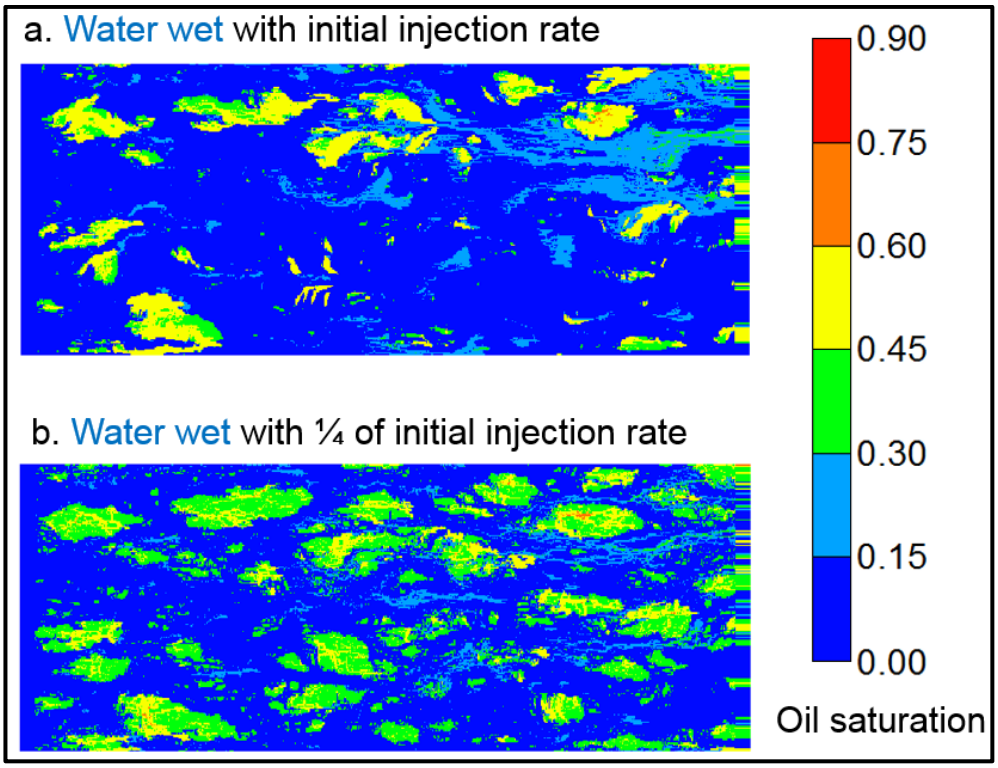

Figure 5-13 Remaining oil saturation after the 2PVI of WAG with water-wet capillary pressure: Case a. initial injection rate; Case b. ¼ initial injection rate.

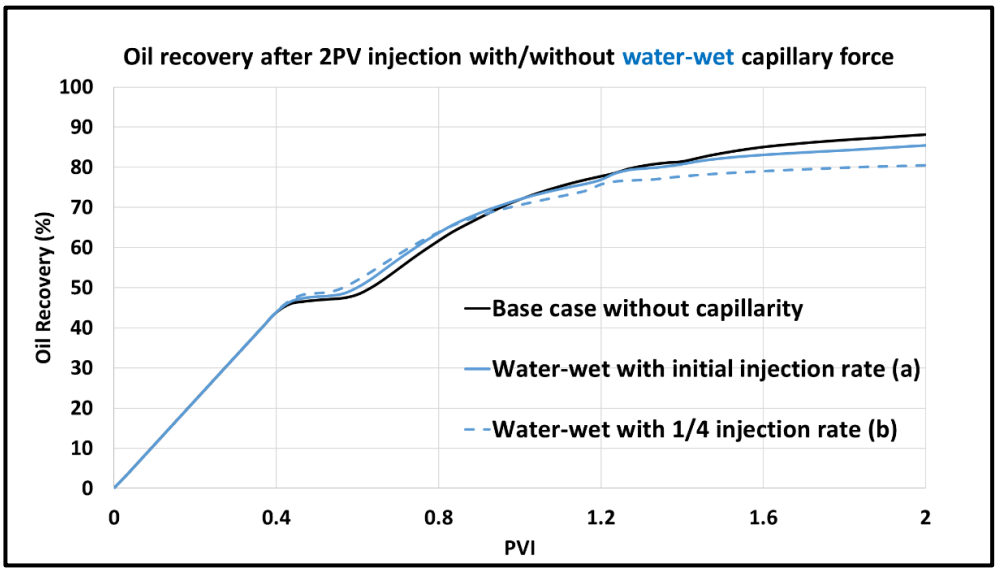

Figure 5-14 Oil recovery with/without the water-wet capillary pressure after 2PV of WAG under near-miscible conditions.

Another interesting finding is that the oil recovery was not uniformly or continuously reduced by the capillary force throughout the injection process. In fact, the water-wet capillarity improves the oil recovery at the early stage of the displacement, although the

oil production approached the plateau much sooner than the case without taking account of the capillary force (Figure 5-14). To investigate this phenomenon, Figure 5-15 is plotted to track the oil recovery of each cycle (except the first water cycle). Note the included capillary pressure is designed to be of negligible impact on the recovery in the first water cycle. In other words, the oil recovery achieved from the first water cycle (0-0.4 PV) is almost identical in all three cases, i.e. the base case without capillarity, the case with capillarity (a) and the case with capillarity and the reduced injection rate (b). In doing so, all three cases are comparable in terms of oil recovery for the subsequent process of WAG injection.

As seen in Figure 5-15, the included water-wet P_{cow} enhances the oil recovery at the first gas cycle (0.4-0.8 PV). The oil recovery in the cases taking account of capillarity is approximately 4% greater than the base case. This is because the included capillary pressure has further driven the injected gas to preferentially flow into the high-permeability zones. At the early stage of displacement, where the dominant gas breakthrough has not occurred, compositional effects are therefore maximised to recover the oil in the preferential routes. Since the oil components are mostly stripped by the injected CO_2 and therefore produced in the "gas" phase, oil recovery during the first gas cycle is greatly accelerated due to the higher mobility of the "gas" phase than oil phase.

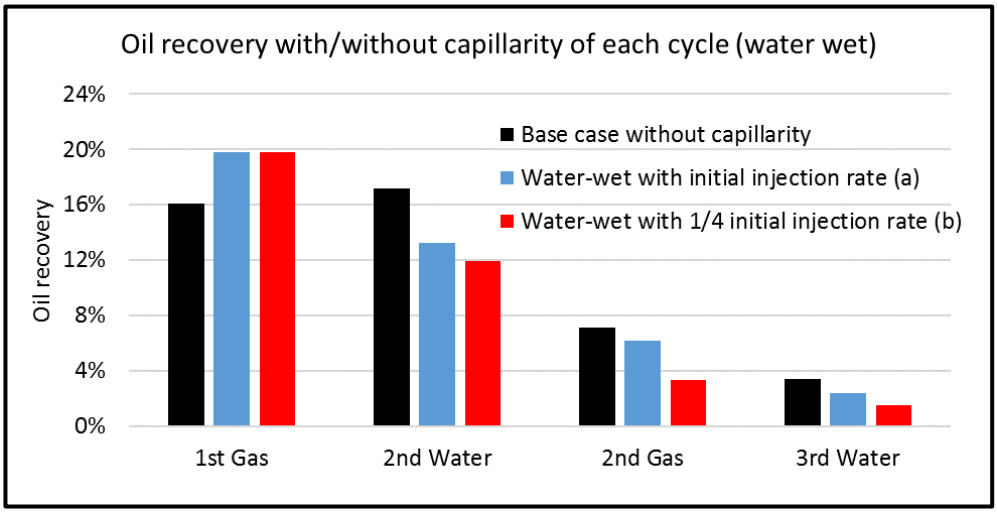

Figure 5-15 Oil recovery of each cycle in the assumed water-wet system.

Although the oil recovery of the first gas cycle is increased, the sweep efficiency is much degraded. Due to the greater entry pressure of the low-permeability areas than the high-permeability areas, gas fingers are further aggravated by the capillary force. The negative impacts of capillary force on the oil recovery start to be evident from the second water

cycle (0.8-1.2 PV). As seen in Figure 5-15, the oil recovery of scenarios (Case a and Case b) taking account of capillarity are persistently lower than the base case without capillarity for the rest of displacement (0.8-2 PV). As seen in Figure 5-3, the added water-wet capillarity based on J-function increases with the decreasing permeability. In other words, the entry pressure for gas flow is much greater in the low-permeability zones than the high-permeability zones. Therefore, both M_{CE} and M_{IFT} are greatly restricted in these low-permeability areas due to the lack of contacts between CO_2 and oil. In particular, the oil recovery in Case b (capillarity and reduced injection rate) is lowered by approximately 5% during the second water cycle (0.8-1.2 PV) compared to the base case.

5.3.3.2 Oil-wet system

Similarly, two scenarios varying the injection rate were both simulated for an oil-wet system. Figure 5-16 shows the remaining oil saturation after 2PV WAG displacement in an assumed oil-wet system. Figure 5-17 is plotted to compare the oil recovery of all three cases, i.e. base case without capillarity, case with oil-wet capillarity (Case c) and case with reduced injection rate and capillarity (Case d) throughout the injection process.

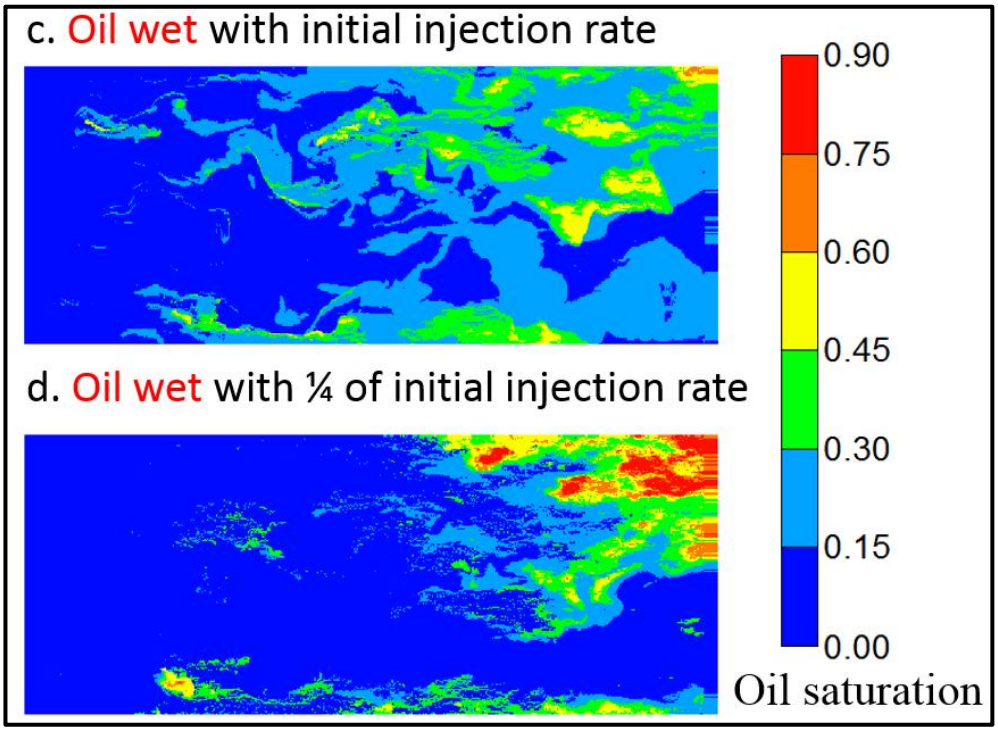

Figure 5-16 Remaining oil saturation after the 2PVI of WAG with oil-wet capillary pressure: c. initial injection rate d. ¼ initial injection rate.

As expected, the flow behaviour in the oil-wet system is quite different from the water-wet system. There are no multiple isolated oil zones present at the end of injection. This is because the included oil-wet capillary pressure ($P_{cow}=P_{cgw}<0$) has led gas to imbibing

into low-permeability areas and therefore lessening the imbalance of the CO_2 concentration between the preferential and non-preferential routes. As a result, the development of gas fingers are mitigated, which improves the overall sweep efficiency in the oil-wet system. However, the volume loss of the injected CO_2 due to its dissolution into oil is increased by the expanded contact area between oil and CO_2. Therefore, the oil recovery of the first gas cycle (0.4-0.8PV), which is mostly dependent on sufficient contacts between oil and CO_2 to maximise the effect of oil stripping (M_{CE}) in the swept zone, is decreased. As seen in Figure 5-17 and Figure 5-18, the oil recovery during the first gas cycle (no dominant breakthrough) is lowest among all three cases.

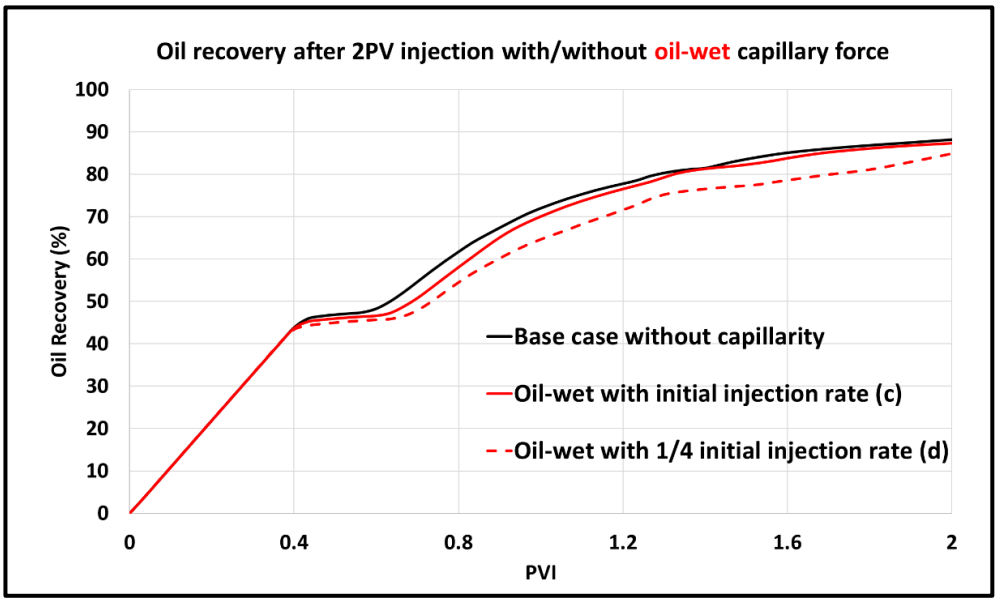

Figure 5-17 with/without the oil-wet capillary pressure after 2PV of WAG under near-miscible conditions.

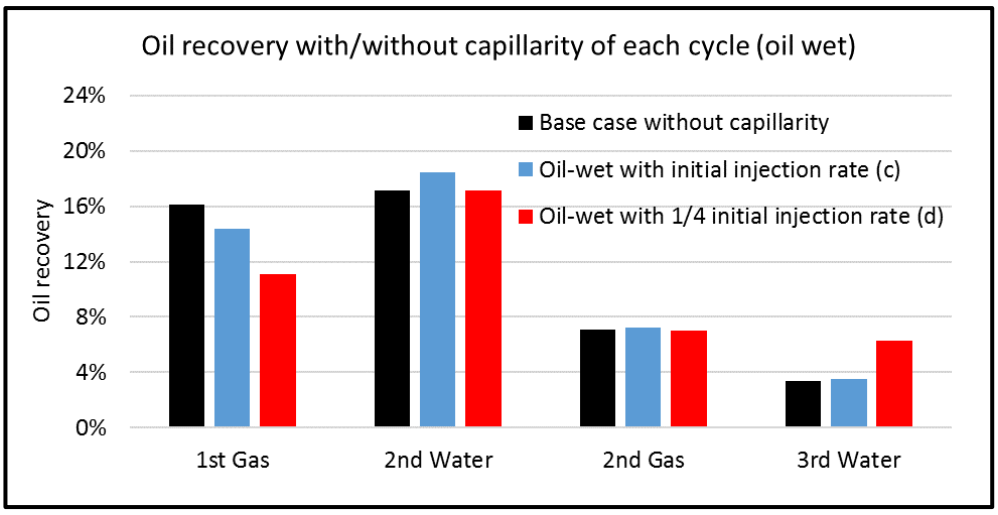

Figure 5-18 Oil recovery of each cycle in the assumed oil-wet system.

On the other hand, oil-wet capillary pressure may have a positive or a non-negative effect during the second water cycle (0.8-1.2PV), as seen in Figure 5-18. The included capillarity has greatly delayed the plateau of the oil production, particularly compared to the water-wet case. Interestingly, there is still a good amount of oil recovery achieved during the third water cycle in the oil-wet system, particularly with the reduced injection rate (Case d). It is conjectured that the oil recovery of the oil-wet case (Case d) during an extended injection would increase evidently whereas the oil recovery of water-wet case does not. In other words, the difference in the oil recovery between the two wetting systems would increase given a longer water injection cycle. To test this conjecture, the displacement was extended with another 0.4 PV of water injection. Figure 5-20 shows the oil recovery during the extended cycle for all three cases with reduced injection rates. As expected, the oil recovery of the oil-wet case (Case d) during the extended injection increases much more than the other two cases. As seen in Figure 5-19, the oil recovery of the oil-wet case (Case d) is almost equal to the base case (89.4%), which is approximately 8% higher than the water-wet case (Case b) at the end of extended water cycle. An additional oil recovery of 3.7% can be achieved during the extended water cycle in the oil-wet system whereas less than 0.5% of additional oil recovery is achieved in the water-wet case.

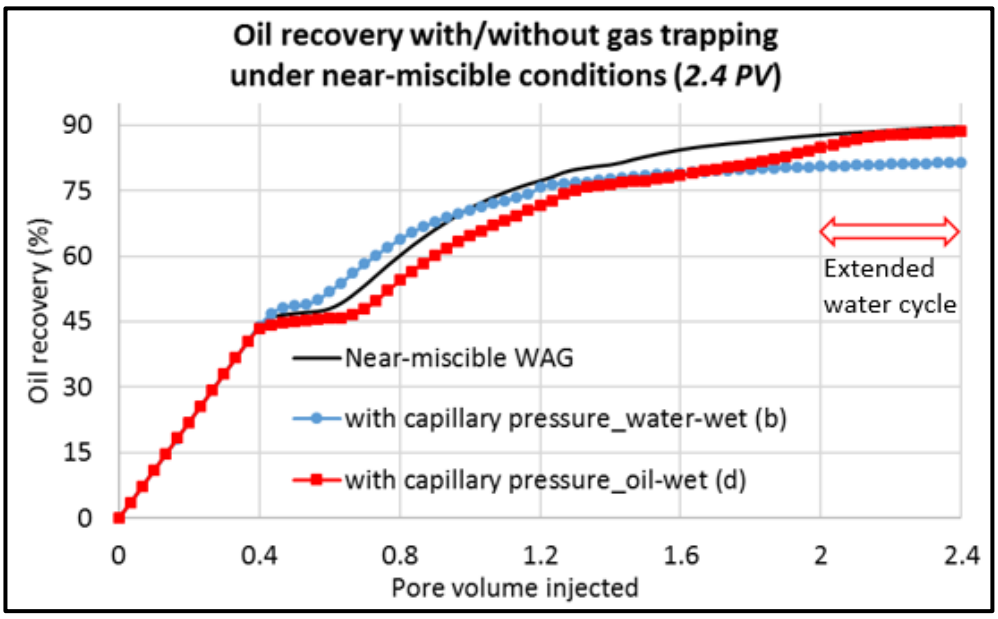

Figure 5-19 Oil recovery taking into accout various wetting conditions.

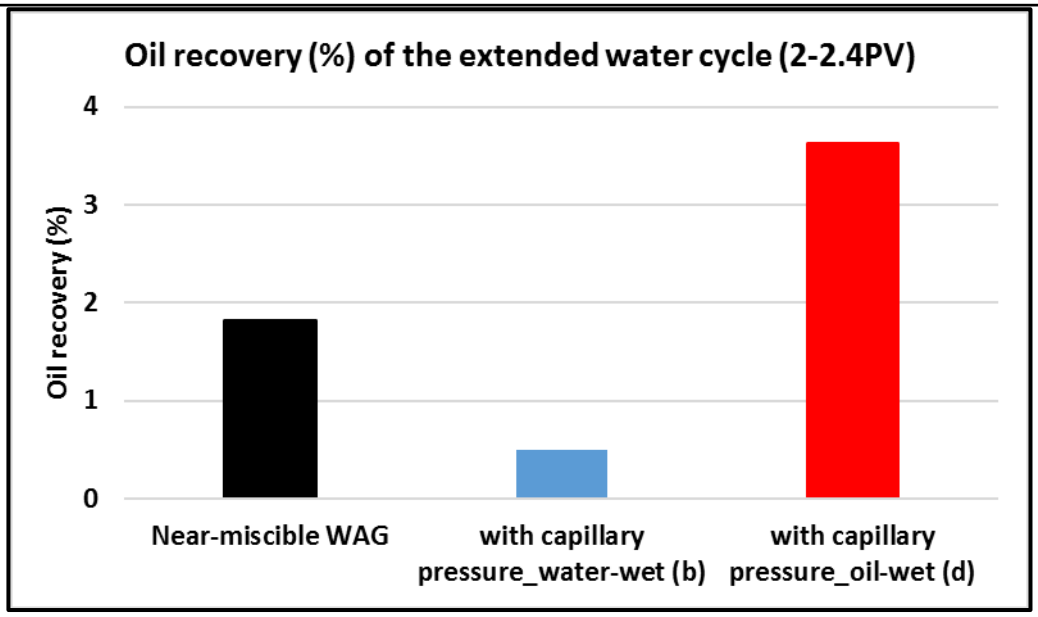

Figure 5-20 Oil recovery of the extended water cycle in cases without capillary pressure, with water-wet capillary pressure and with oil-wet capillary pressure.

5.3.4 Effect of gravity

In order to analyse the impact of the gravity effect on the flow behaviour, a set of flow simulations of near-miscible WAG process was performed in the 2D vertical models. Figure 5-21 shows the remaining oil saturation after 2PV WAG displacement in the 2D vertical model with a k_v/k_h ratio of 0.1. There is no severe gravity segregation in either cases (V1 and V2), although the oil recovery in vertical models on average is approximately 2% lower than that in areal models. The overall displacement performance in the case with M_{CE} acting only (Case V1) is very similar to the areal case in terms of remaining oil saturation. This is because the relatively small density differences between three phases and limited vertical permeability retain the viscous-dominated flow in this particular case. The effect of gravity is mostly masked by the dominant gas fingers. On the other hand, the negative impact of gravity is observable in the case taking into account both M_{CE} and M_{IFT} (Case V2), i.e. the reduced sweep efficiency in the bottom area. As expected, the trend of the gas to flow upwards moderately hampers the viscous crossflow to sweep the bottom area. As seen in Figure 5-22, the combined outcome of M_{CE} and M_{IFT} (Case V2) brings an additional oil recovery of 11% (14% in areal cases) compared to the case with M_{CE} acting only (Case V1).

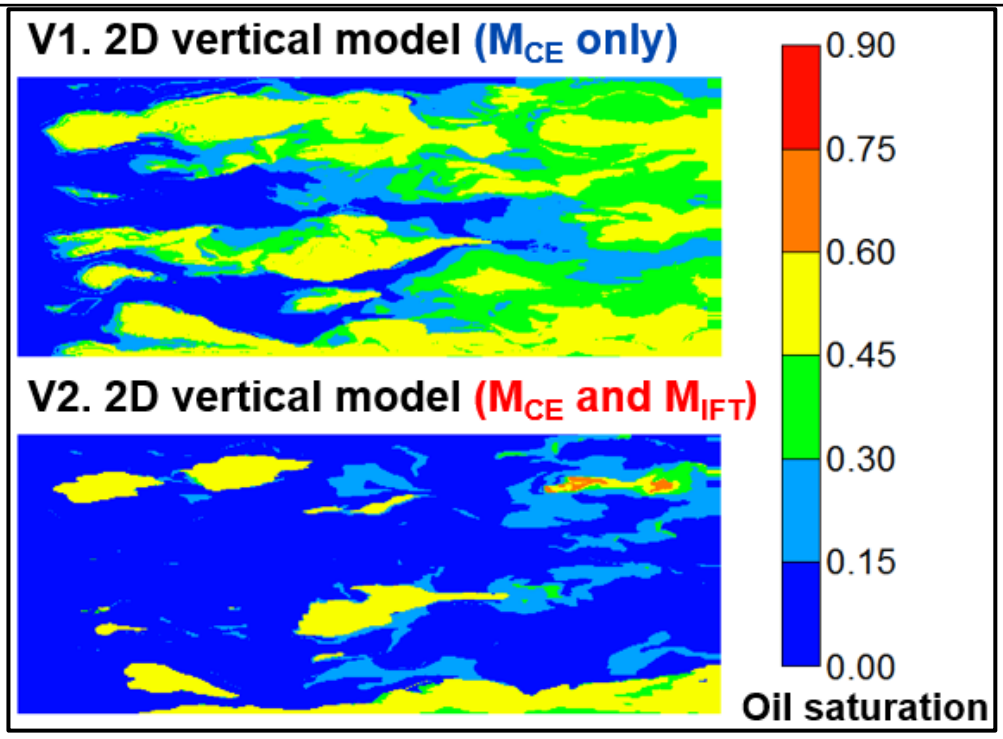

Figure 5-21 Remaining oil saturation after 2PVI of WAG in the 2D vertical model with a Kv/Kh ratio of 0.1: Case V1 (M_{CE} acting only) and Case V2 (M_{CE} and M_{IFT}).

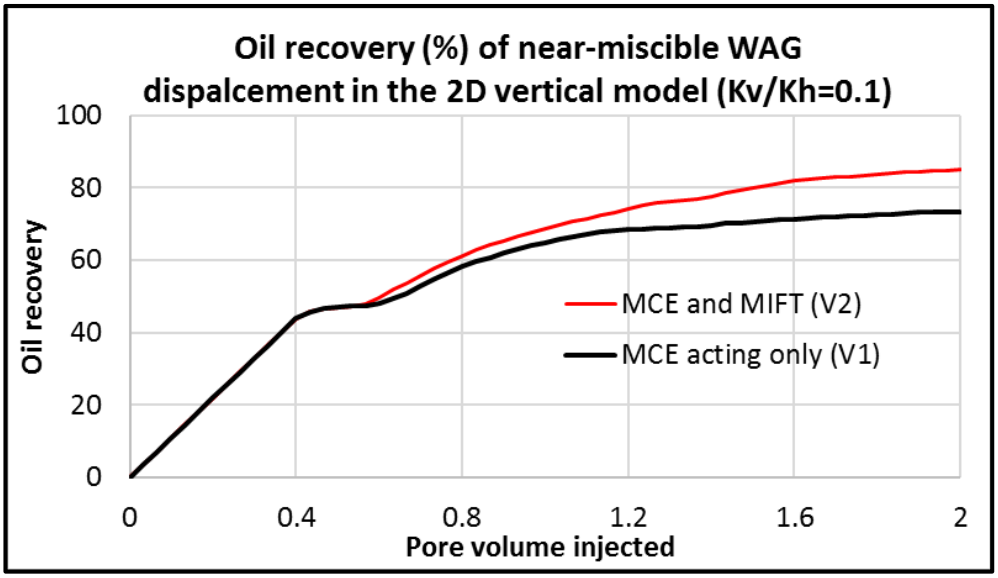

Figure 5-22 Oil recovery in the 2D vertical cases with a Kv/Kh ratio of 0.1: Case V1 (M_{CE} acting only) and Case V2 (M_{CE} and M_{IFT}).

As for the case with a k_v/k_h ratio of 1, the gravity segregation becomes much more evident than in previous cases. The gravity effect has degraded the displacement performance in the bottom zone in both Case V3 (M_{CE} only) and Case V4 (M_{CE} and M_{IFT}). As a result, the average oil recovery in vertical models with a k_v/k_h ratio of 1 is approximately 5% lower than that in the areal models. The tendency of gas to flow upwards was greatly amplified by the large k_v/k_h ratio. As seen in Figure 5-23, a large amount of oil remains

in the bottom area at the end of the injection, particularly in the case taking into account both M_{CE} and M_{IFT} (Case V4). As seen in Figure 5-24, the additional oil recovery resulted from the combined M_{CE} and M_{IFT} (Case V4) is reduced to 9% (14% in areal cases).

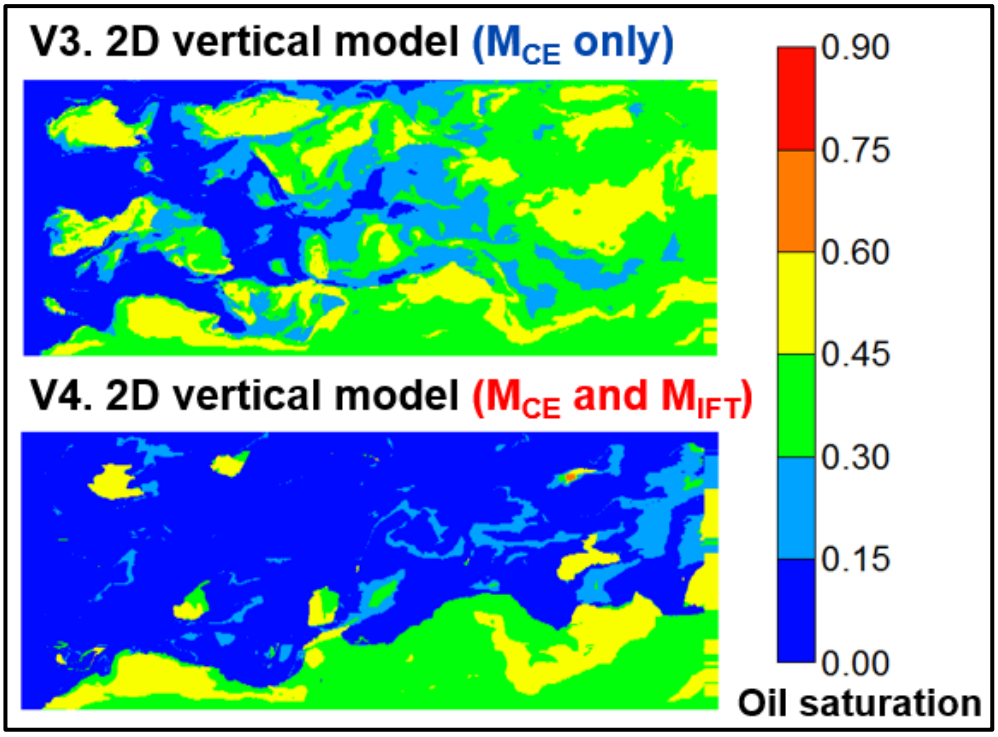

Figure 5-23 Remaining oil saturation after 2PVI of WAG in the 2D vertical model with a Kv/Kh ratio of 1: Case V3 (M_{CE} acting only) and Case V4 (M_{CE} and M_{IFT}).

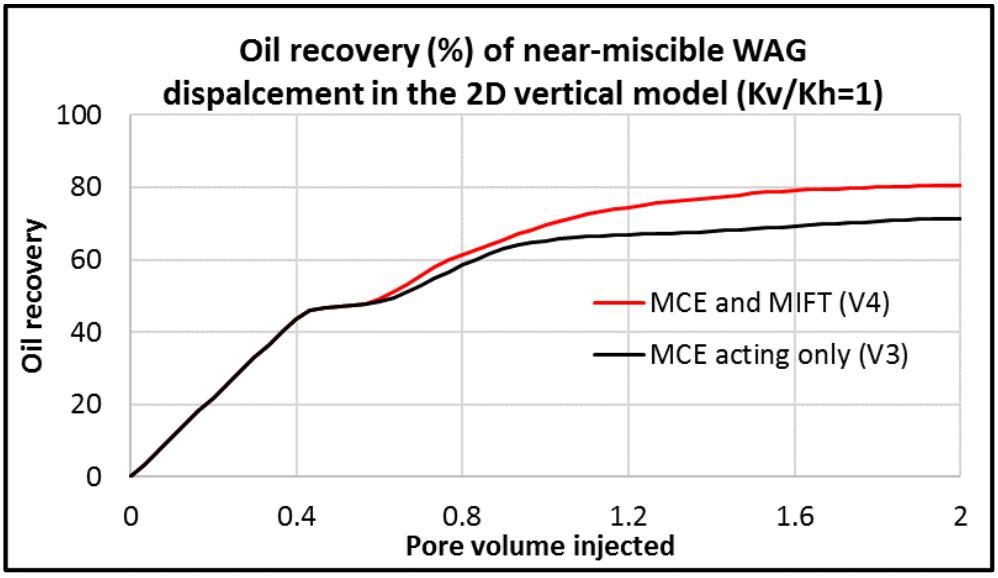

Figure 5-24 Oil recovery in the 2D vertical cases with a Kv/Kh ratio of 1: Case V3 (M_{CE} acting only) and Case V4 (M_{CE} and M_{IFT}).

5.4 Summary

The main objective of this chapter is to investigate the impact of the typical multiphase flow behaviour on the displacement performance in the process of near-miscible WAG injection, where two major mechanisms of oil mobilisations (M_{ce} and M_{IFT}) could occur. With the use of very fine-scale models (Δx=0.05m), the significance of gas trapping, water hysteresis, capillary forces in terms of the oil recovery, has been clearly pointed out. Very importantly, the efforts of studying the key processes separately leads to a greater insight into how these physical processes positively or negatively affect the sweep and local displacement efficiency in the fingering flow regime. Here is a summary of the key findings achieved in this chapter.

1. The effect of gas trapping may degrade the displacement performance of the non-preferential routes, particularly during the second water injection cycle (right after the first gas cycle). This is because the effect of gas trapping has reduced the amount of gas redistributed into non-preferential routes during the second water cycle (1.2-1.6PV). For this reason, the overall amount of oil that can be mobilised by M_{IFT} has decreased. Secondly, the relative permeability of oil under M_{IFT} is also negatively affected when the effect of gas trapping is included in the current modelling method. For these two reasons, the viscous crossflow is moderately restricted, which leads to a reduction of 3% in the oil recovery.

2. The effects of water hysteresis could slightly improve the oil recovery during near-miscible WAG process. This is because the mobility of water is reduced more in the preferential routes than in the non-preferential routes, which leads to an increasing amount of water to flowing into the non-preferential routes during the water cycle. In addition, the special treatment of the residual oil saturation in Larsen and Skauge's model has negligible impact on the oil recovery in the near-miscible WAG process. Such effects have been mostly masked by M_{CE} (preferential routes) and M_{IFT} (non-preferential routes).

3. The effect of capillary force is more complex in the near-miscible WAG process. Specifically, the water-wet capillarity may improve and accelerate the oil recovery at the early stage of displacement but degrade the sweep in the longer term. The water-wet capillary pressure greatly restricts the gas flowing into low-permeability zones and therefore bypassing a large amount of oil. The oil recovery may drop by over 7% in the case with a reduced injection rate. On the other hand, the capillary force assumed in an

oil-wet system may slow and reduce the oil recovery within 2PV WAG injection but improve the displacement performance in the longer-term. This because the oil-wet capillary pressure drives CO_2 into the non-preferential routes (i.e. low-permeability zones) and therefore improves the sweep efficiency. Unlike the base case (no capillarity) or the water-wet case, the oil recovery can be further increased by simply extending the third water injection cycle in the assumed oil-wet system.

4. In the particular case presented here, the gravity effect reduces the benefits of the combine M_{CE} and M_{IFT} compared to the flow simulations in the 2D area model. This is because the issue of gravity segregation, which leads to the degraded sweep efficiency, becomes more severe with increasing K_v/K_h ratio. In the extreme case with the ratio of K_v/K_h as 1, the difference in recovery between the case with M_{CE} acting only and the case with both M_{CE} and M_{IFT} is reduced to 9% (14% between areal cases).

Chapter 6 Conclusions and Future Work

6.1 Conclusions

Hundreds of very fine-scale simulations have been performed to identify the significance of different aspects of multiscale physics, including compositional effects, interfacial tension effects, gas trapping, water hysteresis, capillary forces and gravity effects, all of which could occur in the process of near-miscible CO_2-WAG. The efforts of studying the key processes separately and jointly leads to a greater insight into how these physical processes affect the sweep and local displacement efficiency. The outcome of this research, which fills some knowledge gap of flow behaviour in the transition from immiscible to miscible conditions. In the meantime, the ancillary experiments essential to assessing near-miscible WAG projects also become evident here, i.e. the measurements of interfacial-tension dependent relative permeabilities, hysteresis in relative permeability of gas and capillary pressure between gas and water. The improved understanding of near-miscible WAG is directly beneficial to the theoretical research on flow behaviour in porous media. Although this work has focussed on the increase in oil recovery from near-miscible CO_2 WAG, the simulations also indicate where the mobile and immobile CO_2 is located, which provides valuable insight for the implementation of CO_2 storage. Specifically, three main research questions have been systematically addressed in this thesis:

1. How do compositional effects (M_{CE}) interact with the underlying heterogeneity pattern of the flow field and influence the oil/component recovery?

The compositional effect of mass transfer can have a very significant impact on the prediction of CO_2-EOR projects. Issues such as front stability, local displacement efficiency and formation of fingering or channelling during CO_2 displacement have been extensively discussed in Chapter 3. The unstable phase flow determined by the underlying heterogeneity greatly slows the flow in the unswept area and leads to unequal displacement performance between preferential and non-preferential routes. The process of mass transfer between CO_2 and oil can be hampered to a certain degree by unstable flow depending on the level of heterogeneity. Specifically, lighter components have moved preferentially in high gas saturation zones, and leaving the heavier components behind. In the case of channelling flow, compositional effects were less important since the permeability channel dominated the displacement. Both the ultimate oil recovery and

component recovery are significantly and about equally reduced, when the underlying heterogeneity is of dominant influence.

2. What is the role of interfacial effects (M_{IFT}) in the displacement process under near-miscible conditions?

As the interfacial tension decreases to a level of 1-3 mN/m, i.e. near-miscible conditions, film or layer flow of oil could occur, which may significantly improve the displacement performance. Such film flow effects are denoted as M_{IFT} and described by an enhanced hydrocarbon relative permeability in Chapter 4 of this study. A range of various combinations between the M_{CE} and M_{IFT} mechanisms were tested by numerical simulations to evaluate the impact of each mechanism on the flow behaviour, i.e. their separate and joint effects on quantities such as the local oil displacement efficiency, phase flow vectors and the ultimate oil recovery. When acting in combination, the oil stripping and IFT effects can greatly improve the local displacement performance even when viscous fingering flow occurs. The remaining oil in these non-preferential flow paths (i.e. bypassed oil) can be efficiently recovered by the combined M_{CE} and M_{IFT} mechanisms, but only with the application of Water-Alternating-Gas (WAG). This M_{IFT} mechanism has much less impact in cases with continuous CO_2 injection compared to its efficiency in WAG. This is because during continuous injection, gas fingers are dominant in the preferential flow paths, and therefore the local displacement efficiency is very good, but only in these preferential routes. On the other hand, WAG is able to make full use of the IFT effects because of its relatively stable displacing front, which allows the M_{IFT} mechanism to contribute. An additional and rather interesting finding of study is the significant contribution of viscous crossflow to the recovery mechanism, which has been ascertained with the novel tracer analysis proposed in Chapter 4.

3. Do other physical effects such as hysteresis, capillarity and gravity affect the oil recovery?

Based on the new synthesis developed in this study, the investigation was further extended to take into account of important multiphase flow behaviour occurring in WAG processes. The effect of gas trapping may degrade the displacement performance of the non-preferential routes. This is because the trapping mechanism greatly hampers M_{IFT} acting during the secondary water injection cycle. The viscous crossflow between the non-preferential routes and preferential routes (gas fingers) is restricted, which leads to a lowered sweep efficiency and a reduction of 3% in the oil recovery. Regarding the effect of water hysteresis, the sweep efficiency is slightly boosted due to the fact that an increasing amount of water is forced into non-preferential routes. This leads to a slight

enhancement of M_{IFT} and an increase in oil recovery by approximately 2% compared to the case which accounted for only M_{CE} and M_{IFT}.

The effect of the capillary force is more complex. In a water-wet system, oil recovery may be improved at the early stage of displacement but the oil recovery will be lower at the end of injection. In this case, capillary pressure between gas and water forms entry barriers for the gas flowing into low-permeability zones, which give rises to more severe gas fingers and a larger amount of bypassed oil. The oil recovery may drop by over 7% compared to the case without capillarity. On the other hand, the oil recovery was about 4% higher in the oil-wet system than that in the water-wet system. In addition, such a difference in oil recovery could be further increased by up to 9% through simply extending the final cycle of water injection. This is because the oil-wet capillary pressure enables gas to imbibe into low-permeability zones, which mitigates the dominant gas fingers. The improved sweep efficiency would maximize the benefits of the combined M_{CE} and M_{IFT}, which are increasingly evident at the late stage of the displacement.

Although the gravity segregation is not the central focus of this study, the effect of gravity was briefly investigated to validate the great necessity of the new synthesis for modelling near-miscible WAG process. Therefore, a set of sample simulations in 2D vertical models varying the k_v/k_h ratio (0.1 and 1) was performed. The density difference between three phases (water, oil and gas) has led to an evident gravity segregation only in the example case with a k_v/k_h ratio of 1. In this particular case, the combined beneficial impact of M_{CE} and M_{IFT} in the 2D vertical cases reduces to approximately 9% of the oil recovery compared to the case with M_{CE} acting only. As for the other case (k_v/k_h =0.1), the gravity effect has very limited impact on the oil recovery.

To summarise, Figure 6-1 shows how various mechanisms and the corresponding modelling methods influence predictions of oil recovery. The oil recovery of the immiscible WAG displacement, where none of the mechanisms was included, is approximately 60% (bar in black). The discrepancies in prediction of recovery is less than 3% among the three typical 3PRP models (Stone 1, Stone 2 and Baker). Then, flow simulations of near-miscible displacement were performed. The results shown by orange and blue bars indicate the potential positive and negative impact on the displacement performance if taking into account these effects: M_{CE}, M_{IFT}, gas trapping, water hysteresis, gravity effect and capillary pressure. What should be highlighted here is the oil-wet

capillary pressure (bar in red), which slows/reduces the oil recovery within the 2PV injection but the oil recovery can be further increased by simply extending the third water injection cycle.

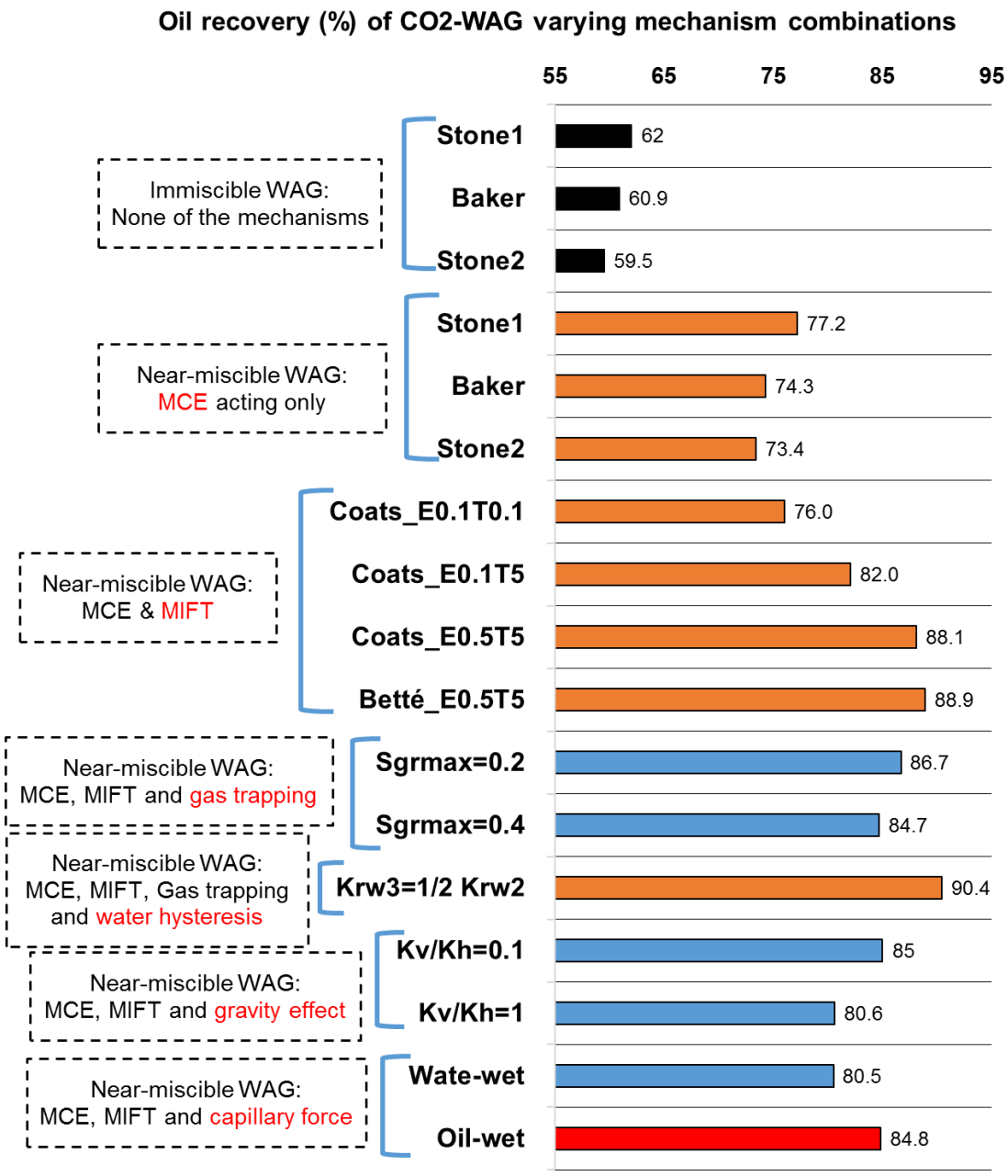

Figure 6-1 Summary of oil revoery varying mechanisms combinations.

6.2 Future work

Upscaling methods for full-compositional flow is an active research topic in numerical flow simulations (Li and Durlofsky, 2016). The results achieved here can be used as "input" for any upscaling work on the compositional flow in the future. In the meantime,

it is aware that findings achieved here are based on a set of specific assumptions, such as certain types of fluid properties and geological structures, which are subject to unavoidable uncertainties. In practice, sources of uncertainties can be resulted from the lack of data, random measurements errors, systematic errors (such as bias and model restrictions) etc. (Bu and Damsleth, 1996). In fact, some preliminary tests have been conducted to investigate uncertainties of central interest, namely the additional realisation of the permeability field, the number of pseudo-components of EOS (4-component VS 7-component), choices of multiphase relative permeability model (Betté VS Coats) and the involved input values. A more extensive work are recommended to further address the uncertainty concerns involved in this work.

6.2.1 Fluid properties

The sample oil analysed here is a typical light oil without much heavy component (see section 3.2.3). This feature enables the injection of CO_2-WAG to maximise the combined benefits of M_{CE} and M_{IFT}. Very importantly, the viscosity of oil is lower than water before entering very late stage of mass transfer. In other words, the displacing front is mostly stable during the water cycles, when the viscous crossflow can be greatly amplified by M_{IFT} to recover the bypassed oil. However, if the oil composition has more heavy components, the mobility of oil may become worse than water at early stages of displacement (or throughout the whole process). This would lead to more unstable flow behaviour and suppressed viscous crossflow. For this reason, a more comprehensive analysis on the fluid properties requires further investigations.

6.2.2 Geological model

For simplicity, the geological model utilized here is a synthetic field with correlated permeability and constant porosity. Obviously, the realistic situations are much more complex. One of the central concerns is the connectivity between flow paths. For example, the connectivity in 3D cases is of much complexity and can be better than 2D cases (Larue and Hovadik, 2006). On the other hand, it is possible that overall displacement performance are significantly degraded by the extensive non-permeable layers, which baffle the viscous crossflow between flow paths. Therefore, this research can be extended to include geological structures of interest in 3D models, such as fault and mud layers, although the computational cost may not be affordable if performing equally fine-scale simulations at this stage. In addition, the assumption of the negligible oil-gas capillarity is only valid for a near-miscible WAG process in a strongly water-wet system. For other complex situations (mixed wet, weekly water/oil wet), where wetting

order is less clear, a more rigorous function for 3-phase capillarity requires further research.

Appendix

Component	Mass frac.	Mole frac.	MW	SG	Tb (C)
CO2	0.0045	0.0118	44.0095	0.8180	-78.4643
N2	0.0004	0.0016	28.0135	0.8094	-195.8100
C1	0.0160	0.1154	16.0425	0.3000	-161.5167
C2	0.0156	0.0601	30.0690	0.3562	-88.6056
C3	0.0247	0.0648	44.0956	0.5070	-42.0833
i-C4	0.0112	0.0222	58.1222	0.5629	-11.7889
n-C4	0.0239	0.0476	58.1222	0.5840	-0.5111
i-C5	0.0205	0.0328	72.1488	0.6247	27.8444
n-C5	0.0231	0.0370	72.1488	0.6311	36.0667
C6	0.0464	0.0651	82.2600	0.6960	63.8889
C7	0.0670	0.0842	91.9314	0.7400	91.9444
C8	0.0883	0.0989	103.1156	0.7659	116.6667
C9	0.0770	0.0784	113.4302	0.8129	142.2222
C10	0.0589	0.0515	132.0084	0.7937	165.8333
C11	0.0399	0.0313	147.0000	0.7930	187.2222
C12	0.0297	0.0213	161.0000	0.8040	208.3333
C13	0.0293	0.0193	175.0000	0.8150	227.2222
C14	0.0238	0.0145	190.0000	0.8260	246.3889
C15	0.0239	0.0134	206.0000	0.8360	266.1111
C16	0.0205	0.0106	222.0000	0.8430	283.3333
C17	0.0185	0.0090	237.0000	0.8510	300.0000
C18	0.0210	0.0097	251.0000	0.8560	312.7778
C19	0.0186	0.0082	263.0000	0.8610	325.0000
C20	0.0127	0.0053	275.0000	0.8660	338.0556
C21	0.0100	0.0040	291.0000	0.8710	351.1111
C22	0.0084	0.0032	300.0000	0.8760	363.3333
C23	0.0064	0.0024	312.0000	0.8810	375.0000
C24	0.0056	0.0020	324.0000	0.8850	386.1111
C25	0.0054	0.0019	337.0000	0.8880	397.2222
C26	0.0056	0.0019	349.0000	0.8920	407.7778
C27	0.0062	0.0020	360.0000	0.8960	417.7778
C28	0.0068	0.0021	372.0000	0.8990	427.7778
C29	0.0070	0.0021	382.0000	0.9020	436.1111
C30+	0.2234	0.0645	400.0000	0.9700	609.2340

Table-A1 Fluid characterization of the 34-component oil. With the use of WINPROP (CMG, 2019), this 34-component oil has been lumped into 4 and 7 components respectively for flow simulatons.

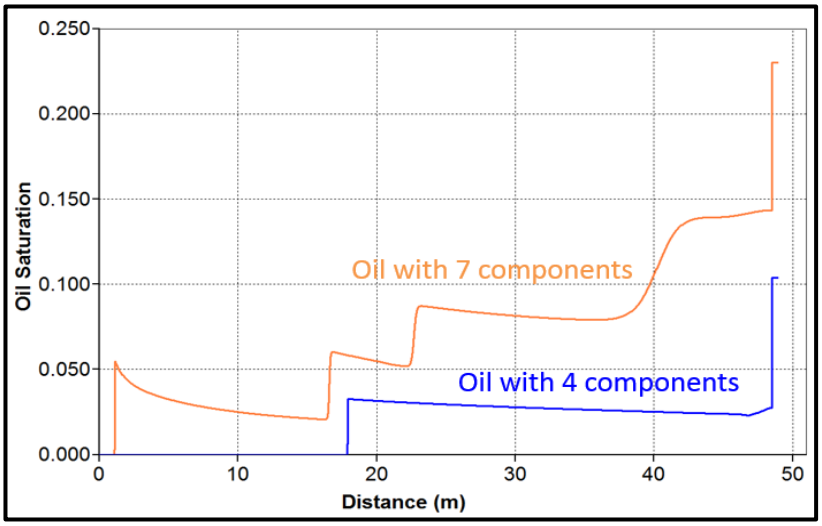

Figure-A1 Oil saturation along the 1D model after 1PV continuous CO_2 injection under near-miscible coniditions (M_{CE} acting only). With the use of 4-componen model, there is no remaning oil saturation in the area adjacent to the injector (0-18m). The important phenomena of heavy oil components left behind cannot be reflected in a 4-component system. As discussed in 3.2.3, the 7-component oil is therefore used for flow simulations performed in this study.

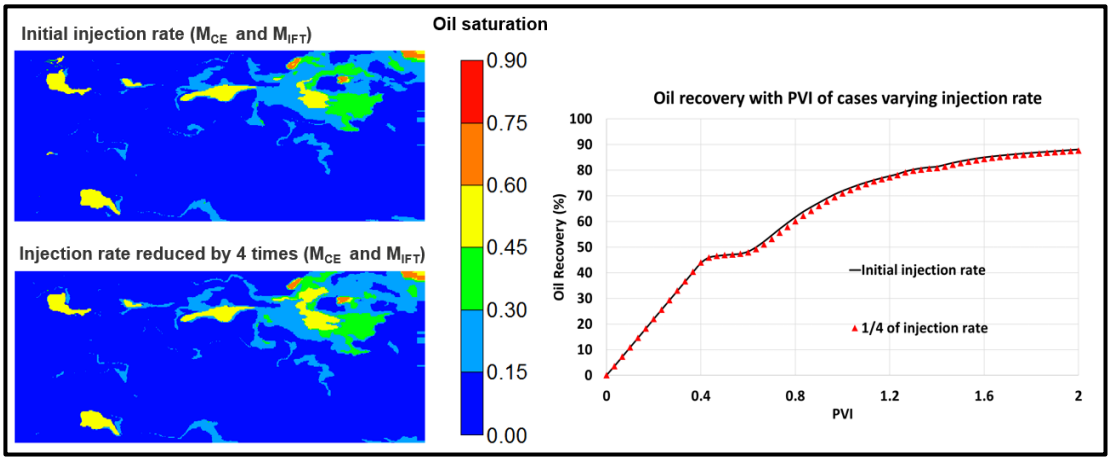

Figure-A2 Remaining oil saturation and oil recovery of cases with the intitial injection rate and one reduced by four times. As mentioned in 5.2.3, there is negilible difference in the remaining oil saturation and oil recovery between the case with the initial injection rate and the case with the reduced injection rate. Through reducing the injection rate, the investigation can be further extended to cover different conditions of balance between the viscous force and capillary force.

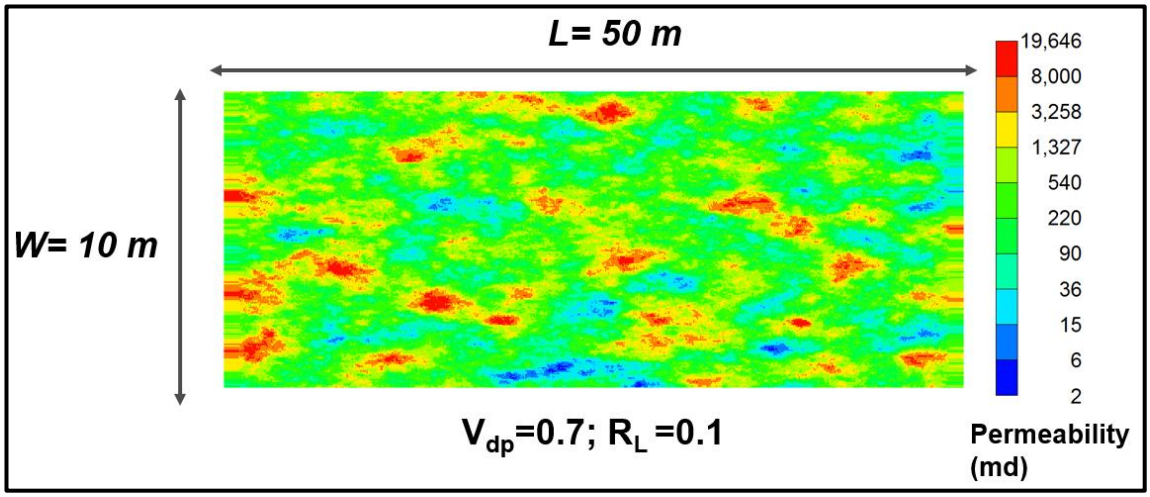

Figure-A3 Permeability field of another realisation (V_{dp}= 0.7 and R_L=0.1). With the use of Petrel (Schlumberger, 2018), another permeability filed is generated with the same value of V_{dp} and R_L.

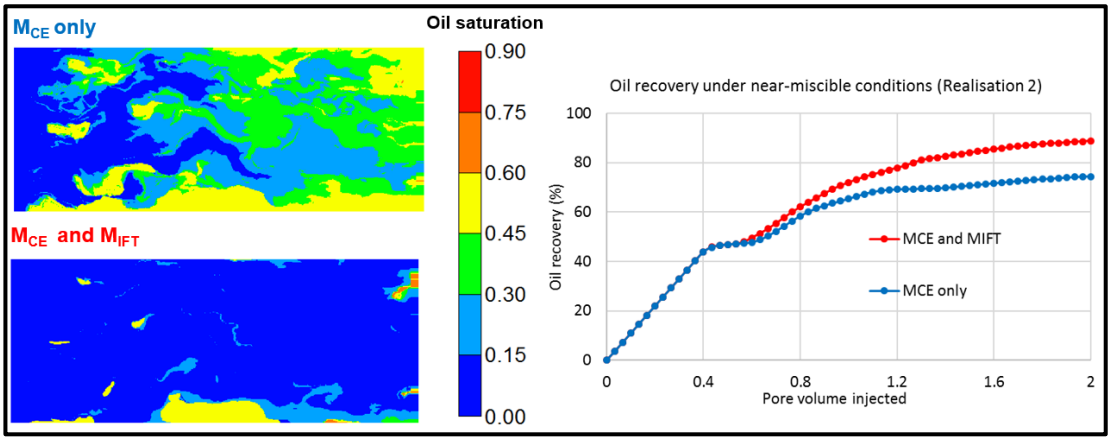

Figure-A4 Remaining oil saturation and oil recovery of cases based on the permeability field of another realisation. In the case with M_{CE} acting only, severe gas fingers still occur, which leaves a large amount of remaining oil saturation. In the case taking into account both M_{CE} and M_{IFT}, the displacement performance has been significantly improved, which is remarkbly similar to the cases shown in 4.4.7. The difference in oil recovery between two cases is up to 15% after 2PV WAG dispalcement. As mentioned in 4.5, these flow simulations based on another realisation were preformed to address the concerns of the potential biased results.

References

Abedini, A. and Torabi, F. (2015) 'Pore size determination using normalized J-function for different hydraulic flow units', *Petroleum*, 1(2), pp. 106-111.

Abou-Kassem, J. H., Farouq-Ali, S. and Islam, M. R. (2013) *Petroleum Reservoir Simulations*. Elsevier

Al-Siyabi, Z., Danesh, A., Tohidi, B. and Todd, A. (1999) 'Variation of gas–oil–solid contact angle with interfacial tension', *Petroleum Geoscience*, 5(1), pp. 37-40.

Al-Wahaibi, Y. M. (2010) 'First-Contact-Miscible and Multicontact-Miscible Gas Injection within a Channeling Heterogeneity System', *Energy & Fuels*, 24(3), pp. 1813-1821.

Alvarado, V. and Manrique, E. (2010) 'Enhanced oil recovery: an update review', *Energies*, 3(9), pp. 1529-1575.

Araktingi, U. G. and Orr Jr, F. M. (1993) 'Viscous Fingering in Heterogeneous Porous Media', *SPE Advanced Technology Series*, 1(01), pp. 71-80.

Arya, A., Hewett, T. A., Larson, R. G. and Lake, L. W. (1988) 'Dispersion and reservoir heterogeneity', *SPE Reservoir Engineering*, 3(01), pp. 139-148.

Asar, H. and Handy, L. L. (1988) 'Influence of Interfacial Tension on Gas/Oil Relative Permeability in a Gas-Condensate System', *SPE Reservoir Engineering*, 3(01), pp. 257-264.

Aziz, K. and Settari, A. (1979) *Petroleum Reservoir Simulation (476)*. Applied Science Publ. Ltd., London, UK

Baker, L. (1988) 'Three-phase relative permeability correlations', SPE-17369-MS, *Proceedings of the SPE Enhanced Oil Recovery Symposium*. Society of Petroleum Engineers, 16-21 April Tulsa, USA. doi: 10.2118/17369-MS.

Barclay, T. H. and Mishra, S. (2016) 'New correlations for CO2-Oil solubility and viscosity reduction for light oils', *Journal of Petroleum Exploration and Production Technology*, 6(4), pp. 815-823.

Bardon, C. (1994) 'Gas/oil relative permeabilities and residual oil saturations in a field case of a very light oil, in the near-miscibility conditions', in *SPE Annual Technical Conference and Exhibition*. Society of Petroleum Engineers.

Berg, R. R. (1975) 'Capillary pressures in stratigraphic traps', *AAPG bulletin*, 59(6), pp.

939-956.

Betté, S., Hartman, K. J. and Heinemann, R. F. (1991) 'Compositional modeling of interfacial tension effects in miscible displacement processes', *Journal of Petroleum Science and Engineering*, 6(1), pp. 1-14.

Blunt, M. J. (2000) 'An empirical model for three-phase relative permeability', *Society of Petroleum Engineers Journal*, 5(04), pp. 435-445.

Blunt, M. J. (2001) 'Flow in porous media—pore-network models and multiphase flow', *Current opinion in colloid & interface science*, 6(3), pp. 197-207.

Bourgeois, M., Joubert, T. and Dominguez, V. (2019) *IOR 2019–20th European Symposium on Improved Oil Recovery*. Available.

BP (2019) *Energy Outlook to 2040*. Available at: https://www.bp.com/en/global/corporate/energy-economics/energy-outlook.html.

Brooks, R. and Corey, T. (1964) 'HYDRAU uc properties of porous media', *Hydrology Papers, Colorado State University*, 24, p. 37.

Brown, H. W. (1951) 'Capillary Pressure Investigations', *Journal of Petroleum Technology*, 3(03), pp. 67-74.

Bu, T. and Damsleth, E. (1996) 'Errors and Uncertainties in Reservoir Performance Predictions', *SPE Formation Evaluation*, 11(03), pp. 194-200.

Burdine, N. (1953) 'Relative permeability calculations from pore size distribution data', *Journal of Petroleum Technology*, 5(3), pp. 71-78.

Cao, H. (2002) 'Development of techniques for general purpose simulators'. Stanford University Stanford, CA.

Carlson, F. M. (1981) 'Simulation of relative permeability hysteresis to the nonwetting phase', SPE-10157-MS, *Proceedings of the SPE Annual Technical Conference and Exhibition*. Society of Petroleum Engineers, 4-7 October San Antonio, Texas. doi: 10.2118/10157-MS.

Chang, Y.-B., Lim, M. T., Pope, G. A. and Sepehrnoori, K. (1994) 'CO2 Flow Patterns Under Multiphase Flow: Heterogeneous Field-Scale Conditions'.

Christensen, J. R., Stenby, E. H. and Skauge, A. (1998) 'Review of WAG field experience', SPE-39883-MS, *Proceedings of the International Petroleum Conference and Exhibition of Mexico*. Society of Petroleum Engineers, 3-5 March, Villahermosa, Mexico. doi: 10.2118/39883-MS.

Christie, M., Muggeridge, A. and Barley, J. (1993) '3D simulation of viscous fingering and WAG schemes', *SPE reservoir engineering*, 8(01), pp. 19-26.

Chung, F. T. H., Jones, R. A. and Nguyen, H. T. (1988) 'Measurements and Correlations of the Physical Properties of CO2-Heavy Crude Oil Mixtures', *SPE Reservoir Engineering*, 3(03), pp. 822-828.

Cinar, Y. and Orr, F. M. (2005) 'Measurement of Three-Phase Relative Permeability with IFT Variation', *SPE Reservoir Evaluation & Engineering*, 8(01), pp. 33-43.

CMG (2017) 'CMG-GEM technical manual', *Computer Modelling Group*.

CMG (2019) 'CMG-GEM technical manual', *Computer Modelling Group*.

Coats, K. H. (1980) 'An Equation of State Compositional Model', *Society of Petroleum Engineers Journal*, 20(05), pp. 363-376.

Corey, A. T. (1954) 'The interrelation between gas and oil relative permeabilities', *Producers monthly*, 19(1), pp. 38-41.

Danesh, A. (1998) *PVT and phase behaviour of petroleum reservoir fluids (47)*. Elsevier

De Gennes, P.-G., Brochard-Wyart, F. and Quéré, D. (2013) *Capillarity and wetting phenomena: drops, bubbles, pearls, waves*. Springer Science & Business Media

Delshad, M. and Pope, G. A. (1989) 'Comparison of the three-phase oil relative permeability models', *Transport in Porous Media*, 4(1), pp. 59-83.

Dullien, F. A. L. (1992) '2 - Capillarity in Porous Media', in Dullien, F. a. L. (ed.) *Porous Media (Second Edition)*. San Diego: Academic Press, pp. 117-236.

Dykstra, H. and Parsons, R. (1950) 'The prediction of oil recovery by waterflood', *Secondary Recovery of Oil in the United States*, 2, pp. 160-174.

Egermann, P., Vizika, O., Dallet, L., Requin, C. and Sonier, F. (2000) 'Hysteresis in Three-Phase Flow: Experiments, Modeling and Reservoir Simulations', SPE-65127-MS, *Proceedings of the SPE European Petroleum Conference*. Society of Petroleum Engineers, 2000/1/1/, Paris, France. p. 14. doi: 10.2118/65127-MS.

Elliott, J. R., Suresh, S. J. and Donohue, M. D. (1990) 'A simple equation of state for non-spherical and associating molecules', *Industrial & Engineering Chemistry Research*, 29(7), pp. 1476-1485.

Faisal, A., Bisdom, K., Zhumabek, B., Zadeh, A. M. and Rossen, W. R. (2009) *SPE Annual Technical Conference and Exhibition*. Society of Petroleum Engineers. Available.

Fayers, F. and Matthews, J. (1984) 'Evaluation of normalized Stone's methods for estimating three-phase relative permeabilities', *Society of Petroleum Engineers Journal*, 24(02), pp. 224-232.

Ferreira, F. C., Booth, R., Oliveira, R., Carneiro, G., Bize-Forest, N. and Wahanik, H. (2015) 'New Rock-Typing Index Based on Hydraulic and Electric Tortuosity Data for Multi-Scale Dynamic Characterization of Complex Carbonate Reservoirs', SPE-175014-MS, *Proceedings of the SPE Annual Technical Conference and Exhibition*. Society of Petroleum Engineers, 2015/9/28/, Houston, Texas, USA. p. 26. doi: 10.2118/175014-MS.

Gardner, J. W. and Ypma, J. G. J. (1984) 'An Investigation of Phase Behavior-Macroscopic Bypassing Interaction in CO2 Flooding'.

Gray, W. G. (1975) 'A derivation of the equations for multi-phase transport', *Chemical Engineering Science*, 30(2), pp. 229-233.

Hassanizadeh, S. M. and Gray, W. G. (1993) 'Thermodynamic basis of capillary pressure in porous media', *Water resources research*, 29(10), pp. 3389-3405.

Holm, L. and Josendal, V. (1974) 'Mechanisms of oil displacement by carbon dioxide', *Journal of petroleum Technology*, 26(12), pp. 1,427-1,438.

Holm, L. W. and Josendal, V. A. (1982) 'Effect of Oil Composition on Miscible-Type Displacement by Carbon Dioxide'.

Holstein, E. D., Lake, L. W. and Engineers, U. S. o. P. (2007) *Petroleum engineering handbook. Vol. 5. Reservoir engineering and petrophysics*. SPE

Homsy, G. M. (1987) 'Viscous fingering in porous media', *Annual review of fluid mechanics*, 19(1), pp. 271-311.

Jessen, K., Stenby, E. H. and Orr Jr, F. M. (2004) 'Interplay of Phase Behavior and Numerical Dispersion in Finite-Difference Compositional Simulation', *SPE Journal*, 9(2), pp. 193-201.

Jhaveri, B. S. and Youngren, G. K. (1988) 'Three-Parameter Modification of the Peng-Robinson Equation of State To Improve Volumetric Predictions', *SPE Reservoir Engineering*, 3(03), pp. 1033-1040.

Johns, R. T. and Garmeh, G. (2010) 'Upscaling of Miscible Floods in Heterogeneous Reservoirs Considering Reservoir Mixing', *SPE Reservoir Evaluation & Engineering*, 13(05), pp. 747-763.

Juanes, R. and Blunt, M. J. (2006) 'Analytical Solutions to Multiphase First-Contact Miscible Models with Viscous Fingering', *Transport in Porous Media*, 64(3), pp. 339-373.

Kargozarfard, Z., Riazi, M. and Ayatollahi, S. (2019) 'Viscous fingering and its effect on areal sweep efficiency during waterflooding: an experimental study', *Petroleum Science*, 16(1), pp. 105-116.

Khabibullin, R., Grin, Z. A., Alkan, H., Grivet, M. and Elgridi, K. (2017) 'Investigation of CO2 Application for Enhanced Oil Recovery in a North African Field-A New Approach to EOS Development', in *IOR 2017-19th European Symposium on Improved Oil Recovery*.

Killough, J. (1976) 'Reservoir simulation with history-dependent saturation functions', *Society of Petroleum Engineers Journal*, 16(01), pp. 37-48.

Lake, L. W. (1989) *Enhanced oil recovery*. Prentice Hall, Englewood Cliffs.

Lake, L. W., Johns, R., Rossen, W. R. and Pope, G. A. (2014) *Fundamentals of enhanced oil recovery*. Society of Petroleum Engineers

Land, C. S. (1968) 'Calculation of Imbibition Relative Permeability for Two- and Three-Phase Flow From Rock Properties', *Society of Petroleum Engineers Journal*, 8(02), pp. 149-156.

Land, C. S. (1971) 'Comparison of calculated with experimental imbibition relative permeability', *Society of Petroleum Engineers Journal*, 11(04), pp. 419-425.

Larsen, J. A. and Skauge, A. (1998) 'Methodology for Numerical Simulation With Cycle-Dependent Relative Permeabilities', *SPE Journal*, 3(02), pp. 163-173.

Larue, D. K. and Hovadik, J. (2006) 'Connectivity of channelized reservoirs: a modelling approach', *Petroleum Geoscience*, 12(4), pp. 291-308.

Leach, M. P. and Yellig, W. F. (1981) 'Compositional Model Studies - CO2 Oil-Displacement Mechanisms'.

Leverett, M. C. (1941) 'Capillary Behavior in Porous Solids', *Transactions of the AIME*, 142(01), pp. 152-169.

Li, H. and Durlofsky, L. J. (2016) 'Upscaling for Compositional Reservoir Simulation', *SPE Journal*, 21(03), pp. 873-887.

Longeron, D. G. (1980) 'Influence of Very Low Interfacial Tensions on Relative

Permeability', *Society of Petroleum Engineers Journal*, 20(05), pp. 391-401.

McPhee, C., Reed, J. and Zubizarreta, I. (2015) 'Chapter 9 - Capillary Pressure', in Mcphee, C., Reed, J. and Zubizarreta, I. (eds.) *Developments in Petroleum Science (64)*. Elsevier, pp. 449-517.

Mirzaei-Paiaman, A., Ostadhassan, M., Rezaee, R., Saboorian-Jooybari, H. and Chen, Z. (2018) 'A new approach in petrophysical rock typing', *Journal of Petroleum Science and Engineering*, 166, pp. 445-464.

Moortgat, J. (2016) 'Viscous and gravitational fingering in multiphase compositional and compressible flow', *Advances in Water Resources*, 89(Supplement C), pp. 53-66.

Muskat, M. (1949) 'Physical principles of oil production: McGraw-Hill Book Company', *Inc., New York*.

Naar, J., Wygal, R. J. and Henderson, J. H. (1962) 'Imbibition Relative Permeability in Unconsolidated Porous Media', *Society of Petroleum Engineers Journal*, 2(01), pp. 13-17.

Negron-Perez, E. A. and Ali, S. M. F. (1973) 'Does Prior Gas Injection Increase Waterflood Recovery? Reservoir Simulator Results Vs Old Theory', SPE-4727-MS, *Proceedings of the SPE Eastern Regional Meeting*. Society of Petroleum Engineers, 1973/1/1/, Pittsburgh, Pennsylvania. p. 14. doi: 10.2118/4727-MS.

Orr, F. M. (2007) *Theory of gas injection processes*. Tie-Line Publications, Copenhagen, Denmark.

Orr, F. M., Jr., Silva, M. K. and Lien, C.-L. (1983) 'Equilibrium Phase Compositions of CO2/Crude Oil Mixtures-Part 2: Comparison of Continuous Multiple-Contact and Slim-Tube Displacement Tests'.

Peng, D.-Y. and Robinson, D. B. (1976) 'A New Two-Constant Equation of State', *Industrial & Engineering Chemistry Fundamentals*, 15(1), pp. 59-64.

Perera, M. S. A., Gamage, R. P., Rathnaweera, T. D., Ranathunga, A. S., Koay, A. and Choi, X. (2016) 'A Review of CO2-Enhanced Oil Recovery with a Simulated Sensitivity Analysis', *Energies*, 9(7), p. 481.

Perkins, T. K. and Johnston, O. C. (1963) 'A Review of Diffusion and Dispersion in Porous Media', *Society of Petroleum Engineers Journal*, 3(01), pp. 70-84.

Pickup, G. E., Stephen, K. D., Ma, J., Zhang, P. and Clark, J. (2005) 'Multi-stage upscaling: Selection of suitable methods', in *Upscaling Multiphase Flow in Porous Media*. Springer, pp. 191-216.

Ranaee, E., Porta, G. M., Riva, M., Blunt, M. J. and Guadagnini, A. (2015) 'Prediction of three-phase oil relative permeability through a sigmoid-based model', *Journal of Petroleum Science and Engineering*, 126, pp. 190-200.

Ranaee, E., Riva, M., Porta, G. M. and Guadagnini, A. (2016) 'Comparative assessment of three-phase oil relative permeability models', *Water Resources Research*, 52(7), pp. 5341-5356.

Rathmell, J., Stalkup, F. and Hassinger, R. (1971) 'A laboratory investigation of miscible displacement by carbon dioxide', SPE-3483-MS, *Proceedings of the Fall Meeting of the Society of Petroleum Engineers of AIME*. Society of Petroleum Engineers, 3-6 October 1971, New Orleans, Louisiana. doi: https://doi.org/10.2118/3483-MS.

Rezk, M. G. and Foroozesh, J. (2019) 'Effect of CO2 mass transfer on rate of oil properties changes: Application to CO2-EOR projects', *Journal of Petroleum Science and Engineering*, 180, pp. 298-309.

Ringrose, P. S., Sorbie, K. S., Corbett, P. W. M. and Jensen, J. L. (1993) 'Immiscible flow behaviour in laminated and cross-bedded sandstones', *Journal of Petroleum Science and Engineering*, 9(2), pp. 103-124.

Rose, W. and Bruce, W. A. (1949) 'Evaluation Of Capillary Character In Petroleum Reservoir Rock', *Journal of Petroleum Technology*, 1(05), pp. 127-142.

Saboorian Jooybari, H., Movazi, G. H. and Jaberi, R. (2010) 'A New Approach for Rock Typing Used in One of the Iranian Carbonate Reservoir (A Case Study)', SPE-131915-MS, *Proceedings of the International Oil and Gas Conference and Exhibition in China*. Society of Petroleum Engineers, 2010/1/1/, Beijing, China. p. 10. doi: 10.2118/131915-MS.

Sanchez, N. L. (1999) *Latin American and Caribbean petroleum engineering conference*. Society of Petroleum Engineers. Available.

Schembre, J. M. and Kovscek, A. R. (2003) 'A technique for measuring two-phase relative permeability in porous media via X-ray CT measurements', *Journal of Petroleum Science and Engineering*, 39(1), pp. 159-174.

Schlumberger (2015) 'Eclipse technical manual', *Schlumberger Limited*.

Schlumberger (2018) 'Petrel technical manual', *Schlumberger Limited*.

Shen, P., Zhu, B. and Wu, Y.-S. (2005) 'The influence of interfacial tension on water-oil two-phase relative permeability'.

Shyeh-Yung, J. G. J. (1991) 'Mechanisms of Miscible Oil Recovery: Effects of Pressure on Miscible and Near-Miscible Displacements of Oil by Carbon Dioxide', SPE-22651-MS, *Proceedings of the* Society of Petroleum Engineers, 1991/1/1/. doi: 10.2118/22651-MS.

Skauge, A. and Sorbie, K. (2014) 'Status of Fluid Flow Mechanisms for Miscible and Immiscible WAG', SPE-169747-MS, *Proceedings of the SPE EOR Conference at Oil and Gas West Asia*. Society of Petroleum Engineers, 31 March-2 April 2014, Muscat, Oman. doi: 10.2118/169747-MS.

Soave, G. (1972) 'Equilibrium constants from a modified Redlich-Kwong equation of state', *Chemical engineering science*, 27(6), pp. 1197-1203.

Sohrabi, M., Danesh, A. and Jamiolahmady, M. (2008b) 'Visualisation of Residual Oil Recovery by Near-miscible Gas and SWAG Injection Using High-pressure Micromodels', *Transport in Porous Media*, 74(2), pp. 239-257.

Sohrabi, M., Danesh, A., Tehrani, D. H. and Jamiolahmady, M. (2008a) 'Microscopic Mechanisms of Oil Recovery By Near-Miscible Gas Injection', *Transport in Porous Media*, 72(3), pp. 351-367.

Sohrabi, M., Tehrani, D., Danesh, A. and Henderson, G. (2004) 'Visualization of oil recovery by water-alternating-gas injection using high-pressure micromodels', *Society of Petroleum Engineers Journal*, 9(03), pp. 290-301.

Sorbie, K. and Mackay, E. (2000) 'Mixing of injected, connate and aquifer brines in waterflooding and its relevance to oilfield scaling', *Journal of Petroleum Science and Engineering*, 27(1-2), pp. 85-106.

Sorbie, K. and Skauge, A. (2019) *IOR 2019–20th European Symposium on Improved Oil Recovery*. Available.

Sorbie, K. S. (2013) *Polymer-improved oil recovery*. Springer Science & Business Media

Sorbie, K. S. and van Dijke, M. I. J. (2010) 'The Mechanism of Oil Recovery by Water-Alternating-Gas Injection at Near-Miscible Conditions in Mixed Wet Systems', SPE-129837-MS, *Proceedings of the SPE Improved Oil Recovery Symposium*. Society of Petroleum Engineers, 24-28 April, Tulsa, Oklahoma. doi: 10.2118/129837-MS.

Spiteri, E. J. and Juanes, R. (2006) 'Impact of relative permeability hysteresis on the numerical simulation of WAG injection', *Journal of Petroleum Science and Engineering*, 50(2), pp. 115-139.

Stalkup, F. I. (1983) *Miscible displacement (8)*. Dallas.

Stone, H. L. (1970) 'Probability Model for Estimating Three-Phase Relative Permeability', *Journal of Petroleum Technology*, 22(02), pp. 214-218.

Stone, H. L. (1973) 'Estimation of Three-Phase Relative Permeability And Residual Oil Data', *Journal of Canadian Petroleum Technology*, 12(04).

Theune, U. (2018) 'Ternary Plots', *MATLAB Central File Exchange*.

Todd, M. R. and Longstaff, W. J. (1972) 'The Development, Testing, and Application Of a Numerical Simulator for Predicting Miscible Flood Performance', *Journal of Petroleum Technology*, 24(07), pp. 874-882.

Tsang, C. F. and Neretnieks, I. (1998) 'Flow channeling in heterogeneous fractured rocks', *Reviews of Geophysics*, 36(2), pp. 275-298.

Van der Waals, J. D. (1873) *Over de Continuiteit van den Gas-en Vloeistoftoestand (1)*. Sijthoff

Van Dijke, M., McDougall, S. and Sorbie, K. (2001) 'Three-phase capillary pressure and relative permeability relationships in mixed-wet systems', *Transport in Porous Media*, 44(1), pp. 1-32.

Waggoner, J. R., Castillo, J. L. and Lake, L. W. (1992) 'Simulation of EOR Processes in Stochastically Generated Permeable Media'.

Wang, F. (1988) 'Effect of wettability alteration on water/oil relative permeability, dispersion, and flowable saturation in porous media', *SPE reservoir engineering*, 3(02), pp. 617-628.

Wegener, D. C. and Harpole, K. J. (1996) 'Determination of Relative Permeability and Trapped Gas Saturation for Predictions of WAG Performance in the South Cowden CO2 Flood', SPE-35429-MS, *Proceedings of the SPE/DOE Improved Oil Recovery Symposium*. Society of Petroleum Engineers, 1996/1/1/, Tulsa, Oklahoma. p. 13. doi: 10.2118/35429-MS.

Whitson, C. H. and Brulé, M. R. (2000) *Phase behavior*. Henry L. Doherty Memorial Fund of AIME, Society of Petroleum Engineers Richardson, TX

Yang, D. and Gu, Y. (2004) 'Visualization of Interfacial Interactions of Crude Oil-CO2 Systems under Reservoir Conditions', SPE-89366-MS, *Proceedings of the* Society of Petroleum Engineers, 2004/1/1/. doi: 10.2118/89366-MS.

Yellig, W. and Metcalfe, R. (1980) 'Determination and Prediction of CO2 Minimum Miscibility Pressures (includes associated paper 8876)', *Journal of Petroleum Technology*, 32(01), pp. 160-168.

Young, L. C. and Stephenson, R. E. (1983) 'A Generalized Compositional Approach for Reservoir Simulation', *Society of Petroleum Engineers Journal*, 23(05), pp. 727-742.

Zapata, V. J. and Lake, L. W. (1981) 'A theoretical analysis of viscous crossflow', SPE-10111-MS, *Proceedings of the SPE Annual Technical Conference and Exhibition*. Society of Petroleum Engineers, 4-7 October, San Antonio, Texas. doi: 10.2118/10111-MS.